

MATHEMATISCHES FORSCHUNGSIINSTITUT OBERWOLFACH

Report No. 39/2006

Mathematical Theory and Modelling in Atmosphere-Ocean Science

Organised by

Oliver Bühler (New York)

Andrew J. Majda (New York)

Rupert Klein (Berlin)

August 20th – August 26th, 2006

ABSTRACT. Mathematical theory and modelling in atmosphere-ocean science combines a broad range of advanced mathematical and numerical techniques and research directions. This includes the asymptotic analysis of multiscale systems, the deterministic and stochastic modelling of sub-grid-scale processes, and the numerical analysis of nonlinear PDEs over a broad range of spatial and temporal scales. This workshop brought together applied mathematicians and experts in the disciplinary fields of meteorology and oceanography for a wide-ranging exchange of ideas and results in this area with the aim of fostering fundamental interdisciplinary work in this important science area.

Mathematics Subject Classification (2000): 76U05, 7606, 86A10, 86A05, 65M12, 65Z05, 35M10.

Introduction by the Organisers

This workshop was the second meeting at Oberwolfach of this kind, following after a highly successful previous meeting in 2002. Again, the meeting was very well attended with over 38 participants from Germany, Europe, and the U.S.A. Most attendees were senior researchers but there was also a handful of post-docs and graduate students. The organizers feel that this mix greatly enhanced the educational outreach and impact of the meeting, which is a significant target in its own right.

The wide range of talks reported here reflected the interdisciplinary breadth of the workshop, with research topics ranging from the physical and mathematical intricacies of tropical convection on the one hand to the abstract geometric interpretations of the governing PDEs of atmosphere–ocean fluid dynamics on the other. This ambitious breadth of research lies at the heart of this interdisciplinary

workshop and it provided a very stimulating environment for lively talks and discussions at Oberwolfach.

The common thread running through the mathematical challenge of atmosphere and ocean dynamics is the inherent multiscale nature of these vast dynamical systems, in which spatial scales interact nonlinearly across scales from millimetre-size rain drops to planetary large-scale waves spanning the globe. Concomitant with the vast range of spatial scale is a range of temporal scales from a few seconds for sound waves to many years for oceanic vortices. A persistent theme of the workshop was how to tackle these multiscale problems theoretically and numerically. Progress was reported on the difficult problem of tropical convection, which features very intricate micro-physics and is unresolvable in its details on present-day supercomputers. Work describing the space-time organization of convection over a broad range of scales is currently underway by a number of researchers and the workshop gave an up-to-date snapshot of a number of models and approaches. Similar approaches in boundary layer modelling were reported on as well.

Viewed over long time scales the faster processes in the atmosphere and oceans begin to resemble stochastic noise and a number of theoretical talks aimed to model the low-frequency variability of the global system based on simplified stochastic representations for the fast processes. This links naturally to the problem of integrating stiff PDEs due to widely different temporal and spatial scales, and a number of talks presented progress in the numerical analysis of schemes that can tackle these stiff systems.

From a physical point of view the distinction between fast and slow processes often overlaps with the distinction between wavelike and vortical motions and a number of talks addressed averaging methods and the nonlinear interactions between fast waves and slow vortices. This overlapped with some theoretical developments in the area of constrained PDEs, in which fast waves are filtered *ab initio* in some manner. The resulting constrained PDE system has a smaller phase space and typically can be viewed as a suitable projection of the original PDE system on a slow manifold. This raises theoretical and numerical issues of long-term accuracy and stability and several such aspects were discussed in the workshop.

Workshop: Mathematical Theory and Modelling in Atmosphere-Ocean Science**Table of Contents**

Mitch W. Moncrieff	
<i>Orogenic Organized Propagating Convective Systems: Dynamics, Parameterization and Numerical Prediction</i>	2313
Boualem Khouider (joint with Andrew J. Majda)	
<i>Multicloud models for tropical convection and convectively coupled waves</i>	2315
Joseph A. Biello (joint with Andrew J. Majda, Mitch W. Moncrieff)	
<i>Meridional momentum flux and superrotation in the multi-scale IPESD MJO model</i>	2321
Joseph Egger	
<i>Statistical flow equations applied to atmospheric circulations</i>	2324
Grant Branstator	
<i>Reduced Models of Tropospheric Planetary Waves</i>	2325
Adam H. Monahan (joint with John C. Fyfe)	
<i>On the nature of zonal jet EOFs</i>	2328
Marcus J. Grote (joint with Andrew J. Majda)	
<i>Stable Time Filtering of Strongly Unstable Spatially Extended Systems</i> ..	2329
Vladimir Zeitlin (joint with G.M. Reznik)	
<i>Nonlinear dynamics in the semi-transparent equatorial waveguide. Part 1. Resonant excitation of Rossby and Yanai waves and their interactions</i> .	2331
Esteban G. Tabak (joint with Paul A. Milewski, Fabio A. Tal)	
<i>A coarse graining approach to quantifying mixing in stratified flows</i>	2333
Paul A Milewski (joint with Ruben R. Rosales, Esteban G. Tabak, Cristina Turner)	
<i>Stability, Breaking Waves, and Mixing in Stratified Flows</i>	2334
Bjorn Stevens (joint with Brian Medeiros)	
<i>Shallow layers of non-precipitating cumulus convection</i>	2336
David M. Holland	
<i>A 1-D Elastic-Plastic Sea-Ice Model Solved with an Implicit Eulerian-Lagrangian Method</i>	2340
Antony Z. Owino (joint with Bjorn Stevens, Rupert Klein)	
<i>Multiple Scale Asymptotics of Cloud Topped Boundary Layer</i>	2341

Elie Bou-Zeid (joint with Marc B. Parlange, Charles Meneveau)	
<i>Modeling and parameterization of regional scale land-atmosphere exchanges</i>	2345
Yann Brenier	
<i>Derivation and discretization of the semi-geostrophic equations</i>	2345
Daan Crommelin (joint with Eric Vanden-Eijnden)	
<i>Reconstruction of effective stochastic dynamics from data</i>	2347
Paola Cessi	
<i>Regimes of thermocline scaling: the interaction of wind-stress and surface buoyancy</i>	2349
J. Gavin Esler (joint with O. J. Rump, E. R. Johnson)	
<i>A Similarity Theory for Transcritical Flow over Orography</i>	2351
Christian Schoof	
<i>Marine ice sheet dynamics</i>	2352
Stamen I. Dolaptchiev (joint with Rupert Klein)	
<i>Reduced Systematic Model Equations For The Planetary And Synoptic Scales In The Atmosphere</i>	2353
Sebastian Reich (joint with Mark Dubal, Andrew Staniforth, Nigel Wood (UK Met Office))	
<i>Semi-implicit semi-Lagrangian time-stepping methods and regularized fluid equations in numerical weather prediction</i>	2355
Ian Roulstone (joint with L.R. Watkinson, A.S. Lawless, N.K. Nichols)	
<i>Data Assimilation and the 2- and 3-body Problems</i>	2356
Lars Mentrup (joint with Jörn Behrens)	
<i>Unstructured adaptive grid refinement in atmospheric and ocean modeling</i>	2359
Andrew Majda and Xiaoming Wang	
<i>The Emergence of Large Scale Coherent Structure under Small Scale Random Bombardments</i>	2361
Paul David Williams (joint with Thomas W. N. Haine, Peter L. Read [1])	
<i>Inertia-gravity waves emitted spontaneously from quasi-balanced flow: properties and consequences</i>	2362
Ulrich Achatz	
<i>The primary nonlinear dynamics of modal and nonmodal perturbations of monochromatic inertia-gravity waves</i>	2364
David J Muraki (joint with Youngsuk Lee, David Alexander & Craig Epifanio)	
<i>A Resonant Instability of Finite-Amplitude Mountain Waves</i>	2366
Onno Bokhove (joint with Marcel Oliver)	
<i>Spherical Hamiltonian Isentropic 2-Layer Model for Atmospheric Dynamics</i>	2369

Eileen Mikusky (joint with Antony Owinoh, Rupert Klein)	
<i>On the motion and structure of 3D - mesoscale vortices</i>	2372
Oswald Knoth	
<i>Compressible atmospheric modeling at all scales</i>	2374
Almut Gassmann	
<i>Time-splitting techniques in nonhydrostatic compressible modeling</i>	2377
Leo R.M. Maas	
<i>Waves in rotating fluids: geometric effects</i>	2379
Riwal Plougonven and Chris Snyder	
<i>The spontaneous generation of inertia-gravity waves in idealized baroclinic life cycles</i>	2381
Jacques Vanneste (joint with I. Yavneh, E. I. Ólafsdóttir and A. B. Olde Daalhuis)	
<i>Exponential smallness of inertia-gravity-wave generation</i>	2383
Tapio Schneider (joint with Simona Bordoni and Christopher C. Walker)	
<i>Macroturbulence and Hadley Circulation Dynamics</i>	2386
K. Shafer Smith	
<i>Linear baroclinic instability in the world's oceans</i>	2388

Abstracts

Orogenic Organized Propagating Convective Systems: Dynamics, Parameterization and Numerical Prediction

MITCH W. MONCRIEFF

Precipitating convection in the lee of major mountain chains (e.g., Rocky Mountains, Andes, Ethiopian Highlands, Tibetan Plateau, European Alps) organizes into *long-lived coherent dynamical systems*. These powerful transporters of mass, energy and momentum propagate at $\approx 10\text{m/s}$ so their effects on the environment can extend across the entire US continent. The sources of energy are primarily latent heating, evaporation of falling precipitation, mean-flow kinetic energy, and work done by the convectively-generated pressure gradient. Environmental shear interacting with vorticity generated (baroclinically) by horizontal gradients of heating organizes coherent circulations on scales 10 km - 1000 km; namely, mesoscale atmospheric motion.

The key dimensionless quantities are: i) the ratio of the work done by the pressure gradient to the kinetic energy of propagation expressing a hydraulic work-energy principle, and ii) a convective Richardson number, the ratio of convective available potential energy to the mean-flow kinetic energy [1, 2]. Steady-state two-dimensional dynamical models are based on a nonlinear eigenvalue/free-boundary problem defined by the elliptic integro-differential (vorticity) equation

$$\nabla^2 \psi = G(\psi) + \int_{z_0}^z \frac{\partial F}{\partial \psi} dz$$

where G is the environmental shear, $F = F(z, \psi, c)$ is the buoyancy generated by latent heat release/evaporative cooling, ψ is the streamfunction, c is the propagation speed (eigenvalue), and z is the vertical displacement of the streamfunction from its inflow level. Along with appropriate boundary conditions, solutions to this equation define a hierarchy of dynamical models. Lateral boundary conditions are provided by the far-field solution of the above equation.

A key dynamical property is the characteristic backward tilt of convective systems relative to their direction of propagation. Tilting affects the vertical transport of horizontal momentum. The flow acceleration and the heating has a first-baroclinic (couplet) form. For example, an eastward-traveling system generates lower-tropospheric eastward and upper-tropospheric westward accelerations. Furthermore, the momentum transport by the tilted flow organization results in a positive dynamical feedback: momentum transport generates the sheared environment in which propagating systems tend to develop [1, 4].

Global numerical models used for weather prediction and climate research have great difficulty with representing organized propagating convective systems. The dynamical processes of convective organization are missing from these parameterizations, which were not designed to represent the upscale fluxes of energy and

momentum generated by organized convection [4]. Moreover, in modern higher-resolution global numerical weather prediction models (apart from convective-system resolving models) the grid-scale is not adequately separated from the dynamical scale of convective organization. This has serious implications since scale-separation is a keystone of contemporary parameterization methods.

The above issues associated with mesoscale convective organization are addressed by a hybrid parameterization called a predictor-corrector approach [4]. In this approach organized mesoscale circulations are represented by a first-baroclinic couplet based on a dynamical model (a special case of the above equation). The first-baroclinic perturbation approximates the stratiform heating/mesoscale down-draft couplet and the accompanying momentum transport [1, 2]. It is functionally related to the convective parameterization needed to represent the cumulus convection embedded in the organized circulation. Explicit circulations at 10-km grid-spacing are the “predictor” but the circulations are under-resolved. Under-resolution causes systematic warming of the lower troposphere since the mesoscale downdrafts are too weak. This weakness is alleviated by the “corrector”, defined as the cooling perturbation in the heating couplet.

The predictor-corrector hybrid parameterization was evaluated using a hierarchy of numerically simulated summertime convective systems over the continental United States. In turn, the simulations were validated by comparison with radar measurements of precipitation. Issues of horizontal resolution were quantified by comparing control simulations (3-km and 1-km grid-pacing) to simulations at 10-km grid-spacing (grid-resolution of next-generation global numerical weather prediction models). The convective momentum transport was found to be particularly vulnerable to the horizontal resolution.

Issues in need of further study include: i) the effects of convective momentum transport in prediction models; ii) the dynamics of upslope flow driven by solar-heated mountainous terrain and orographic effects on convection; iii) the interaction between orographically generated gravity-inertial waves and convective organization; iv) the application of power laws for organized precipitating systems to stochastic parameterization methods; and v) the design of generalized numerical solvers for elliptic free-boundary problems.

REFERENCES

- [1] Moncrieff, M.W., 1992: Organized convective systems: archetypal dynamical models, mass and momentum flux theory, and parameterization. *Quart. J. Roy. Meteor. Soc.*, **118**, 819-950.
- [2] Moncrieff, M.W., 2004: Analytic representation of the large-scale organization of tropical convection. *J. Atmos. Sci.*, **61**, 1521-1538.
- [3] Grabowski, W. W., and M. W. Moncrieff, 2001: Large-scale organization of tropical convection in two-dimensional explicit numerical simulations. *Quart. J. Roy. Met. Soc.*, **127**, 445-468.
- [4] Moncrieff, M.W., and C. Liu, 2006: Representing convective organization in prediction models by a hybrid strategy. *J. Atmos. Sci.*, (in press).

Multicloud models for tropical convection and convectively coupled waves

BOUALEM KHOUIDER

(joint work with Andrew J. Majda)

1. INTRODUCTION

Moist convection in the tropics is organized into a hierarchy of propagating cloud clusters and superclusters ranging from hundreds to a few thousand kilometers to planetary scale disturbances. Especially, the intra-seasonal oscillation, observed to propagate in the eastern Pacific warm pool as an 'envelope' of the clouds clusters and/or superclusters [18, 20, 21]. The most energetic clouds consist however of deep penetrative, so called hot towers which are believed to be the heat engine for local and large-scale tropical circulation, because of the latent heat gained because precipitation which is abundant in those clouds. Idealized models with crude vertical resolutions reduced to one to two vertical baroclinic modes are therefore commonly used for both theoretical and numerical studies of this complex physical phenomenon [3, 5, 6, 19, 16, 15]. It is observed however, that organized tropical convection involves three cloud types shallow-non precipitating cumulus clouds with cloud tops ranging from one to two kilometers, congestus clouds which are mildly precipitating and with clouds around 5 to 6 km. The third and most important cloud-type in terms of precipitation and latent heat release, are the deep penetrative clouds with tops near the tropopause [7]. The tropical atmosphere has three layers which are stable to moist convection; one near the top of the planetary boundary layer, the trade inversion layer—characterized by a big jump in the temperature's vertical profile, thus capping the trade cumulus clouds, one near the middle troposphere, the 0° C layer beyond which ice forms, also called the milting layer, associated with the cumulus congestus clouds, and the third layer is near the tropopause, blocking the deep convective towers. Above the milting layer, another cloud-type forms perhaps because of the solidification of liquid water to ice called stratiform anvil clouds because of their shape. The stratiform clouds are also believed to play an important role in the dynamics of organized tropical convection and the moist convective instability associated with convectively coupled waves [17, 16, 15].

During decades, two schools of thought have dominated the arena of convective parametrization theory, leading to two types of models. The so-called convergence models are based on the Convective Instability of the Second Kind (CISK) [22, 6, 13] where the amount of heating is basically set proportional to the low level convergence of mass or water vapor, therefore assuming a constant source of instability for convection. The second type of models on the other hand rely on the quasi-equilibrium theory pioneered apparently by Arakawa and Shubert [1]. The tropical atmosphere is assumed/believed to be always near a radiative-convective equilibrium state. A small deviation from this equilibrium is quickly compensated

by convection acting to restore the equilibrium [2, 4]. For this theory to be complete, convective processes must be triggered and amplified by 'external' sources in order to sustain and maintain large scale tropical disturbances. One of such mechanisms is the wind-induced surface heat exchange (WISHE) introduced and used by Emanuel [3] and Emanuel et al. [2]. Idealized models relying on these two theories are based on only one baroclinic mode for the free tropospheric dynamics coupled to thermal or a dynamical boundary layer, with barotropic advection sometimes added, thus accounting only for the direct heating mode, namely, associated with the deep penetrative clouds, ignoring completely the trimodal nature of tropical convection [7].

Convective model parametrizations with two heating modes were first introduced by Mapes [17]; a deep convective mode as in one-baroclinic models plus a stratiform mode associated with the stratiform anvil clouds. Majda and Shefter [16] introduced a simplified version of the stratiform models which is further analyzed in Majda et al. [15]. Although these stratiform models capture many key observed features of convectively coupled waves, they have some short comings. In addition to their simplification of the congestus clouds, the stratiform models also rely on the WISHE mechanisms to amplify and sustain the convective disturbances in non-linear simulations.

Using the two-baroclinic mode framework, Khouider and Majda, [9, 10, 11, 12] have recently introduced and analyzed a new family of convective parametrization using all the three cloud-types in their heating field. The multicloud models are based on a crude vertical resolution of the primitive equations in the equatorial beta plane assuming a three cloud-type convective parametrization providing the heat sources. Congestus clouds heat the lower half of the troposphere and cool the upper half while deep convective clouds heat the entire troposphere. Stratiform clouds on the other hand heat the upper troposphere and cool the lower troposphere through evaporation of rain falling into dry air. The resulting phenomenological model is then analyzed in [9, 10, 11, 12] both by linear stability analysis and non-linear simulations. It is found that the multicloud model captures many key features of convectively coupled waves as observed in the tropics which are confirmed by the non-linear simulations—without the use of WISHE or CISK. Linear stability analysis [9] reveals scale selective instability of moist gravity waves at the synoptic scale reminiscent of the convectively coupled Kelvin waves or superclusters. Furthermore the nonlinear simulations in [10], the convectively coupled waves are somehow organized into envelopes moving at slower speeds than the waves themselves. Moreover, it is demonstrated in [9, 12] that the congestus heating plays a major role in moistening and preconditioning the atmosphere for deep convection on the wave front essentially by driving the second baroclinic moisture convergence. The bulk of the model equations are given below while the linear and nonlinear results are found in [9, 10, 11, 12].

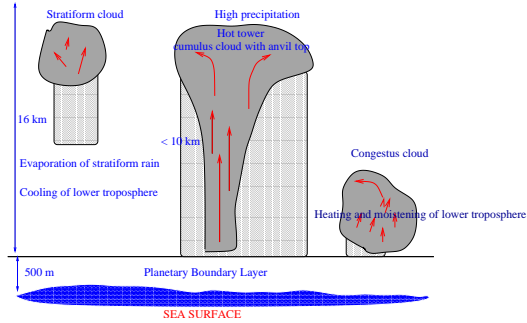


FIGURE 1. The multicloud models are based on the dynamical interactions of three cloud types coupled a sea surface layer.

2. THE MULTICLOUD MODEL PARAMETRIZATION

The multicloud cloud parametrizations assume three cloud types, deep, stratiform and congestus, that coexist and dynamically interact with each other and through a thermal sea surface layer: Deep convective clouds spanning the whole tropospheric height, congestus clouds within the lower half of the troposphere and stratiform clouds within the upper half, as shown in Figure 1. The multicloud models use a crude vertical resolution of the primitive equations in the equatorial beta plane based on these three cloud-types providing the heat sources in the free troposphere,

$$(1) \quad \begin{aligned} H_d(z) &= H_d \sin(z), \quad 0 \leq z \leq \pi \\ H_s(z) &= \begin{cases} 0, & 0 \leq z \leq \pi/2 \\ -H_s \sin(2z), & \pi/2 \leq z \leq \pi \end{cases} \\ H_c(z) &= \begin{cases} H_c \sin(2z), & 0 \leq z \leq \pi/2 \\ 0, & \pi/2 \leq z \leq \pi \end{cases} \\ E_c(z) &= \begin{cases} 0, & 0 \leq z \leq \pi/2 \\ -\delta_c H_c \sin(2z), & \pi/2 \leq z \leq \pi \end{cases} \\ E_s(z) &= \begin{cases} -\delta_s H_s \sin(2z), & 0 \leq z \leq \pi/2 \\ 0, & \pi/2 \leq z \leq \pi \end{cases} \end{aligned}$$

Here $H_c(z)$ and $E_c(z)$ refer to congestus clouds respectively heating the lower half of the troposphere and cooling the upper half while $H_d(z)$ is the effect of deep convective clouds heating the entire troposphere. Stratiform clouds on the other hand heat the upper troposphere and cool the lower troposphere through evaporation of rain falling into dry air. These latter effects are represented respectively by $H_s(z)$ and $E_s(z)$. Closed forms for the quantities H_d, H_s, H_c are provided below while δ_s and δ_c are prescribed fractions of unity. A conceptual picture of the heating and cooling profiles associated with the three cloud types is given in Figure 2. The

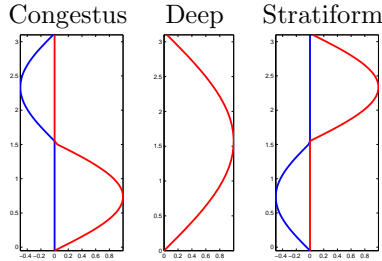


FIGURE 2. Heating and cooling profiles

following basis functions, consistent with the heating profiles in (1):

$$(2) \quad \begin{aligned} \mathbf{V} &= \bar{\mathbf{U}} + \sqrt{2} \cos\left(\frac{\pi z}{H_T}\right) \mathbf{v}_1 + \sqrt{2} \cos\left(\frac{2\pi z}{H_T}\right) \mathbf{v}_2 \\ w &= -\frac{H_T}{\pi} \sqrt{2} \left[\sin\left(\frac{z\pi}{H_T}\right) \operatorname{div} \mathbf{v}_1 + \frac{1}{2} \sin\left(\frac{2\pi z}{H_T}\right) \operatorname{div} \mathbf{v}_2 \right] \\ \Theta &= z + \sqrt{2} \sin\left(\frac{\pi z}{H_T}\right) \theta_1 + 2\sqrt{2} \sin\left(\frac{2\pi z}{H_T}\right) \theta_2. \end{aligned}$$

are used to project the primitive equations onto the first and second baroclinic modes, leading to the 2 shallow water-like systems coupled through the surface layer and the cloud-cloud interactions.

$$(3) \quad \begin{aligned} \text{1st Baroclinic} &\quad \left\{ \begin{array}{l} \frac{\bar{d}\mathbf{v}_1}{dt} + \beta y \mathbf{v}_1^\perp - \nabla \theta_1 = -C_d(u_0) \mathbf{v}_1 - \frac{1}{\tau_R} \mathbf{v}_1 \\ \frac{d\theta_1}{dt} - \operatorname{div} \mathbf{v}_1 = H_d + \xi_s H_s + \xi_c H_c + S_1 \end{array} \right. \\ \text{2nd Baroclinic} &\quad \left\{ \begin{array}{l} \frac{\bar{d}\mathbf{v}_2}{dt} + \beta y \mathbf{v}_2^\perp - \nabla \theta_2 = -C_d(u_0) \mathbf{v}_2 - \frac{1}{\tau_R} \mathbf{v}_2 \\ \frac{d\theta_2}{dt} - \frac{1}{4} \operatorname{div} \mathbf{v}_2 = (-H_s + H_c) + S_2. \end{array} \right. \\ \text{Moisture: } & \frac{\bar{dq}}{dt} + \operatorname{div} \left[(\mathbf{v}_1 + \tilde{\alpha} \mathbf{v}_2) q + \tilde{Q}(\mathbf{v}_1 + \tilde{\lambda} \mathbf{v}_2) \right] = -P + \frac{D}{H_T} \\ & P = \frac{2\sqrt{2}}{\pi} (H_d + \xi_s H_s + \xi_c H_c) \\ \text{Boundary layer: } & \frac{\partial \theta_{eb}}{\partial t} = \frac{1}{h_b} (E - D) \end{aligned}$$

Here $S_{1,2}$ represent the radiative cooling rates, D is the downdraft which connects directly the boundary layer to upper troposphere, and P is precipitation with ξ_s, ξ_c are the fractional contributions of stratiform and congestus clouds to surface precipitation depending on the parameters δ_s, δ_c in (1). For simplicity, the fraction ξ_s, ξ_c are set to zero, in [9, 10, 11, 12], so that there is contribution from stratiform and congestus clouds to surface precipitation. This is equivalent to setting

$\delta_s = \delta_c = 1$ in (1) so that the cooling in the lower troposphere induced by the evaporation of stratiform rain balances exactly the stratiform heating aloft and the congestus heating in the lower troposphere is also balanced by the associated cooling aloft.

As the reader would expect, the moisture equation plays an important role in the convective dynamics. The fluid dynamics on the other hand have a strong feedback on this quantity namely through both the first and second baroclinic moisture convergence.

Details on the derivation and more discussion on these equations are found in [9, 12]. Notice however, that the derivation was constrained to conserve moist static energy, namely,

$$\frac{\partial \langle \theta_e \rangle_z}{\partial t} = \frac{1}{H_T} E + \frac{2\sqrt{2}}{\pi} S_1 \quad (= 0 \text{ at RCE})$$

where

$$\langle \theta_e \rangle_z = \frac{h_b}{H_T} \theta_{eb} + \frac{1}{H_T} \frac{2\sqrt{2}}{\pi} \theta_1 + q.$$

An other important feature of the present model parametrization resides in the introduction of a moisture-switch function which permits to switch back and forth from a congestus to a deep convective regime according to whether the atmosphere is dry or moist.

A moisture based trigger depending on the middle tropospheric equivalent potential temperature $\theta_{em} = q + \frac{2\sqrt{2}}{\pi}(\theta_1 + \alpha_2 \theta_2)$ is introduced, $\Lambda^* \leq \Lambda = \Lambda(\theta_{em}) \leq 1$. The left and right limits are reached when the atmosphere is most and dry respectively. Therefore, the convective closure is achieved as follows. The precipitation and downdrafts are highly depending on the switch function and are given by

$$H_d = \frac{1 - \Lambda}{1 - \Lambda^*} Q_c, \quad D = \Lambda D_0$$

and the stratiform and congestus heating rates are given by

$$(4) \quad \begin{aligned} \frac{\partial H_s}{\partial t} &= \frac{1}{\tau_s} (\alpha_s H_d - H_s); \\ \frac{\partial H_c}{\partial t} &= \frac{1}{\tau_c} \left(\alpha_c \frac{\Lambda - \Lambda^*}{1 - \Lambda^*} \frac{D}{H_T} - H_c \right). \end{aligned}$$

Moreover, a CAPE and Betts-Miller like combination scheme is used.

$$Q_c = \frac{1}{\tau_{conv}} \left[a_1 \theta_{eb} + a_2 (q - \hat{q}) - a_0 (\theta_1 + \gamma_2 \theta_2) \right]^+$$

and the downdrafts are closed by

$$D_0 = \frac{m_0}{Q_{R,1}^0} \left[\bar{Q}_{R,1}^0 + \mu (H_s - H_c) \right]^+ (\theta_{eb} - \theta_{em})$$

while a Newtonian radiative cooling is used for

$$S_j = -Q_{R,j}^0 - \frac{1}{\tau_D} \theta_j, \quad j = 1, 2$$

REFERENCES

- [1] Arakawa, A., and W. H. Shubert, *Interaction of a cumulus cloud ensemble with the large-scale environment. Part I.* J. Atmos. Sci., **31**, (1974), 674–701.
- [2] Emanuel, K. A, J. D. Neelin, and C. S. Bretherton, *On large-scale circulations in convecting atmosphere.* Quart. J. Roy. Meteor. Soc., **120** (1994), 1111–1143.
- [3] Emanuel, K. A., *An air-sea interaction model of intraseasonal oscillations in the tropics.* J. Atmos. Sci., **44** (1987), 2324-3240.
- [4] Emanuel, K. A, *Atmospheric convection.* Oxford Press (1994), 592 pages.
- [5] Fuchs, Z. and D. Raymond, *Large-scale modes of a nonrotating atmosphere with water vapor and cloud-radiation feedbacks.* J. Atmos. Sci., **59**, (2002) 1669–1679.
- [6] Hayashi, Y., *Large-scale equatorial waves destabilized by convective heating in the presence of surface friction.* J. Meteor. Soc. Japan., **49**, (1971), 458–466
- [7] Johnson, R. H., T. M. Rickenbach, S. A. Rutledge, P. E. Ciesielski, and W. H. Schubert, *Trimodal characteristics of tropical convection.* J. of Climate., **12**, (1999), 2397-2407.
- [8] Kiladis, G. N., K.Straub, and P. Haertl, *Zonal and vertical structure of the Madden-Julian oscillation.* J. Atmos. Sci., **62** (2005), 2790–2809.
- [9] Khouider B. and A. J. Majda, *A simple multicloud parametrization for convectively coupled tropical waves. Part I: Linear analysis.* J. Atmos. Sci., **63** (2006), 1308-1323.
- [10] Khouider B. and A. J. Majda, *A simple multicloud parametrization for convectively coupled tropical waves. Part II: Nonlinear simulations.* J. Atmos. Sci., (2006), In press.
- [11] Khouider B. and A. J. Majda, *Model multicloud parametrizations for convectively coupled tropical waves: Detailed wave evolution.* Dynamics of Oceans and Atmospheres, (2006), In press.
- [12] Khouider B. and A. J. Majda, *Multicloud convective parametrizations with crude vertical structure.* Theoretical and Computational Fluid Dynamics, (2006), In press.
- [13] Lindzen, R. S., *Wave-CISK in the tropics,* J. Atmos. Sci., **31**, (1974), 156–179.
- [14] Lin, X. and R. H. Johnson *Kinematic and thermodynamic characteristics of the flow over the Western Pacific Warm Pool during TOGA COARE.* J. Atmos. Sci., **53**, (1996), 695–715.
- [15] Majda, A. J., B. Khouider, G.N. Kiladis, K. H. Straub, and M. G. Shefter, *A model for convectively coupled tropical waves: Nonlinearity, rotation, and comparison with observations,* J. Atmos. Sci., **61**, (2004), 2188–2205.
- [16] Majda, A. J. and M. Shefter, *Models for stratiform instability and convectively coupled waves.* J. Atmos. Sci., **58**, (2001), 1567-1584.
- [17] Mapes, B. E., *Convective inhibition, subgridscale triggering energy, and “stratiform instability” in a toy tropical wave model.* J. Atmos. Sci., **57**, (2000), 1515-1535.

- [18] Nakazawa, T., *Tropical super clusters within intraseasonal variations over the western Pacific*. J. Meteor. Soc. Japan, **66**, (1988), 823-839.
- [19] Neelin J. D., and N. Zeng, *A quasi-equilibrium tropical circulation model-formulation*. J. Atmos. Sci., **57**, (2000), 1741-1766.
- [20] Wheeler, M., and G. N. Kiladis, *Convectively coupled equatorial waves: Analysis of clouds and temperature in the wavenumber-frequency domain*. J. Atmos. Sci., **56**, (1999), 374-399.
- [21] Wheeler, M., G. N. Kiladis, and P. J. Webster, *Large scale dynamical fields associated with convectively coupled equatorial waves*. J. Atmos. Sci., **57**, (2000), 613-640.
- [22] Yamasaki, M., *Large-scale disturbances in a conditionally unstable atmosphere in low latitudes*. Pap. Meteor. Geophys., **20**, (1969), 289–336

**Meridional momentum flux and superrotation in the multi-scale
IPESD MJO model**

JOSEPH A. BIELLO

(joint work with Andrew J. Majda, Mitch W. Moncrieff)

We present the derivation of the meridional momentum flux arising from a multi-scale horizontal velocity field in the IPESD multi-scale models of the equatorial troposphere [8, 3]. It is shown that, due to the balance dynamics on the synoptic scales, the synoptic scale component of the meridional momentum flux convergence must always vanish at the equator. Plausible MJO models are presented along with their planetary scale meridional momentum fluxes. These models are driven by synoptic scale heating fluctuations that have vertical and meridional tilts. Irrespective of the sign of the synoptic scale meridional momentum flux (direction of the tilts) in each of the four MJO examples, the zonal and vertical mean meridional momentum flux convergence from the planetary scales always drives westerly winds near the equator: this is the superrotation characteristic of actual MJOs. Since there is an analytic expression of the upscale flux in the IPESD model, we are able to analytically demonstrate that equatorial superrotation occurs when the planetary flow due to the vertical upscale momentum flux from synoptic scales reinforces the horizontally convergent flow due to planetary scale mean heating.

We are interested in the zonal mean of the zonal momentum flux vector due to the *total* flow from all scales in our multi-scale theory,

$$(1) \quad \left\langle \vec{F}^U \right\rangle = -\frac{1}{C_E} \int_0^{C_E} \left[(uv) \hat{j} + (uw) \hat{k} \right] dx.$$

The ansatz of the IPESD model is that the velocities can be separated into their zonal planetary scale means plus synoptic scale fluctuations. In the model, the zonal velocity has a mean which is comparable to its fluctuations whereas the planetary scale means of the vertical and meridional velocities are small compared to their synoptic scale fluctuations. It is the synoptic scale mean of the flux

convergences which drive planetary scale motion. Using primes to denote the fluctuations and overbars to denote means, we find

$$(2) \quad \langle \vec{F}^U \rangle = -\frac{1}{C_*} \int_0^{C_*} \left\{ [(\overline{u'v'}) + \epsilon (\overline{U}\overline{V})] \hat{j} + [(\overline{u'w'}) + \epsilon (\overline{U}\overline{W})] \hat{k} \right\} dX.$$

There are two contributions to each component of the flux; one from each of the planetary and synoptic scales. Due to the IPESD scaling of the planetary mean vertical and meridional flow, both vertical and meridional fluxes are dominated (at least formally) by their synoptic scale fluctuations: the planetary mean contribution is weaker by a factor of ϵ .

In the MJO models [1, 2, 3] the synoptic scale fluctuations themselves are concentrated in a moving envelope of convective activity which only covers 10000 km longitudinally whereas the planetary scale response is global. Therefore it is not clear whether which component of the flux dominates the planetary scale mean. In fact, we show in [3] that the relative contribution of these two components depends on the details of the synoptic scale flow in a variety of examples, all of which give a plausible structure for the MJO. Furthermore equatorial superrotation arises in all four MJO models irrespective of the synoptic scale meridional tilt.

It is natural to inquire as to which property of the planetary scale flow causes this superrotation. Using a Helmholtz-Hodge-Weyl decomposition in a purely first baroclinic analytic example, we can express the horizontal velocity as

$$(3) \quad \begin{aligned} U &= -\Psi_y + \Phi_x \\ V &= \Psi_x + \Phi_y \end{aligned}$$

where Ψ expresses purely rotational motion in the plane and Φ describes horizontally divergent flow; this arises vertical component of the circulation through incompressibility. The flow is convergent at the base of the troposphere if $w_z > 0$ yielding a potential which is negatively curved, for example, $\Phi = \Phi_0 e^{-(x^2+y^2)/2}$ with $\Phi_0 > 0$. Considering flows which are symmetric about the origin further requires that Ψ be anti-symmetric; $\Psi = -\Psi_0 y e^{-((x-x_0)^2+y^2)/2}$ with $\Psi_0 > 0$ describes equatorially symmetric pair of cyclonic gyres, zonally shifted with respect to the potential flow. It is a straightforward calculation to show that, for small values of the shift in this simple example, the zonal mean meridional momentum flux is

$$(4) \quad \overline{\langle UV \rangle} \propto -y\Psi_0 \Phi_0 e^{-y^2/2}$$

near $y = 0$, which is to say that only the correlation of rotation and convergence contribute to this flux. Because of the assumed separability of the rotational and convergent components of the flow, the other terms in the fluxes due to rotational/rotational and convergent/convergent velocity correlations vanish. Though this is not the most general flow possible, it does highlight an important fact: equatorial superrotation is a result of the correlation of convergent and vortical components of the flow in the horizontal plane. In particular, both cyclonic/ lower troposphere convergent flow and anti-cyclonic/lower troposphere divergent flow drive equatorial westerlies.

The next question we pose is, what are the necessary features of the planetary scale heating and upscale momentum flux which create equatorial superrotation? Since equatorial superrotation occurs even in the canonical model of vertically tilted superclusters and congestus heating (the first example), it is sufficient to consider zonal momentum forcing due to vertical upscale flux and planetary scale heating alone: the upscale temperature flux in the canonical model is extremely small near the equator.

In order to get a closed form analytic expression for the upscale flux, we approximate the IPESD long wave equations [1, 8] using undissipated, balanced dynamics [3]. Focusing on the first baroclinic mode, the direct heating is symmetric about the center of the envelope whereas the upscale momentum flux is antisymmetric and a simple form for these functions is

$$(5) \quad S^\theta = S \cos(x/2) e^{-y^2/2}, \quad F^U = -F \sin(x) e^{-y^2/2}$$

where $S, F > 0$ in the canonical model. It is an elementary calculation to show that the lowest order y -dependence of the zonal mean meridional momentum flux is

$$(6) \quad \overline{UV} \propto -y S F e^{-y^2}.$$

Therefore, when $S F > 0$, the meridional momentum flux is convergent at the equator and drives a mean westerly wind. Clearly, equation (6) implies that if either the upscale momentum flux from the synoptic scales or the planetary scale mean heating vanish, then there is no meridional flux of zonal momentum near the equator. However, in the canonical MJO model [1, 3] the zonal momentum flux convergence at the base of the troposphere, F^U , drives westerlies in the western half of the envelope and easterlies in the eastern half of the envelope. The planetary scale mean heating forces a horizontal convergence at the base of the troposphere, also driving westerlies in the western half of the envelope and easterlies in the eastern half. Therefore, the flow associated with the zonal momentum and mean heating reinforce one another and this is the source of the superrotation.

REFERENCES

- [1] Biello, J.A. and A.J. Majda, 2005: A new multi-scale model for the Madden-Julian Oscillation. *J. Atmos. Sci.*, **62**, 1694–1721.
- [2] Biello, J.A. and A.J. Majda, 2006: Modulating synoptic scale convective activity and boundary layer dissipation in the IPESD models of the Madden-Julian Oscillation. *Dynam. Atmos. Oceans* (in press).
- [3] Biello, J.A., A.J. Majda and M.W. Moncrieff, 2006: Meridional momentum flux and superrotation in the multi-scale IPESD MJO model. *J. Atmos. Sci.* (in press).
- [4] Hendon, H. and B. Leibmann, 1994: Organization of convection within the Madden-Julian Oscillation. *J. Geophys. Res.*, **99**, 8073–8083.
- [5] Hendon, H. and M. Salby, 1994: The life cycle of the Madden-Julian Oscillation. *J. Atmos. Sci.*, **51**, 2225–2237.

- [6] Johnson, R.H. and X. Lin, 1997: Episodic trade wind regimes over the Western Pacific Convective Envelope. *J. Atmos. Sci.*, **54**, 2020–2034.
- [7] Kiladis, G., K.H. Straub and P.T. Haertel, 2005: Zonal and vertical structure of the Madden-Julian Oscillation. *J. Atmos. Sci.*, **62**, 2790–2809.
- [8] Majda, A.J. and R. Klein, 2003: Systematic multi-scale models for the tropics. *J. Atmos. Sci.*, **60**, 393–408.
- [9] Moncrieff, M., 2004: Analytic Representation of the Large-scale Organization of Tropical Convection. *J. Atmos. Sci.*, **61**, 1521–1538.
- [10] Nakazawa, T., 1988: Tropical super clusters within intraseasonal variations over the western pacific. *J. Meteor. Soc. Japan*, **66**, 823–839.
- [11] Wang, B., 2005: *Intraseasonal Variability in the Atmosphere-Ocean System*, Ch 10., “Theory”, W.K. Lau, & D.E. Waliser (eds.), Praxis Publishing Ltd.
- [12] Weickmann, K. M., G. N. Kiladis, and P.D. Shardeshmukh, 1997: The dynamics of intraseasonal angular momentum oscillations. *J. Atmos. Sci.*, **54**, 1445–1461.
- [13] Zhang, C.D., 2005: Madden-Julian Oscillation. *Rev. Geophys.*, **43**, Art. # RG2003.

Statistical flow equations applied to atmospheric circulations

JOSEPH EGGER

Modern analysis projects make global data sets available which cover more than forty years at fairly high spatial and temporal resolution. This allows one to step forward from case studies to a statistical analysis of flow evolutions. To fix ideas we will deal only with flows affected by mountains. A parameter has to be found which captures the interaction of the flow with a mountain massif. The flow observations are then regressed against this parameter. To explain the resulting fields, basic equations of dynamic meteorology are transformed in a statistical form suited to this regression procedure. In particular, the vorticity and the potential temperature turn out to be helpful where statistical trajectories are calculated.

At the moment, the only type of interaction parameters used are the components of the mountain torque exerted by a selected mountain massif. This torque represents essentially the difference of the surface pressure across the mountain. There is essentially one torque per standard direction. Regressions against this parameter are performed for the three-dimensional wind field, for the vorticity and the divergence, for potential temperature, for humidity and precipitation as well as for selected transports.

Applications for these techniques to Greenland are described in Egger and Hoinka (2006: Dynamics of atmospheric regression patterns: regional mountain torque events; *J. Atmos. Sci.*; in print) where it is shown that the dynamics of the flow evolution are captured astonishingly well by the statistical vorticity equation provided the ‘turbulent fluxes’ are included as observed.

Further work will address the issue of topographic instability. Although many corresponding theories have been published tests are lacking so far. The framework described above is ideally suited for such tests.

It is also planned to apply these methods to the circulations near the Tibetan Plateau where moisture effects are more important than near Greenland. Finally work on perturbations in the Mediterranean is under way where again mountain torques exerted by the Alps and other prominent features of the Mediterranean topography will be used as parameters.

Reduced Models of Tropospheric Planetary Waves

GRANT BRANSTATOR

One would think that there is the potential to represent the statistical behavior of atmospheric planetary-scale disturbances on longer than synoptic timescales by a highly reduced system. After all, a very large fraction of atmospheric low-frequency variability can be represented by just a few structures. But data analysis shows that the problem is not that simple; these large-scale, low-frequency disturbances are profoundly affected by rectified effects of smaller scale synoptic disturbances that have high-frequencies. It turns out, however, that in spite of this being a multi-scale problem, there are two good reasons to believe that a highly reduced representation of the system is in fact possible.

The first reason is that, in a statistical sense, the high-frequency disturbances are strongly slaved to the low-frequency disturbances. This means that the statistics of high-frequency disturbances and the fluxes that result from them and feedback onto the low-frequencies are potentially a well-defined function of the low-frequency state. The second reason for optimism is that synoptic perturbations react to low-frequency disturbances on very fast time-scales. This means that if one is formulating a reduced model of the low-frequency planetary waves, it is reasonable to assume that for a time-step of a couple of days the reaction of the statistics of the synoptic disturbances is instantaneous. Moreover, data analysis of tendencies in reduced spaces indicates that time-steps of this length are sufficiently short to resolve the important dynamics of the system. Of special importance is that time-steps of this length are sufficient to resolve nonlinearities that appear to be crucial for creation of nonGaussian features in PDFs of the leading planetary wave structures (Branstator and Berner, 2005).

As a means of determining the potential of highly reduced models to well-approximate the statistical behavior of prominent tropospheric disturbances and for learning about the factors that such models must include to be successful, we have constructed a reduced model that should capture all of the dynamics that are potentially representable in a reduce system. The procedure used to construct this model requires a very long record of the behavior of the full system. For this reason we have set as our goal the construction of a reduced model of the prominent planetary wave disturbances in an atmospheric general circulation model (AGCM)

that has been integrated for four million days of perpetual January. This AGCM has over 18000 spatial degrees of freedom, so finding a low-dimensional counterpart is not a trivial undertaking. As reported by Branstator and Berner (2005), Berner (2005) and Berner and Branstator (2006), amplitudes of the leading patterns of the midtropospheric state in this AGCM, as given by empirical orthogonal function analysis of 500 hPa geopotential heights, have autocorrelations that decay to $1/e$ for lags in the one to two week range. And in some planes defined by these EOFs, the joint PDFs of these pattern amplitudes have distinctly nonGaussian, though not multimodal, features consisting of radial ridges of enhanced probability. It is these two characteristics that we are interested in capturing in a reduced model. Specifically, for the purposes of this report, we focus on these characteristics for amplitudes of EOFs 1 and 3 because in this plane the nonGaussianity is prominent and because these patterns have counterparts in nature. EOF1 is similar to the Northern Annular Mode (Thompson and Wallace, 1998) and EOF3 is a commonly observed high latitude zonal wave two pattern.

Our reduced model is based on analogs. In this model, the state of the system is defined by a low-dimensional vector representing the large-scale planetary waves of the AGCM. To begin with we assume this low-dimensional state consists of only the two directions we are interested in, namely EOFs 1 and 3. To form a dynamical model we need to associate any low-dimensional state with a low-dimensional tendency in order to advance the system forward in time. (In the case we have investigated we have used a discrete representation of time, so stated more carefully, we need to associate any given low-dimensional state with a temporal increment.) The function we use to map a given low-dimensional state into an increment is based on finding a full-dimensional state from the AGCM trajectory whose projection onto the low-dimensional state is as close to the given low-dimensional state as possible. We then apply the increment that actually occurred in the AGCM to advance the reduced model in time. Since the AGCM trajectory is affected by all of the degrees of freedom of that model, this procedure incorporates the unresolved scales into the dynamics of the reduced model. Indeed, when we carry out this procedure with a time step of 72 hours we find that both in terms of lag correlations and PDFs the reduced model acts in a manner that is very similar to the AGCM. Hence we conclude that it is possible to construct a reduced model with dimension as small as two for the AGCM.

Though the analog marching procedure demonstrates that reduced models of planetary wave patterns can be constructed, the model that results is not defined in a compact form. Indeed, it takes 8 million parameters to describe this model. Furthermore there is a certain ambiguity in the definition in that for any given state there are actually very many potential increments that are suggested by the AGCM trajectory, because there are many AGCM high-dimensional states all with very similar projections onto the reduced space but with very different low-dimensional temporal increments. Of course the increments for these various analogs differ because the states need not be similar in the directions not resolved in the low-dimensional system. However, experimentation with the analog model

demonstrates that the statistics of its trajectory is independent of which of these similar states is picked at any particular time step. So apparently what is important are statistical attributes of increments of those states that have a specified two-dimensional projection, not the increments of any one particular state.

As a step toward replacing the analog reduced model with a reduced model that can be described using far fewer parameters we explore what are the important characteristics of temporal increments associated with full-dimensional states that have similar low-dimensional projections. It turns out that such states have a small, but non-negligible mean that is a function of the low-dimensional state. We also find that dispersion of increments about this mean is well approximated by Gaussian distributions and that these distributions are a function of the low-dimensional state. Thus we can produce a reduced model that is nearly as effective as the analog-based model by drawing temporal increments from these Gaussian distributions and adding them to the low-dimensional state dependent mean increment.

As a final step in the simplification process we test how important it is to take into account the low-dimensional state dependence of the temporal increments. We find that the state dependence of the mean increments is crucial while the state dependence of the distributions, though making noticeable contributions to the behavior of the reduced model, is of less importance. A third aspect of the statistics of increments that is very important is a strong anisotropy that is present in their distributions. Reduced models formed in such a way as to ignore this anisotropy do not produce one of the most distinct nonGaussian features in the joint PDF. However, further analysis of the situation reveals that this anisotropy can be traced to an oscillation in a plane that is orthogonal to the plane of the reduced model. This oscillation was found by Selten and Branstator (2005) in this same AGCM dataset and is similar to an oscillation found in nature (Branstator, 1987). Interestingly, rather than account for it via incorporating anisotropy into the distributions from which temporal increments are drawn, it can also be represented simply by adding a third dimension to the reduced model.

The implications of these calculations is that it is possible to represent key aspects of the statistics of prominent planetary wave patterns in a highly reduce model with just a few parameters. These parameters represent the state dependence of the statistics of tendencies in the reduced space in terms of a state-dependent deterministic tendency and a Gaussian distribution of increments about that tendency. In additional calculations we have found that it is adequate to represent the state-dependence of the deterministic component in terms of a small basis set of sigmoid functions fit using neural net methodologies. It is likely that the state dependence of parameters defining the state dependence of tendency distributions can be approximated in a similar fashion.

Though in our work we have formulated and analyzed the system in terms of temporal increments found from analogs, it is obvious our results can be interpreted and described in the more commonly used language of stochastic models. In this framework what we have done is construct a low-dimensional Langevin

model in which the drift term for a given low-dimensional state is found as the average of temporal increments from the full system for all states whose projections match the given low-dimensional state. And the noise term in the Langevin model comes from a Gaussian fit to the distribution of temporal increments associated with those same states. From this standpoint, the results we have described lead to a Langevin counterpart to Siegert et al.'s (1998) procedure for fitting a Fokker-Planck equation to the data from a system.

REFERENCES

- [1] J. Berner, *Linking nonlinearity and non-gaussianity of planetary wave behavior by the Fokker-Planck equation*, J. Atmos. Sci. **62** (2005), 2098-2117.
- [2] J. Berner and G. Branstator, *Linear and nonlinear signatures in the planetary wave dynamics of an AGCM: Probability density functions*, to appear in J. Atmos. Sci. (2006).
- [3] G. Branstator and J. Berner, *Linear and nonlinear signatures in the planetary wave dynamics of an AGCM: Phase space tendencies*, J. Atmos. Sci. **62** (2005), 1792-1811.
- [4] S. Siegert, R. Friedrich, and J. Peinke, *Analysis of data sets of stochastic systems*, Physics Letters A **243** (1998), 275-280.
- [5] D. Thompson, and J. Wallace, *The Arctic Oscillation signature in the wintertime geopotential height and temperature fields*, Geophys. Res. Lett. **25** (1998), 1297-1300.

On the nature of zonal jet EOFs

ADAM H. MONAHAN

(joint work with John C. Fyfe)

Analytic results are obtained for the mean and covariance structure of an idealised jet in zonal-mean zonal wind $u(\phi, t)$ which fluctuates in strength ($U(t)$), position ($\lambda(t)$), and width ($\sigma(t)$):

$$(1) \quad u(\phi, t) = U(t) \exp\left(-\frac{(\phi - \phi_0 - \lambda(t))^2}{2\sigma^2(t)}\right).$$

Through a systematic perturbation analysis, the leading spatial pattern (EOF) and time series (PC) of an Empirical Orthogonal Function analysis (also known as Principal Component Analysis or Proper Orthogonal Decomposition) are obtained. These EOFs are built up of linear combinations of basic patterns corresponding to monopole, dipole, and tripole structures:

$$(2) \quad f_n(\phi) = \frac{1}{\sqrt{\sigma_0 2^n \Gamma(n + 1/2)}} H_n\left(\frac{\phi - \phi_0}{\sqrt{2}\sigma_0}\right) \exp\left(-\frac{(\phi - \phi_0)^2}{2\sigma_0^2}\right)$$

($n = 0, 1, 2$, where σ_0 is the mean of $\sigma(t)$). The analytic results demonstrate that in general the individual EOF modes cannot be interpreted in terms of individual physical processes. In particular, while the dipole EOF (similar to the leading

EOF of the midlatitude zonal mean zonal wind, known as the zonal index) describes fluctuations in jet position to leading order, its time series also contains contributions from fluctuations in strength and width. No simple interpretations of the other EOFs in terms of strength, position, or width fluctuations are possible.

Results are extended to the EOF structure of geopotential $\Phi(\phi, t)$ through the imposition of geostrophic balance and mass conservation

$$(3) \quad \Phi(\phi, t) = - \int_{\phi_1}^{\phi} f(\phi') u(\phi', t) d\phi' + \int_{\phi_1}^{\phi_2} \mu(\phi) \int_{\phi_1}^{\phi} f(\phi') u(\phi', t) d\phi' d\phi$$

where $f(\phi)$ is the Coriolis parameter and $\mu(\phi)$ is a geometrical weighting function. When sphericity of the domain is accounted for in $f(\phi)$ and $\mu(\phi)$, the leading EOF of $\Phi(\phi, t)$ is in excellent agreement with that of observations; the associated time series is correlated with both jet position and width, and with the first and third PC time series of $u(\phi, t)$. The annular mode is therefore not associated with a single jet degree of freedom, and is not simply the manifestation in geopotential of variability associated with the zonal index. On a flat domain, analytic results are available; these demonstrate that the EOFs of geopotential are much more sensitive to the analysis domain than are the EOFs of zonal-mean zonal wind.

REFERENCES

- [1] E. Gerber and G. Vallis, *A stochastic model for the spatial structure of annular patterns of variability and the North Atlantic Oscillation*, J. Climate **18** (2005), 2102-2118.
- [2] A. Monahan and J. Fyfe, *On the nature of zonal jet EOFs*, J. Climate **in press** (2006).
- [3] A. Monahan and J. Fyfe, *On annular modes and zonal jets*, in preparation.
- [4] M. Wittman, A. Charlton, and L. Polvani, *On the meridional structure of annular modes*, J. Climate **18** (2005), 2199-2222.
- [5] G. Vallis, E. Gerber, P. Kushner, and B. Cash, *A mechanism and simple dynamical model of the North Atlantic Oscillation and annular modes*, J. Atmos. Sci., **61**, 264-280.

Stable Time Filtering of Strongly Unstable Spatially Extended Systems

MARCUS J. GROTE

(joint work with Andrew J. Majda)

Many contemporary problems in science ranging from protein folding in molecular dynamics to scale up of small scale effects in nanotechnology to making accurate predictions of the coupled atmosphere-ocean system involve partial observations of extremely complicated systems with many degrees of freedom. Novel mathematical issues arise in the attempt to quantify the behavior of such complex multi-scale systems [1, 2]. For example, in the coupled atmosphere-ocean system,

the current practical models for prediction of both weather and climate involve general circulation models where the physical equations for these extremely complex flows are discretized in space and time and the effects of unresolved processes are parametrized according to various recipes; the result of this process involves a model for the prediction of weather and climate from partial observations of an extremely unstable, chaotic dynamical system with several billion degrees of freedom. The nature of the physical instabilities which strongly affect the predictive properties of this system range from A) comparatively low dimensional large scale instabilities involving synoptic scale weather activity to B) inherently statistical instabilities on shorter spatio-temporal scales such as those involving moist convection which crucially affects the water vapor in the atmosphere and rainfall.

Bayesian hierarchical modeling [3] and reduced order filtering strategies [4, 5, 6, 7, 8, 9, 10, 11] have been developed with some success in these extremely complex systems including the role of observations in tracking the instabilities of type A). The basis for such dynamic prediction strategies for the complex spatially extended systems is the classical Kalman filtering algorithm [12, 13, 14, 15]. New issues arise in the practical application of these filtering strategies to complex spatially extended systems and this is the focus for the present contribution.

One new mathematical issue that emerges is the following one: ensemble filtering requires multiple realizations of an extremely expensive dynamical system with many degrees of freedom; with these practical limitations, it is extremely interesting to see whether it is possible to utilize large time steps which violate the classical CFL-stability condition for an explicit difference scheme [16] and, nevertheless, obtain stable and statistically accurate filtering. Such counter-intuitive behavior has emerged in recent practical applications [7, 3, 8] without documentation or mathematical understanding of this potentially practically important phenomenon.

Our present work [17] is devoted to elucidating this phenomenon as well as the emerging reduced order filtering strategies for tracking physical instabilities of types A) and B) mentioned earlier. First, some elementary mathematical theorems are developed to supply a context and justification for the possibility for various types of stable filtering strategies for strongly unstable systems. Then, these mathematical results are utilized as guidelines for a detailed investigation of the key issue raised at the beginning of this paragraph for a prototype model involving an unstable finite difference approximation for a convection-diffusion equation.

REFERENCES

- [1] Majda, A. & Wang, X., *Nonlinear Dynamics and Statistical Theories for Basic Geophysical Flow*, Cambridge Univ. Press, New York, 2005.
- [2] Majda, A., Abramov, R., & Grote, M. J., *Information Theory and Stochastics for Multi-scale Nonlinear Systems*, Amer. Math. Society, Providence, 2005.
- [3] Berliner, L. M., Milliff, R. E., & Wikle, C. K., *J. Geophys. Res.* **108** (2003), 3104–3120.
- [4] Miller, R., Carter, E., & Blue, S., *Tellus* **51** (1999), 167–194.
- [5] Ghil, M. & Malanotte-Rizzoli, P., *Adv. Geophys.* **33** (1991), 141–266.

- [6] Todling, R. & Ghil, M., *Mon. Weather Rev.* **122** (1994), 183–204.
- [7] Anderson, J. L., *Mon. Weather Rev.* **129** (2001), 2884–2903.
- [8] Anderson, J. L., *Mon. Weather Rev.* **131** (2003), 634–642.
- [9] Farrell, B. & Ioannou, P., *J. Atmos. Sci.* **58** (2001), 3666–3680.
- [10] Farrell, B. & Ioannou, P., *J. Atmos. Sci.* **62** (2005), 460–475.
- [11] Ott, E., Hunt, B., Szunyogh, I., Zimin, A., Kostelich, E., Corrazza, M., Kalnay, E., & Yorke, J., *Tellus* **56A** (2004), 415–428.
- [12] Chui, C. K. & Chen, G., *Kalman Filtering*, Springer, Berlin, 1987.
- [13] Jazwinski, A., *Stochastic Processes and Filtering Theory*, Academic Press, New York, 1970.
- [14] Kiapio, J. & Somersalo, E., *Statistical and Computational Inverse Problems*, Springer Verlag, New York, 2005.
- [15] Cohn, S. & Dee, D., *SIAM J. Num. Anal.* **25** (1988), 586–617.
- [16] Richtmeyer, R. & Morton, K. W., *Difference Methods for Initial-Value Problems*, Wiley-Interscience, New York, 1967.
- [17] Grote, M. J. & Majda, A. J., *Proc. Natl. Acad. Sci. USA* **103** (2006), 7548–7553.

Nonlinear dynamics in the semi-transparent equatorial waveguide.

Part 1. Resonant excitation of Rossby and Yanai waves and their interactions

VLADIMIR ZEITLIN

(joint work with G.M. Reznik)

With the help of multi time- and space- scale asymptotic expansions applied to the weakly nonlinear perturbations in the framework of the two- layer rotating shallow water model in the equatorial tangent plane we study the interactions between the baroclinic Rossby and/or Yanai waves trapped in the equatorial waveguide (e.g. [1]) and the barotropic Rossby waves freely propagating across the equator. We demonstrate that, depending on its parameters, a barotropic wave can resonantly excite a single, or a pair of baroclinic waves with frequencies lower than its proper one. This process, hence, is of the parametric resonance type. We show that nonlinear saturation of the amplitudes of the baroclinic waves at the level much greater than the amplitude of the barotropic wave takes place. The envelopes of the baroclinic waves obey the modulation equations of the Ginzburg - Landau type. Formation of characteristic "domain wall" and "dark soliton" patterns in the envelopes of the baroclinic waves is displayed [2]. The growing trapped waves also generate a barotropic response modifying the primary barotropic wave.

The physical picture arising from our results is as follows. In the linear approximation the equatorial wave-guide is transparent for the barotropic Rossby waves. Due to nonlinear effects, the barotropic wave resonantly excites, for instance from the pre-existing noise, a pair of the baroclinic wave-guide modes with exponentially growing amplitudes. This process may be alternatively seen as a destabilisation of a given barotropic wave by baroclinic equatorial perturbations.

The process is generic as the unstable in this sense barotropic waves are dense in the phase-space. A given barotropic wave generally excites a pair of the baroclinic waves, although the cases of excitation of a single baroclinic mode, or of two pairs of baroclinic modes are possible. The case of a single mode corresponds to pure parametric resonance, when the excited mode has time and space periods twice the periods of the initial barotropic wave.

The nonlinear stage of this instability is as follows. The interacting baroclinic waves give rise to an exponentially growing secondary barotropic mode. This mode has the form of reflected and transmitted wave structures spreading with time out of the equator. Its interaction with the baroclinic modes arrests the growth of these latter. The amplitudes of the excited baroclinic waves are thus gradually saturated. The saturation, however, is not stationary in the general case, as saturated amplitudes continue to oscillate slowly with frequencies depending on the constant amplitude moduli. The saturation is stationary only in the pure parametric resonance case. A general tendency observed by calculating typical increments and saturation levels is that two waves saturate at considerably different values, the saturation level of longer wave being higher.

When the effects of spatial modulation are taken into account, a Ginzburg - Landau type equation arises in the parametric resonance case with solutions exhibiting characteristic domain-wall like phase defects and "dark soliton" structures. In the general case of a pair of waves a hyperbolic system of coupled nonlinear equations arises, with the behaviour predicted by the non-modulated equations in the domain of influence of initial conditions modified by possible shock formation.

We believe that the behaviour we displayed is generic for semi-transparent wave-guides, although the only example treated in literature we are aware of is the beach edge waves. These waves trapped near the shore may be resonantly excited by the waves coming on-shore from the open ocean [3], [4]. Although the scales, the physics of the system, and the dispersion properties of the waves are very different from the equatorial waves, the resulting modulation equations are close. However they were not, as to our knowledge, exhaustively studied.

REFERENCES

- [1] Gill, A.E., 1982, *Atmosphere - ocean dynamics*, AP.
- [2] Reznik, G.M., and Zeitlin, V., 2006, Phys.Rev. Lett., **96**, 034502.
- [3] Minzoni A.A., and Whitham G.B., 1977, J. Fluid Mech. **79**, 273.
- [4] Akylas, T.R. , 1983, J. Fluid Mech., **132**, 197.

A coarse graining approach to quantifying mixing in stratified flows

ESTEBAN G. TABAK

(joint work with Paul A. Milewski, Fabio A. Tal)

Quantifying mixing among fluid layers with different properties is crucial for modeling climate dynamics. Yet obtaining such quantification is a difficult task: one is typically interested in fluid masses that extend over at least hundreds of kilometers horizontally and a few kilometers in the vertical, while the physical processes involved in mixing take place at scales smaller than a millimeter. In order to bridge this gap, one needs to find a way to parameterize the full cascade of “turbulent” fluid motion occupying many decades of unresolved scales.

In this talk, an alternative way of modeling mixing is described, reminiscent of statistical physics. In this approach, one defines an “entropy” associated with the degree of mixing of a flow, and attempts to maximize this entropy, subject to the constraints provided by the large-scale equations of motion (see Figure 1).

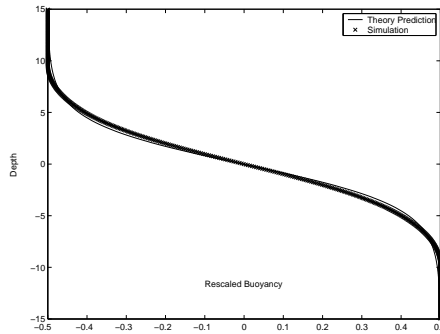


FIGURE 1. Buoyancy profile resulting from the mixing of two initially distinct layers, subject to an injection of turbulent energy at their interface. The two profiles displayed correspond to the theoretical prediction based on maximal mixing, and the actual numerical results following the dynamics of a turbulent diffusive model.

We have applied this scheme to diapycnal mixing in two scenarios: the localized mixing driven by stirring at the horizontal interface between two semi-infinite fluid layers of different density [2], and the entrainment of ambient fluid into mixed layers through breaking waves [1].

REFERENCES

- [1] T. Jacobson, P. A. Milewski and E. G. Tabak, *A closure for mixing at internal breaking waves*, submitted to Journal of Fluid Mech. (2006).
- [2] E. G. Tabak and F. A. Tal, *Mixing in simple models for turbulent diffusion*, CPAM, **57** (2004), 1–27.

Stability, Breaking Waves, and Mixing in Stratified Flows

PAUL A MILEWSKI

(joint work with Ruben R. Rosales, Esteban G. Tabak, Cristina Turner)

The shallow water or hydraulic limit for wave propagation and breaking in one layer is well understood. The problem is well posed, and arbitrary initial data form shocks. There, integral formulations of conservation of mass and momentum completely define the jump, and the energy equation gives, a posteriori, the rate at which large scale energy is lost and "internal" energy (mostly in the form of small scale turbulence) is generated. For the case of two-layer shallow water, bounded above and below by horizontal walls, the equations for the lower layer height and velocity are given by

$$\begin{aligned} h_t + (hu)_x &= 0 \\ u_t + \frac{1-3h}{1-h}uu_x + \left((1-h) - \frac{1}{(1-h)^2}u^2 \right) h_x &= 0. \end{aligned}$$

Even though the system has been derived before, the evolution of smooth solutions was not completely understood since there is the possibility for the system to be elliptic, leading to ill-posedness. The condition for hyperbolicity, in dimensional variables is

$$g \frac{(\Delta\rho/\rho)/(h_1 + h_2)}{(u_1/h_2)^2} = Ri > 1$$

The ellipticity in the system, is present for strong shear and is a remnant of the Kelvin-Helmholtz instability. We first show that these flows are nonlinearly stable for Richardson number greater than unity. That is, solutions from smooth initial data with $Ri > 1$ everywhere never cross the sonic surface into the elliptic domain, at least until breaking. (Reasonable jump conditions will also preclude instabilities after breaking.) An illustration of the dynamics is in Figure 1.

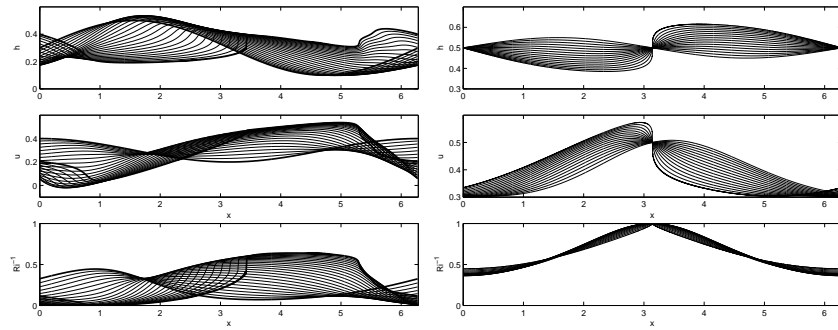


FIGURE 1. Computation of h , u , Ri^{-1} for the two-layer flow until breaking. The figure on the left depicts the wave regime and the figure on the right shows that when $Ri = 1$ at one point, the solution is reminiscent of Kelvin-Helmholtz rolls there.

The proof of the stability is based on writing the system in terms of Riemann Invariants and showing that, since the characteristic speeds are smooth functions of the Riemann invariants on the sonic curve, the elliptic region is unattainable. Preliminary results indicate that for more layers, the dynamics can cross the sonic surface and waves can dynamically give rise to Kelvin-Helmholtz instabilities.

Next, we consider shocks at the interface of miscible fluids in a simpler one-and-a-half layer system shown in Figure 2. We assume all mixing occurs at shocks, through the turbulent entrainment of upper fluid into the lower layer. Even in its simplicity, this scenario is realistic for many flows of geophysical significance [1], such as dense overflows over sills.

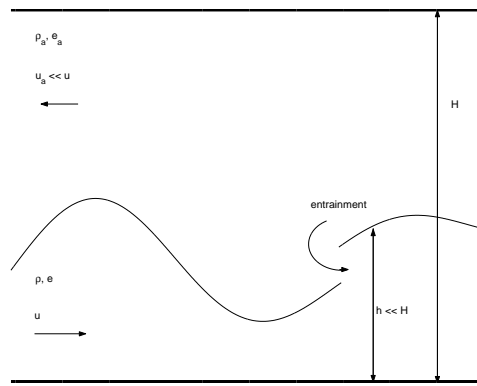


FIGURE 2. Two-layer flow with entraining internal hydraulic jump

The problem is governed by the following system of equations of conservation of mass, momentum and energy for the height h , velocity u , buoyancy b and internal turbulent energy e of the layer:

$$(bh)_t + (bhu)_x = 0$$

$$(hu)_t + \left(hu^2 + \frac{bh^2}{2} \right)_x = 0$$

$$\left(\frac{hu^2}{2} + \frac{bh^2}{2} + he \right)_t + \left(\frac{hu^3}{2} + bh^2u + heu \right)_x = 0.$$

To close this problem we require an additional equation. Focussing on the shock one can imagine that the energy dissipated can flow into small scale turbulence or into mixing the fluid (which takes work to raise heavy fluid). The partition between these sinks of macroscopic energy is unknown.

We propose a closure which maximizes the amount of entrainment and mixing (subject to the constraint that energy is dissipated, and that the Lax condition is satisfied). This condition is given in terms of the shock speed and not as an

additional conservation law. For the system above, for a shock in the right-going characteristic the shock speed is:

$$c = u_+ - \sqrt{b_+ h_+}.$$

In related work presented by E. Tabak, this closure is justified in terms of entropy production.

REFERENCES

- [1] J. Nash, J. Moun *Internal hydraulic flows on the continental shelf: High drag states over a small bank*, J. Geophys. Res. **106** (2001), 4593-4612.

Shallow layers of non-precipitating cumulus convection

BJORN STEVENS

(joint work with Brian Medeiros)

The representation of clouds has long been recognized as a weak link in attempts to model the climate system and how it might change with changing atmospheric composition. More than 30 years ago Arakawa [1] wrote that

the modelling of time dependent clouds is perhaps the weakest aspect of the existing general circulation models and may be the most difficult task in constructing any reliable climate model.

Subsequent reports by governmental and intergovernmental panels [5, 3] echoed, and even amplified, his view. To this day the representation of clouds contribute the most uncertainty to our representation of short term (a hundred years or less) climate change.

More recent work [2] suggests that among the varied cloud regimes, shallow cumulus layers (as are often found in regions of large-scale subsidence) contribute most strongly to the different predictions of climate change by general circulation models. Calculations by our group show that differences among models are well reproduced even in much simplified planetary geometries, such as for planets with specified zonally and hemispherically symmetric sea-surface temperatures, no land surface, or sea-ice; suggesting that such differences are robust to modest changes in atmospheric circulation [4]. The inference being that differences in the representation of how clouds change in a changing climate embody the tendencies of different representations (sub-grid models) of clouds to behave differently for a given change in the large-scale thermodynamic environment in which the clouds are embedded.

Although clouds are complex expressions of their physical environment, which intricately couple a wide variety of physical processes (radiation, myriad microphysical processes, waves, surface heating and moistening, mixing) and thus take expression in a wide variety of regimes, the shallow cloud regimes that appear to contribute most to uncertainty in calculations of climate change are perhaps the simplest, and most amenable to idealizations [6]. We report on recent work

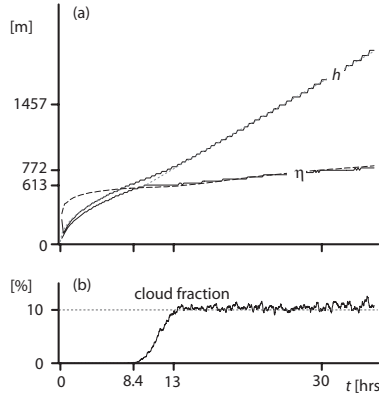


FIGURE 1. (a) Time series of PBL top, h , and lifting condensation level η . A gray dotted line (which is effectively overlaid by other lines) shows the fit to h_θ for $t < 8.4$ hrs and $t > 13$ hrs respectively. The early time fit is proportional to $t^{1/2}$ and the late time fit is proportional to t . (b) Time series of cloud fraction, defined as the percent of columns with condensate.

devoted to developing such idealizations for layers of shallow cumulus convection, and the key physical interactions thought to govern their behavior. Most of our results are taken from work recently submitted for publication [6], the idea being that such simple models can help constrain existing parameterizations of clouds, thereby reducing uncertainty in climate prediction.

The idealization we consider is developed in the spirit of the model problem for the dry convective boundary layer [7], wherein one considers how the horizontally averaged thermal structure (as measured by the potential temperature $\theta(z, t)$) evolves in space (z denotes the vertical) and t time for an initial condition of uniform stratification ($d\theta/dz = \Gamma$ initially constant) and under the action of a uniform and fixed surface heat flux, which we denote by Q . This problem admits three non-dimensional numbers, a Prandtl number a Reynolds/Rayleigh like number, and the ratio of the gravity wave timescale in the free layer to the overturning timescale of the developing thermal boundary layer. Assuming similarity in latter two, it follows straightforwardly that for a given Prandtl number this problem admits only one length scale, h which grows as

$$(1) \quad h \propto (2Qt/\Gamma)^{1/2}.$$

Tests with large-eddy simulation suggest that (1) provides a good description of this layer.

A simple representation of the cumulus-topped boundary layer can be developed from a generalization of this problem, for which we allow moisture, which contributes to the buoyancy and permits saturation. The initial moisture profile, $q(z, 0) = q_0 \exp(-z/z_0)$ is chosen to maintain a decreasing equivalent potential

temperature profile through the lower troposphere, while the temperature profile is adjusted to maintain a uniform lapse rate in buoyancy (equivalently virtual potential temperature, θ_v). The surface flux, Q is calculated by specifying the temperature of a saturated lower boundary to be that required to maintain a constant surface buoyancy flux. The addition of moisture to the problem introduces several new parameters, including the moisture parameters z_0 and q_0 and a scale height $\frac{R_v c_p \Theta_{v,0}^2}{Lg}$ where R_v is the gas-constant for water vapor, c_p is the isobaric specific enthalpy for air, L is the enthalpy of vaporization, $\Theta_{v,0}$ is a base state virtual potential temperature and g is gravity. The ensuing development of the layer is shown in Fig. 1. At early times, before the development of a cloud the layer grows like the dry convective boundary layer, with $h \propto t^{1/2}$ while at late time (after clouds develop) a new growth regime emerges in which the layer depth grows proportionally to time.

The proliferation of parameters makes it difficult to argue on dimensional grounds for the growth law of the late-time regime. Instead we appeal to the energetics. By a consideration of the buoyancy budget of the inversion layer (that layer which separates the developing thermal boundary layer and from the unperturbed part of the initial profile) subject to the following constraints on the flow:

- the liquid water content is stationary,
- the sub-cloud and cloud layer buoyancy changes at the same rate,
- and, the sub-cloud layer evolves as a dry convective boundary layer,

it can be shown that

$$(2) \quad \frac{dh}{dt} \propto \left[\frac{Q(1 - 1.3\frac{h}{\eta})}{\Theta_{v,0} + \Gamma h - (\hat{\theta}_v + \Gamma_c(h - \eta))} \right],$$

where η is the height of the sub-cloud layer, Γ_c is a fixed cloud layer lapse rate, $\Theta_{v,0}$ is the basic state virtual temperature and $\hat{\theta}_v$ is the average virtual temperature in the sub-cloud layer. This equation does a reasonably good job of predicting the growth rates seen in the LES, as is illustrated in Fig. 2.

The interpretation is that the effective flux of buoyancy into the inversion layer is given by the numerator of (2) and is proportional to h for $h \gg \eta$, while the stratification that must be overcome by this flux is given by the denominator which grows as $(\Gamma - \Gamma_c)h$, hence the growth rate dh/dt is approximately constant, i.e., h grows linearly in time. In contrast, for the convective boundary layer, the effective buoyancy flux (numerator) is fixed in time while the inversion grows with the depth of the layer, hence $h \propto t^{1/2}$. If one breaks down the effective flux of buoyancy into the inversion it can be shown to consist of two terms: one being proportional to the liquid water flux, the other being proportional to the rate of conversion of potential to kinetic energy. The former, which grows with the depth of the cloud layer, dominates. Physically one can think of this in terms of the evaporation rate of liquid water into the inversion layer, which gradually imbues that layer with the properties of the cloud layer. This describes a fundamentally different growth mechanism than that available to the dry convective boundary

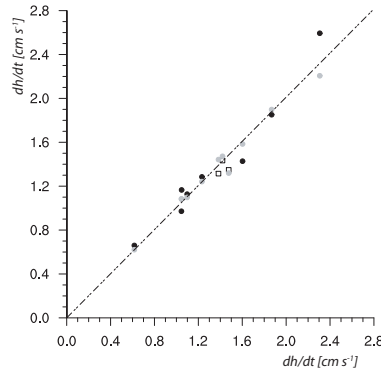


FIGURE 2. Predicted versus actual growth rate for range of simulations. Three simulations solved using different numerical formulations (grids) are shown by the open squares. Simulations in which dh/dt is calculated using the actual cloud lapse from each simulation rather than a fixed constant are shown by gray points.

layer. As a consequence of these arguments one would expect precipitation to limit the flux of liquid water into the inversion, and hence limit, or even quench the growth of the cloud layer.

In summary we find that: (i) low clouds contribute significantly to climate sensitivity of global circulation models; (ii) simple abstractions appear relevant and amenable to analysis; (iii) the cumulus layer grows by injection and more readily than its dry analog; (iv) this has important implications for studies of how the aerosol affects precipitation development and hence the statistics of clouds and eventually climate.

REFERENCES

- [1] A. Arakawa, *Modelling clouds and cloud processes for use in climate models*, Appendix 4 in The Physical Basis of Climate and Climate Modelling, GARP Publications Series No. 16, (1975), 100–120.
- [2] Sandrine Bony and Jean-Louis Dufresne, *Marine boundary layer clouds at the heart of tropical cloud feedback uncertainties in climate models*, Geophys. Res. Lett. **32** (2005), L20806.
- [3] J. T. Houghton, Y. Ding, D. J. Griggs, M. Noguer, P. J. van der Linden, X. Dai, K. Maskell, and C. A. Johnson, eds. *IPCC. 2001. Climate Change 2001: The Scientific Basis. Contribution of Working Group I to the Third Assessment Report of the Intergovernmental Panel on Climate Change*, Cambridge, U.K.: Cambridge University Press.
- [4] Brian Medeiros, Bjorn Stevens, David Williamson, Jerry Olson, Isaac Held and Ming Zhao *Aquaplanets climate sensitivity and cloud feedbacks*, in preparation for the Journal of Climate, available from first author, (2006).

- [5] NRC (National Research Council) *Carbon Dioxide and Climate: A Scientific Assessment*. Washington, D.C. National Academy Press, (1979).
- [6] Bjorn Stevens *On the growth rate of layers of non-precipitating cumulus convection*, J. Atmos. Sci, submitted, (2006).
- [7] H. Tennekes *A model for the dynamics of the inversion above a convective boundary layer*, J. Atmos. Sci, **30**, (1973).

A 1-D Elastic-Plastic Sea-Ice Model Solved with an Implicit Eulerian-Lagrangian Method

DAVID M. HOLLAND

A physical model for an elastic-plastic rheology is developed and implemented in a numerical sea-ice model. The rheology describes sea ice as behaving as an elastic material for relatively small deformations and as a plastic material for larger ones. The model equations are solved using an Eulerian-Lagrangian method in which the displacement of granular aggregates from an original Eulerian grid is computed in a Lagrangian sense and the resulting mass distribution is mapped back onto the Eulerian grid. The equations are integrated in time using Krylov solvers in a fully-implicit framework. The model distinguishes itself from previous sea-ice models in a combination of attributes: the absence of a viscous dependence within the rheology, the employment of an Eulerian-Lagrangian grid, and in the use of an fully-implicit time-stepping scheme allowing for a large time step. Model results and efficiency are presented from a one-dimensional simulation; plans for extension of the physics and numerics to two-dimensions are outlined.

A particular formulation of the physics and numerics of an elastic-plastic sea-ice rheology has been adapted. The physics describes the sea-ice deformation as being elastic for relatively small deformations, a feature that fits with observations from AIDJEX. For large deformations the sea-ice is modeled to behave in a plastic manner, meaning that the stress reaches finite limit and remains constant. The yielding stress is formulated both for compressive failure and tensile failure, the latter is generally neglected in large-scale sea-ice models used in climate studies, but yet may be of relevance in such simulations. The numerics is based on an algorithm in which a combined Eulerian-Lagrangian scheme allows granular aggregates to be advected in a Lagrangian sense and subsequently be remapped to an underlying, fixed Eulerian grid. The particular connection of the numerics to the physics is that the physics describes an elastic behavior and hence the tracking of particle displacement thorough time, and the numerics is tailored to solve for particle displacement. Further, the numerics use an implicit in time scheme thus allowing relatively large time steps than an explicit scheme would permit.

It is the distinguishing physical and numerical attributes, combined with the one-dimensional simulation results, that is offered as proof-of-concept that a fully-developed two-dimensional sea-ice model, including realistic geometry and forcing, and thermodynamics, would be a viable future investigation. The Coriolis force and shear stresses would be implemented, with the latter be treated as Columbic,

hence taken as proportion of the compressive normal stress as presented here. These physical and numerical properties of such a model make it an intriguing candidate for use in a large-scale climate model.

Multiple Scale Asymptotics of Cloud Topped Boundary Layer

ANTONY Z. OWINOH

(joint work with Bjorn Stevens, Rupert Klein)

The presence of clouds has a large impact on the boundary layer structure. In cloudy boundary layer the surface and radiative fluxes may produce local sources of heat and cooling within the interior of the boundary layer and can greatly influence its turbulence structure and dynamics.

In this talk we present preliminary results of an asymptotic analysis of the the cloud topped boundary layer (CTBL) and in particular, stratocumulus clouds. The idealised structure is showed in Fig 1. It consists of layer below the cloud where the liquid water potential temperature θ_l and the total water mixing ratio q_t are constant with height to leading order. These quantities are assumed to vary linearly with height in the cloud layer. An infinitesmally thin inversion layer caps the cloud layer with jumps in the thermodynamic variables θ_l and q_t . The structure above this layer is given by different scaling formulation and is a subject of future studies.

We use the unified approach to meteorological modelling based on multiple scale asymptotics techniques as developed in [1] or [2]. The key steps of this technique involve (a) non dimensionalization of the 3D compressible flow equations on the rotating earth (b) identifying scales valid uniformly such as (c) choice of a particular distinguished limit and (d) construction of solutions to the governing equations based on multiple scale expansions in terms of ε . The main equations for which the asymptotics are performed are

$$(1) \quad \varrho_t + \nabla_{\parallel} \cdot (\varrho \mathbf{v}_{\parallel}) + (\varrho w)_z = 0$$

$$(2) \quad (\varrho \mathbf{v}_{\parallel})_t + \nabla_{\parallel} \cdot (\varrho \mathbf{v}_{\parallel} \circ \mathbf{v}_{\parallel}) + (\varrho \mathbf{v}_{\parallel} w)_z + \varepsilon (\widehat{\boldsymbol{\Omega}} \times \varrho \mathbf{v})_{\parallel} + \varepsilon^{-4} \nabla_{\parallel} p = 0$$

$$(3) \quad (\varrho w)_t + \nabla_{\parallel} \cdot (\varrho \mathbf{v}_{\parallel} w) + (\varrho w w)_z + \varepsilon (\widehat{\boldsymbol{\Omega}} \times \varrho \mathbf{v})_{\perp} + \varepsilon^{-4} p_z = -\varepsilon^{-4} \varrho$$

$$(4) \quad \theta_{lt} + \mathbf{v}_{\parallel} \cdot \nabla_{\parallel} \theta_l + w \theta_{tz} = \mathcal{R}$$

$$(5) \quad q_{tt} + \mathbf{v}_{\parallel} \cdot \nabla_{\parallel} q_t + w q_{tz} = \mathcal{S}_q$$

where the symbols have the usual meaning and have been scaled with reference values as indicated in [1]. We close these equations with equation of state

$$(6) \quad \begin{aligned} \varrho \theta_l &= (1 + q_t) p^{[1 - \Gamma \varepsilon (1 + R^{**} q_t) (1 + c_p^{**} q_t)^{-1}]} (1 + R^{**} q_v)^{[-1 + \Gamma \varepsilon (1 + R^{**} q_t) (1 + c_p^{**} q_t)^{-1}]} \\ &\quad (R^{**} q_v)^{[-\Gamma \varepsilon R^{**} q_t (1 + c_p^{**} q_t)^{-1}]} \exp(-L_v^{**} \Gamma \frac{\varrho q_l}{p} (1 + R^{**} q_v) (1 + q_t)^{-1}) \end{aligned}$$

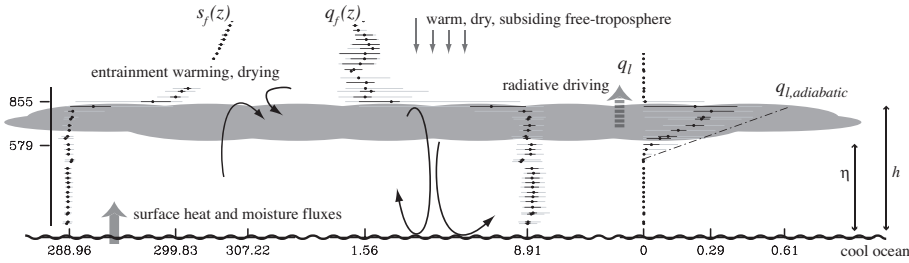


FIGURE 1. Idealized Boundary Layer Structure

The symbols $(.)^{**}$ in (6) are order one variables. Though the equation of state looks complicated, we use the liquid water potential temperature, instead of the usual potential temperature, to circumvent the paramterization of the microphysical processes. The total moisture content $q_t = q_v + q_l$, where q_v is water vapour mixing ratio and q_l is the liquid water mixing ratio, is a conserved quantity in absence of precipitation.

We would like to resolve a shallow layer of fluid of depth of 1 km (i.e εh_{sc}) where h_{sc} is the pressure height scale and horizontal length scales of approximately 1km (i.e εh_{sc}) embedded in a 100 km (i.e $\varepsilon^{-\frac{3}{2}} h_{sc}$). Thus the co-ordinate system is $\xi_{\parallel} = \varepsilon^{-1} \mathbf{x}_{\parallel}$, $\mathbf{X}_{\parallel} = \varepsilon^{\frac{3}{2}} \mathbf{x}_{\parallel}$ and $\eta = \varepsilon^{-1} z$. We consider the time scales associated with the horizontal advection of the gravity wave i.e. $T = \varepsilon t$ and faster time scale associated with 1 km scale $\tau = \varepsilon^{-1} t$. Note that the gravity wave speed is given by $c_g = \sqrt{g \frac{\Delta \theta}{\theta_0} H} \sim \sqrt{g \varepsilon^3 h_{sc}} \sim \varepsilon^{-\frac{1}{2}} u_{ref}$. We expand any dependent flow variables as

$$(7) \quad U = \sum_{i=0} \delta^i U^{(i)}(\tau, \mathbf{X}_{\parallel}, \eta), \quad \text{where } \delta = \varepsilon^{\frac{1}{2}}.$$

The leading order equations of mass and momentum reveal that the fast time - short space averaging leads to

$$(8) \quad \frac{\partial}{\partial \eta} \left\langle (\varrho w)^{(i)} \right\rangle = 0 \quad i = 0, 1, 2, 3, 4 \quad \text{and} \quad \frac{\partial}{\partial \eta} \left\langle (\varrho \mathbf{v}_{\parallel} w)^{(i)} \right\rangle = 0 \quad i = 0, 1, 2, 3.$$

It has been shown in [4] how (8) represents the turbulent fluxes terms.

The non trivial averaged equations are

$$(9) \quad \nabla_{\mathbf{x}} \cdot \mathbf{v}_{\parallel}^{(0)} + w_{\eta}^{(5)} = 0$$

$$(10) \quad \mathbf{v}_{\parallel T}^{(0)} + (\widehat{\boldsymbol{\Omega}} \times \mathbf{v}^{(0)})_{\parallel} + \nabla_{\mathbf{x}} p^{(7)} = - \frac{\partial}{\partial \eta} \left\langle (\varrho \mathbf{v}_{\parallel} w)^{(5)} \right\rangle$$

$$(11) \quad p_{\eta}^{(6)} + \varrho^{(4)} = 0$$

$$(12) \quad p_\eta^{(7)} + \varrho^{(5)} = 0$$

with densities given by

$$(13) \quad \varrho^{(4)} = \frac{\eta^2}{2} + \Gamma\eta - \theta_l^{(4)} + q_t^{(4)} - L_v^{**}\Gamma q_l^{(4)} - R^{**}q_v^{(4)}.$$

$$(14) \quad \varrho^{(5)} = -\theta_l^{(5)} + q_t^{(5)} - L_v^{**}\Gamma q_l^{(5)} - R^{**}q_v^{(5)}$$

The liquid water potential temperature equations are

$$(15) \quad \theta_{lT}^{(4)} = \mathcal{R}^{(6)} - \frac{\partial}{\partial\eta} \left\langle (\varrho\theta_l w)^{(8)} \right\rangle$$

$$(16) \quad \theta_{lT}^{(5)} + \mathbf{v}_{\parallel}^0 \nabla_x \theta_l^{(4)} + w^{(5)} \theta_{l\eta}^{(4)} = \mathcal{R}^{(7)}$$

and total moisture content

$$(17) \quad q_{tT}^{(4)} = \mathcal{S}_q^{(6)} - \frac{\partial}{\partial\eta} \left\langle (\varrho q_t w)^{(8)} \right\rangle$$

$$(18) \quad q_{tT}^{(5)} + \mathbf{v}_{\parallel}^0 \cdot \nabla_x q_t^{(4)} + w^{(5)} q_{t\eta}^{(4)} = \mathcal{S}_q^{(7)}$$

Here we have omitted $\langle \cdot \rangle$ and all variables unless otherwise indicated represents averaged quantities.

We note that the time evolution of the averaged horizontal component of velocity (10) is determined by the coriolis term, turbulent fluxes and pressure gradient which is computed from pressures determined by moist processes given by (11)–(14). The pressure $p^{(7)}$ may also be altered by the large scale motion.

Further, (15) and (17) simply relate to the time variation of the leading order liquid water potential temperature and total water mixing ratio to the radiative flux and convective fluxes in the layer.

The above equations can be vertically averaged further, to obtain depth averaged equations, as follows. We define vertically averaged quantity $\bar{\phi}^H$ over depth $H(\mathbf{X}_{\parallel}, T)$ of ϕ as

$$(19) \quad \bar{\phi}^H = \frac{1}{H} \int_0^H \phi d\eta$$

and boundary condition

$$(20) \quad w = 0 \quad \text{on} \quad z = 0$$

Free surface kinematic boundary conditions on $\eta = H(\mathbf{X}_{\parallel}, T)$

$$(21) \quad \frac{\partial H}{\partial T} = (\mathbf{v} + \mathbf{v}_e - \mathbf{v}_m) \cdot \mathbf{n}$$

where \mathbf{v}_e is the entrainment velocity, \mathbf{v}_m is the mass flux velocity and \mathbf{n} is the normal to the surface $\eta = H(\mathbf{X}_{\parallel}, T)$

$$(22) \quad \frac{\partial H}{\partial T} + \nabla_x \cdot (H \bar{\mathbf{v}}_{\parallel}^{(0)H}) = w_e(\mathbf{X}_{\parallel}, H, T) - w_m(\mathbf{X}_{\parallel}, H, T)$$

We assume that

$$(23) \quad \theta_l = 1 + \delta^4 \theta_l^{(4)}(\mathbf{X}_{\parallel}, T) + \delta^5 \theta_l^{(5)}(\mathbf{X}_{\parallel}, T) + \delta^6 \theta_l^{(6)}(\mathbf{X}_{\parallel}, \eta, T) + \mathcal{O}(\delta^7)$$

$$(24) \quad q_t = 1 + \delta^4 q_t^{(4)}(\mathbf{X}_{\parallel}, T) + \delta^5 q_t^{(5)}(\mathbf{X}_{\parallel}, T) + \delta^6 q_t^{(6)}(\mathbf{X}_{\parallel}, \eta, T) + \mathcal{O}(\delta^8),$$

then averaged momentum and thermodynamics equations are

$$(25) \quad \begin{aligned} \frac{\partial}{\partial T}(H\overline{\mathbf{v}_{\parallel}^{(0)}}^H) &+ \nabla_{\mathbf{x}} \left(\frac{H^2}{2}(\theta_l^{(5)} - q_t^{(5)} + L_v^{**}\Gamma q_l^{(5)} + R^{**}q_v^{(5)}) \right) \\ &+ (\widehat{\boldsymbol{\Omega}} \times H\overline{\mathbf{v}_{\parallel}^{(0)}}^H)_{\parallel} = \mathbf{v}_{\parallel}^{(0)}(\mathbf{X}_{\parallel}, H, T) \frac{\partial H}{\partial T} + \left\langle (\varrho \mathbf{v}_{\parallel} w)^{(5)} \right\rangle_s \end{aligned}$$

$$(26) \quad \frac{\partial}{\partial T}(H\theta_l^{(5)}) + H\overline{\mathbf{v}_{\parallel}^{(0)}}^H \nabla_{\mathbf{x}} \theta_l^{(4)} = H\overline{\mathcal{R}^{(6)}}^H + \theta_l^{(5)} \frac{\partial H}{\partial T}$$

$$(27) \quad \frac{\partial}{\partial T}(Hq_t^{(5)}) + H\overline{\mathbf{v}_{\parallel}^{(0)}}^H \nabla_{\mathbf{x}} q_t^{(4)} = H\overline{\mathcal{S}_q^{(6)}}^H + q_t^{(5)} \frac{\partial H}{\partial T}$$

These depth averaged equations derived represent the time variation of the boundary layer structure in terms of the large scale dynamics, convective, radiative and turbulent fluxes. They are similar to those derived in [3].

Finally, suppose we assume that in the layer that the profile of q_l is given by

$$(28) \quad q_l^{(5)} = \begin{cases} \alpha\eta & \text{for } z_B \leq \eta \leq H \\ 0 & \text{for } 0 \leq \eta < z_B \end{cases}$$

where $z_B = z_B(\mathbf{X}_{\parallel}, T)$ is the cloud base and varies in time and horizontal space. Then the averaged horizontal momentum equation becomes

$$(29) \quad \begin{aligned} \frac{\partial}{\partial T}(H\overline{\mathbf{v}_{\parallel}^{(0)}}^H) &+ (\widehat{\boldsymbol{\Omega}} \times H\overline{\mathbf{v}_{\parallel}^{(0)}}^H)_{\parallel} + \nabla_{\mathbf{x}} \left(\frac{H^2}{2}[\theta_l^{(5)} - (R^{**} - 1)q_v^{(5)}] \right) \\ &+ (R^{**} - 1)z_B H \nabla_{\mathbf{x}} q_v^{(5)} + \frac{\alpha}{2}(1 - L_v^{**}\Gamma)H \nabla_{\mathbf{x}}(H^2 - z_B^2) \\ &= \mathbf{v}_{\parallel}^{(0)}(\mathbf{X}_{\parallel}, H, T) \frac{\partial H}{\partial T} + \left\langle (\varrho \mathbf{v}_{\parallel} w)^{(5)} \right\rangle_s \end{aligned}$$

An equation is needed to predict the height of the subcloud layer z_B .

We conclude by noting that the equations derived in this talk formalize the time variation of the cloud topped boundary layer structure as described by various authors e.g. [5].

REFERENCES

- [1] A. J. Majda and R. Klein, *Systematic Multiscale Models for the Tropics*, Journal of the Atmospheric Sciences, **60**, (2003), 393–408
- [2] R. Klein and A. J. Majda, *Systematic Multiscale Models for Deep Convection on Mesoscales*, Theoretical and Computational Fluid Dynamics, (2006), In Press
- [3] B. Stevens, *Bulk Boundary Layer Concepts for Simplified Models on Tropical Dynamics*, Theoretical and Computational Fluid Dynamics, (2006), In Press

- [4] R. Klein, E. Mikusky and A. Owino, *Multiple Scale Asymptotics for Atmospheric Flows*, 4ECM Stockholm, (2004), 201–220
- [5] J. R. Garratt, *The Atmospheric Boundary Layer*, Cambridge University Press, 316pp. (1992).

Modeling and parameterization of regional scale land-atmosphere exchanges

ELIE BOU-ZEID

(joint work with Marc B. Parlange, Charles Meneveau)

Large eddy simulation (LES) dynamically captures the effect of changes in land cover on atmospheric flow and hence is a very useful tool for the modeling of the non-linear land atmosphere interaction over heterogeneous terrain. However, to be faithful to the physics of atmospheric boundary layer (ABL) flow over heterogeneous and complex terrain, the LES needs a fully local subgrid-scale (SGS) model that does not require any directions of statistical homogeneity for averaging. We have implemented such an SGS model, the Lagrangian dynamic scale-dependent model, in LES and validated the code against classic results for flow over homogeneous terrain and against field experimental results (Bradley's 1968 experiment) for flow over an abrupt change in surface roughness.

Subsequently, we performed LES of ABL flow over random distributions of surface roughness and looked at the effect of roughness heights and heterogeneity distribution on land-atmosphere interaction. The “effective surface roughness” and “blending height” were computed to quantify momentum transfer at the earth surface. An “integral length scale” was defined to characterize the spatial scale of surface heterogeneity, based on the structure function (variogram) of the surface roughness.

As one can expect, for surfaces with low variation of the roughness heights, land atmosphere interaction is rather insensitive to the spatial distribution of the roughness and the effective surface roughness changes little with the scale of heterogeneity. On the other hand, for surfaces with significant variation of the roughness height, momentum transfer at the earth surface is significantly enhanced as the heterogeneity scale is decreased. Furthermore, we show that the effective surface roughness for random patches can be well estimated using a parameterization we previously developed and tested for regular patches.

Derivation and discretization of the semi-geostrophic equations

YANN BRENIER

This is a short review of the mathematical analysis of the SG equations. We start from the Euler equations for an incompressible fluid moving in a bounded domain D in R^3 , subject to constant rotation in the horizontal plane (x_1, x_2) and gravity in the x_3 direction. It is convenient to use particle trajectories $t \rightarrow X(t, a) \in D$, where

a is the particle label, typically the position at $t = 0$ (so that $X(0, a) = a \in A$). With these coordinates, using Boussinesq's approximation, we can write the Euler equations:

$$(1) \quad \partial_{tt}X(t, a) + (\nabla p)(t, X(t, a)) + J \cdot \partial_t X = \theta(a)e_3 ,$$

where J is the rotation generator $Jx = (-x_2, x_1, 0)$, $p(t, x)$ is the pressure at time t and point $x \in D$, and θ depends only on the label a . The incompressibility of the fluid means that, at each t , $a \in D \rightarrow X(t, a) \in D$ belongs to the set $S(D)$ of all volume preserving maps of D . Differentiating (1) with respect to t and eliminating ∂_{tt} by using (1) again, leads to:

$$(2) \quad \partial_{ttt}X + \partial_t\{(\nabla p)(t, X)\} + J \cdot (-(\nabla p)(t, X) - J\partial_t X) = 0,$$

where gravity terms have disappeared. Introducing

$$(3) \quad \Phi(t, x) = p(t, x) + \frac{x_1^2 + x_2^2}{2},$$

we can write (2) as:

$$(4) \quad \partial_{ttt}X + \partial_t\{(\nabla\Phi)(t, X)\} + J \cdot (-(\nabla\Phi)(t, X) + X) = 0.$$

Introducing, for each t , the map

$$(5) \quad M(t, a) = (\nabla\Phi)(t, X(t, a)),$$

we get

$$(6) \quad \partial_{ttt}X + \partial_t M = J \cdot (M - X)$$

where X is valued in $S(D)$ and M is of form (5). Next, assuming $\Phi(t, x)$ to have positive second derivatives in x , following the 'Cullen-Purser' energy principle (which, roughly speaking, means strong rotation and stable vertical stratification), we deduce from the polar factorization theorem for maps [3] that, for each t , $X(t, \cdot)$ is determined as the unique closest point $\pi(M)$ to $M(t, \cdot)$ on $S(D)$ in L^2 distance, which means:

$$(7) \quad \int_D \|X(t, a) - M(t, a)\|^2 da \leq \int_D \|Y(a) - M(t, a)\|^2 da, \quad \forall Y \in S(D).$$

Therefore, under the Cullen-Purser principle, we finally get for M :

$$(8) \quad \partial_{ttt}(\pi(M)) + \partial_t M = J \cdot (M - \pi(M)).$$

Now, the semi-geostrophic equations are simply obtained, after a suitable rescaling, by dropping the third order derivative in time:

$$(9) \quad \partial_t M = J \cdot (M - \pi(M)).$$

A variant (the 'Vlasov-Monge-Ampère' equation)

$$(10) \quad \partial_{tt}M + M - \pi(M) = 0$$

has been recently studied in [6]. A natural discretization of (9) is obtained by splitting the domain D in a large number N of cells D_i of equal volume and center of mass A_i for $i = 1, \dots, N$. Then the map $M(t, \cdot)$ is replaced by the position of N points ('semi-geostrophic vortices') $M_i(t)$ in R^3 and the set of all volume

preserving maps $S(D)$ is replaced by the discrete set of all permutations σ of the centers A_i . So, (9) becomes:

$$(11) \quad \frac{d}{dt} M_i = J \cdot (M_i - A_{\sigma_i}), \quad i = 1, \dots, N$$

where σ is a time-dependent permutation updated so that

$$(12) \quad \sum_{i=1}^N \|A_{\sigma_i} - M_i(t)\|$$

stays minimal at any time. Notice that each SG vortices follows a piecewise circular trajectory.

Results and References. The SG equations go back to Hoskins (see references in [9]) and, earlier, to Eliassen (1948). Global existence of weak solutions was proven in [2] using Eulerian coordinates and by [7] using Lagrangian coordinates. See also [10]. The hamiltonian nature of the SG equations has been investigated in [11]. The discrete approximation (11) was considered in [4] and [1]. See also [5]. Its convergence to the continuous SG equations (in Eulerian coordinates) has been recently proven in [8], which contains further interesting references.

REFERENCES

- [1] Baigent, Norbury, Phys. D 109 (1997) 333.
- [2] Benamou, Brenier, SIAM J. Appl. Math. 58 (1998) 1450.
- [3] Brenier, Comm. Pure Appl. Math. 44 (1991) 375.
- [4] Brenier, A geometric presentation of the semi-geostrophic equations, unpublished note, Newton Institute, 1996.
- [5] Brenier, Comm. Math. Phys. 212 (2000) 93.
- [6] Brenier, Loeper, Geom. Funct. Anal. 14 (2004) 1182.
- [7] Cullen, Feldman, SIAM J. Math. Anal. 37 (2006) 1371.
- [8] Cullen, Gangbo, Pisante, The Semigeostrophic Equations Discretized in reference and dual variables, Arch. Rat. Mech. Analysis (to appear).
- [9] Cullen, Purser, J. Atmospheric Sci. 41 (1984) 1477.
- [10] Loeper, Calc. Var. Partial Differential Equations 22 (2005) 343.
- [11] Roulstone, Norbury, J. Fluid Mech. 272 (1994), 211.

Reconstruction of effective stochastic dynamics from data

DAAN CROMMELIN

(joint work with Eric Vanden-Eijnden)

Construction of stochastic models that describe the effective dynamics of observables of interest is an useful instrument in various fields of application, such as physics, climate science, and finance. We present a new technique for the construction of such effective models from timeseries. The approach centers on the

minimization of an object function that measures the difference between the eigen-spectrum of the generator of the stochastic process (for example, the Fokker-Planck operator) and a reference eigenspectrum obtained from the data.

Denoting the reference spectrum by $\{\psi_k(x), \phi_k(x), \lambda_k\}$, the generator by L and its adjoint by L^* , the object function to be minimized is

$$E = \sum_k \left(\alpha_k \|L^* \psi_k - \lambda_k \psi_k\|^2 + \beta_k \|L \phi_k - \lambda_k \phi_k\|^2 + \gamma_k |\langle \psi_k, L \phi_k \rangle - \lambda_k|^2 \right),$$

where $\alpha_k, \beta_k, \gamma_k$ are nonnegative weights. In [1], L is the generator matrix of a continuous-time Markov chain (in which case the state-space variable x takes on discrete values). The case of a diffusion process, where the generator is the elliptic operator

$$L = b(x) \cdot \nabla + \frac{1}{2}a(x) : \nabla \nabla,$$

is treated in [2]. For both types of generators, the object function E is convex, and quadratic in the quantities over which to minimize (matrix elements L_{ij} in the Markov chain case, drift and diffusion functions $b(x)$ and $a(x)$ in the diffusion case). Moreover, the appropriate constraints ($L_{ij} \neq 0$ if $i \neq j$; $a(x)$ positive semi-definite for all x) define a convex domain. Therefore, minimization of E is a quadratic programming problem, with well-established numerical solution methods, and a unique minimum.

The reference eigenvectors $\psi_k(x), \phi_k(x)$ and eigenvalues λ_k are obtained from data by binning the timeseries and computing the associated transition probability matrix P . The eigenvectors of P can be used as reference eigenvectors (or as spatial discretizations of the reference eigenfunctions, in case of a diffusion). The reference eigenvalues are $\lambda_k = (\Delta t)^{-1} \log \Lambda_k$, with Λ_k the eigenvalues of P and Δt the sampling interval of the timeseries. Minimization of E results in a generator L with an eigenspectrum that resembles the reference spectrum as closely as possible. The invariant distribution of the stochastic process is part of the eigenspectrum.

As an example, consider a 1-dimensional diffusion process with periodic boundary conditions and a domain $[-\pi, \pi]$. The drift and diffusion are given by $b(x) = 1 + \cos x$ and $a(x) = 1 + \frac{1}{2} \sin x$, respectively. From a timeseries of 10^6 datapoints, generated by numerical integration of the 1-dimensional stochastic differential equation associated with this diffusion process, we reconstructed $b(x)$ and $a(x)$. The results of the reconstruction are shown in figure 1. More details, as well as other examples, can be found in [2].

For the reconstruction of drifts and diffusions, the approach allows for both non-parametric and parametric estimation. It is not necessary to assume specific functional forms for $b(x)$ and $a(x)$, and thus non-parametric estimation is possible. For parametric estimation, one assumes expansions $b(x) = \sum_n b_n f_n(x)$ and $a(x) = \sum_m a_m g_m(x)$ with known functions $f_n(x)$ and $g_m(x)$. Minimization of the object function E must now be carried out under variation of the expansion coefficients b_n and a_m . The quadratic structure of E is preserved. By limiting the number of

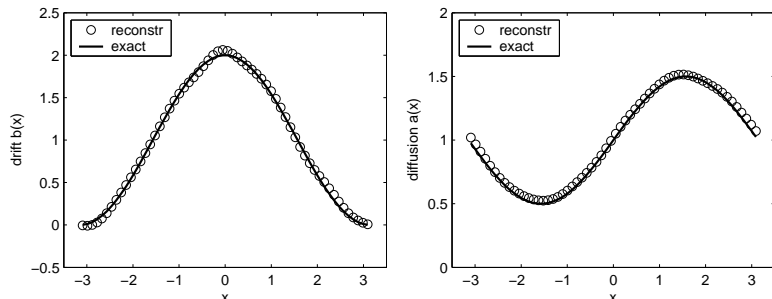


FIGURE 1. Reconstructed drift $b(x) = 1 + \cos(x)$ and diffusion $a(x) = 1 + \frac{1}{2} \sin(x)$ from data.

terms in the expansions, the dimensionality of the minimization problem can be reduced significantly.

REFERENCES

- [1] D.T. Crommelin, E. Vanden-Eijnden, *Fitting timeseries by continuous-time Markov chains: A quadratic programming approach*, J. Comp. Phys., in press (2006)
- [2] D.T. Crommelin, E. Vanden-Eijnden, *Reconstruction of diffusions using spectral data from timeseries*, Comm. Math. Sci., in press (2006)

Regimes of thermocline scaling: the interaction of wind-stress and surface buoyancy

PAOLA CESSI

The role of the relative geometry of wind-stress and buoyancy forcings in enhancing or suppressing the generation of oceanic baroclinic eddies is studied. The dependence of the eddy-component of buoyancy transport on the external parameters such as diapycnal mixing, dissipation rate and forcing is examined through direct numerical simulations of the primitive equations in simplified, zonally-reentrant domains. Qualitatively different regimes are found depending on the relative phase of the wind-stress and surface buoyancy distribution. In some regimes a substantial eddy-field is generated, which fundamentally contributes to the poleward heat transport. In other regimes the eddies are very weak, and the bulk of the transport is effected by the steady, mean circulation. These differences are rationalized in terms of the energetics of the eddies.

The most efficient arrangement for eddy generation has eastward wind-stress in conjunction with negative poleward buoyancy gradient. This correspond to the situation found in the mid-latitudes, where the surface Ekman flow carries buoyancy towards the high buoyancy region, i.e. upgradient of the surface buoyancy.

In this case, strong eddy-fluxes are generated in order to counteract the upgradient buoyancy transport by the Ekman cell. This arrangement of wind-stress provides a large source of available potential energy on which the eddies can grow, so the mechanical energy balance for the eddies is consistent with a substantial eddy buoyancy flux. The competition between upgradient buoyancy transport by the Ekman circulation and downgradient buoyancy transport by the eddies results in a thermocline whose depth is independent of the diapycnal diffusivity.

When the same buoyancy gradient is paired with westward wind-stress, the mean flow produces a sink, rather than a source, of available potential energy and eddies are suppressed. With this arrangement, typical of low latitudes and the sub-polar regions, the Ekman overturning cell carries buoyancy down gradient of the surface distribution. Thus, the net buoyancy transport is almost entirely due to the Ekman flow, and the thermocline is a thin, diffusive boundary layer.

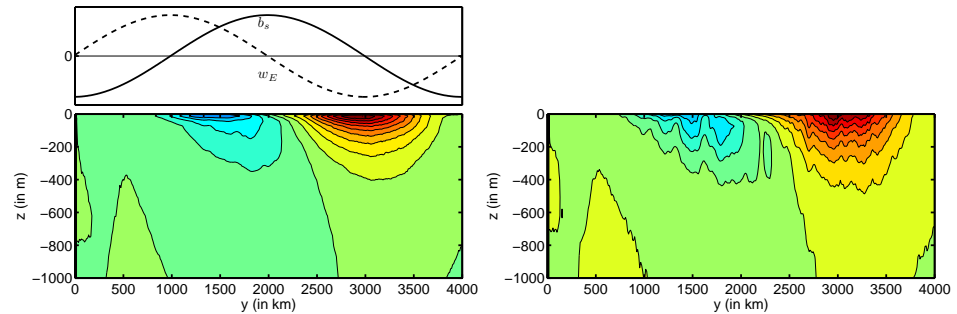


FIGURE 1. The left panel shows the zonally averaged eddy buoyancy fluxes, $\overline{v'b'}$ as a function of depth and latitude, diagnosed from a direct numerical simulation. Motion is driven by prescribed surface forcings shown in the top left panel: the surface buoyancy $b_s(y)$ is shown as a solid line and the surface wind-stress leads to the Ekman pumping, w_E , shown as a dashed line. The right panel shows the corresponding $-\sqrt{\overline{v'^2}} \bar{b}_y$ (diagnosed for the same simulation), illustrating that the RMS barotropic streamfunction is an excellent measure of the eddy diffusivity for buoyancy.

A quantitative theory for the eddy fluxes of buoyancy on the f -plane is developed and compared with the simulations, based on the following assumptions:

- 1) The interior of the thermocline has constant Ertel potential vorticity on isopycnals. This implies that the zonally-averaged, quasi-geostrophic potential vorticity eddy fluxes, $\overline{v'q'} \approx (\overline{v'b'})_z$, is zero (b is the buoyancy, q is the potential vorticity and v is the velocity; $\bar{\cdot}$ denotes the zonal average, and $'$ denotes the departure from zonal average).

- 2) The zonally averaged eddy-fluxes of buoyancy, $\overline{v'b'}$, can be approximated by a down-gradient diffusion closure, $\overline{v'b'} \approx -\kappa_e \bar{b}_y$, with $\kappa_e = \sqrt{\overline{\psi'^2}}$ (ψ' is the barotropic eddy streamfunction, linearly proportional to the vertically averaged pressure fluctuations).
- 3) The barotropic eddy streamfunction variance, $\overline{\psi'^2}$, is proportional to the eddy available potential energy, EAPE, times a mixing length square, ℓ^2 . The EAPE can be calculated explicitly in terms of the imposed forcing and the mean buoyancy. Various closures are examined for the mixing length and compared with the numerical simulations.

The theory shows that, regardless of the choice for ℓ , it is essential to include information about the EAPE in the eddy-flux closure, in order to capture the different eddy regimes.

Figure 1 compares the directly computed eddy buoyancy fluxes, $\overline{v'b'}$, (left panel), with the parametrised fluxes, estimated using $-\sqrt{\overline{\psi'^2}} \bar{b}_y$, for one typical computation.

A Similarity Theory for Transcritical Flow over Orography

J. GAVIN ESLER

(joint work with O. J. Rump, E. R. Johnson)

Non-dispersive and weakly dispersive single layer flows over axisymmetric obstacles of nondimensional height M , measured relative to the layer depth, are investigated. The case of transcritical flow, for which the Froude number F of the oncoming flow is close to unity is considered. For transcritical flow, a similarity theory is developed for small obstacle height, and for non-dispersive flow the problem is shown to be isomorphic to that of transonic flow of a compressible gas over a thin aerofoil. The nondimensional drag exerted by the obstacle on the flow takes the form $D(\Gamma)M^{5/3}$, where $\Gamma = (F - 1)M^{-2/3}$ is a transcritical similarity parameter, and D is a function which depends on the shape of the ‘equivalent aerofoil’ specific to the obstacle. The theory is verified numerically by comparing results from a shock-capturing shallow water model with corresponding solutions of the transonic small disturbance equation, and is generally found to be accurate for $M \lesssim 0.4$ and $|\Gamma| \lesssim 1$. In weakly dispersive flow the equivalent aerofoil becomes the boundary condition for the Kadomtsev-Petviashvili equation and (multiple) solitary waves replace hydraulic jumps in the resulting flow patterns. For $\Gamma \gtrsim 1.5$ the transcritical similarity theory is found to be inaccurate and for small M flow patterns are well described by a supercritical theory, in which the flow is determined by the linear solution near the obstacle. In this regime drag is shown to be $c_d M^2 / F \sqrt{F^2 - 1}$. The transition between the two regimes is discussed.

REFERENCES

- [1] J. G. Esler, O. J. Rump and E. R. Johnson *Non-dispersive and weakly dispersive single layer flow over an axisymmetric obstacle: The equivalent aerofoil formulation*, J. Fluid Mech., to appear.

Marine ice sheet dynamics

CHRISTIAN SCHOOF

Ice sheets affect the dynamics of atmospheres and oceans in numerous ways, for instance through their effect on albedo, freshwater supply and sea level changes. Ice sheets behave as highly viscous thin films, and are typically modelled using a diffusion equation known in glaciology as the ‘shallow ice’ model.

Provided the margins of an ice sheet rest on land, this model is analogous to generic models for the flow of non-Newtonian thin viscous films in the absence of surface tension, and can be cast in the framework of parabolic obstacle problems [1]. Although certain challenges remain in the mathematical analysis of the standard shallow ice model, notably when the bed of the ice sheet is not flat and the obstacle problem leads to a non-monotone variational inequality, a great deal of theoretical progress is possible.

A much harder situation to model is the case of a marine ice sheet, whose edges do not rest on land but parts of which are afloat (as is, for instance, the case in Antarctica). In that case, ice thickness in the part of the ice sheet that does rest on land — the *grounded* part — still satisfies a nonlinear diffusion equation. However, the boundary of the grounded part of the ice sheet is a free boundary (also known as the *grounding line*), and the correct choice of boundary conditions that apply is not obvious. One condition derives from the fact that the ice at the free boundary attains a known thickness given by the fact that it is just thin enough to float. This renders the problem somewhat similar to a Stefan problem, in which temperature on the surface of a melting or solidifying object must attain a given value, the melting point. A second boundary condition, analogous to the Stefan condition, is also required.

We demonstrate using matched asymptotic expansions [2] that in one dimension this second boundary condition is a prescription for ice flux in terms of ice thickness (or equivalently, depth of the ice sheet bed below sea level, as the ice is at flotation). An important outstanding problem is then to understand how bed geometry affects the stability of steady solutions to the marine ice sheet problem. Naïvely, stability can be expected to depend on the slope of the bed at the location of the grounding line, as this controls the change in ice flux caused by perturbations in the position of the free boundary. This simplistic argument, which is supported by numerical solutions, suggests that stable steady solutions must have their grounding line where the bed is angled sufficiently steeply downwards. Current work aims at providing a mathematical proof of this conjecture.

REFERENCES

- [1] N. Calvo, J. Díaz, J., J. Durany, E. Schiavi and C. Vázquez, *On a doubly nonlinear parabolic obstacle problem modelling ice sheet dynamics*, SIAM J. Appl. Math. **63** (2002), 683–707.
- [2] C. Schoof, *Marine ice sheet dynamics. Part I: The case of rapid sliding*, J. Fluid Mech. (2006), in press.

**Reduced Systematic Model Equations For The Planetary And
Synoptic Scales In The Atmosphere**

STAMEN I. DOLAPTCHEV

(joint work with Rupert Klein)

Observations show the existence of large number of low-frequency atmospheric regimes (periods longer than 10 days) with planetary spatial scales (scales larger than 3000 km), which have an important contribution to the variability of the atmosphere (e.g. the thermally and orographically induced quasi-stationary planetary Rossby waves; teleconnection patterns; mean meridional circulations (Hadley, Ferrel and the polar cells); zonally mean flows (subtropical and polar jets)). On the other hand the local wind fields and precipitation patterns are influenced by synoptic disturbances (periods of 3 to 6 days and spatial scales of 1000 km). Both types of regimes - on the planetary and on the synoptic scales, are essential for the weather variations and also for the climate, since they are responsible for the heat, momentum and water vapor transport in the atmosphere.

We use an unified multiple scales asymptotic approach in order to derive reduced model equations describing the relevant atmospheric phenomena on the planetary and synoptic scales. The method was presented in [1, 2]. This technique allows one in a systematic way to capture the important interactions between the two scales. Considering processes on the planetary scales we have to take into account effects due to the sphericity of the earth, large variations of the Coriolis parameter and of the background stratification and the presence of a background zonal flow (resulting from the equator-to-pol temperature gradient).

In the simple case, when we focus on the planetary scales only and the background zonal flow is neglected, we obtain the classical planetary geostrophic (PG) equations: for the ocean see [3, 4] and for the atmosphere see [5, 6]. In the next order asymptotic expansion an evolution equation for the relative vorticity has been derived. It is a subject of current investigation if this equation can provide a boundary condition for the PG equations.

When in the asymptotic scaling the synoptic processes are also resolved but the background zonal flow is still neglected, then we obtain a set of two equations. They are the analogon for the atmosphere of Pedlosky's equations for the ocean [7]. One equation describes the dynamics on the planetary scale of the background stratification $\partial\Theta^{(2)}/\partial r$, where r is a vertical coordinate and $\Theta^{(2)}$ is the first non-trivial term in the potential temperature expansion. This equation is identical to

the potential vorticity (PV) equation in the PG case and there is no influence from the synoptic scales on $\Theta^{(2)}$. The other equation describes the synoptic-scale dynamics. It is a modified quasigeostrophic (QG) potential vorticity equation, where the synoptic scale PV consists of planetary vorticity, relative vorticity due to the horizontal variations on the synoptic scale of the deviations from the background pressure, denoted by $\pi^{(3)}$, and a stretching term due to the vertical variations of this deviations. In comparison with the classical QG theory there are two additional terms resulting from interactions with the planetary scales. These terms are representing the advection of synoptic scale PV by the planetary scale velocity field (velocities due to the planetary scale variations of $\pi^{(2)}$) and the advection by the synoptic velocity field (velocities due to the synoptic scale variations of $\pi^{(3)}$) of PV due to the planetary scale gradient of $\Theta^{(2)}$.

The most interesting case is when we consider both scales and include a geostrophically balanced background zonal flow (denoted by $\mathbf{u}^{(-1)}$), resulting from a prescribed meridional temperature gradient of $\Theta^{(1)}(\phi, r)$. To make the discussion as simple as possible we presented in the talk the results for the planetary scales only and for a Boussinesq fluid. It is interesting to note that the next order velocity field $\mathbf{u}^{(0)}$ (due to $\pi^{(2)}$ variations) is not in geostrophic balance, since metric terms appear in the momentum equation. The PV equation for $\pi^{(2)}$ has additional terms compared with the classical PG equation: horizontal and vertical advection of relative vorticity, divergency term, twisting term and advection by the ageostrophic components of planetary vorticity and of stretching vorticity due to vertical variations of $\Theta^{(1)}$. When the averaged effects from the synoptic scales on the planetary scales are taken into account, spatial averages over the synoptic eddy fluxes appear as a source term in the PV equation. Thus the inclusion of a background zonal flow allows additional interactions between the two scales.

REFERENCES

- [1] A. Majda and R. Klein, *Systematic multi-scale models for the tropics*, J. Atmos. Sci. **2** (2003), 393–408.
- [2] R. Klein, *An Applied Mathematical View of Theoretical Meteorology*, Applied Mathematics Entering the 21st Century, invited talks at the ICIAM 2003 Conference (2004)
- [3] A. Robinson and H. Stommel, *The oceanic thermocline and the associated thermohaline circulation*, Tellus **11** (1959), 259–308.
- [4] Welander, *An advective model of the ocean thermocline*, Tellus **11** (1959).
- [5] N. A. Phillips, *Geostrophic Motion*, Reviews of Geophysics **1** (1963), 123–175.
- [6] A. P. Burger, *Scale Consideration for Planetary Motion in the Atmosphere*, Tellus **10** (1958), 195–205.
- [7] J. Pedlosky, *The Equations for Geostrophic Motion in the Ocean*, J. Phys. Ocean. **14** (1984), 448–455.
- [8] T. Matsuno, *Vertical Propagation of Stationary Planetary Waves in the Winter Northern Hemisphere*, J. Atmos. Sci. **27** (1970), 871–883.

Semi-implicit semi-Lagrangian time-stepping methods and regularized fluid equations in numerical weather prediction

SEBASTIAN REICH

(joint work with Mark Dubal, Andrew Staniforth, Nigel Wood (UK Met Office))

The fundamental components of a numerical weather prediction (NWP) code are provided by (i) data assimilation, (ii) dynamic core, and (iii) parameterization of unresolved phenomena such as precipitation. The talk is primarily concerned with numerical aspects of the dynamic core, which is defined by the inviscid Euler equations of stratified and rotating ideal fluid dynamics. I first summarize two popular approaches to deal numerically with the large variety of length and time scales of atmospheric circulation. These are (i) filtered equations such as the anelastic or the hydrostatic approximation on the one hand and (ii) semi-implicit methods on the other hand. Our focus is on approach (ii) and the semi-implicit semi-Lagrangian (SISL) time-stepping method. The SISL method is, for example, used by the UK Met Office to overcome the severe step-size restrictions due to unresolved waves as well as strong advection in their non-hydrostatic Unified Model. The idea of the Unified Model is to only use unapproximated Euler equations for the dynamic core and to have the spatial and temporal approximations select the desired spatial and temporal resolution. The practical implementation of the Unified Model methodology poses challenging questions to the practitioners and theoreticians alike. Our own current work focuses on an interpretation of the semi-implicit method as a regularization of the unapproximated Euler equations and the implementation of such a regularization within an explicit time-stepping method [2, 3, 4, 5, 6, 7, 8]. Some preliminary results for a vertical slice Euler model are presented at the end of my talk. It is also worth noting that a regularized set of equations has been used in [1] for the implementation of a particle-mesh method.

The ultimate goal of this work is to implement the regularized time-staggered semi-Lagrangian method for the three-dimensional Euler equations.

REFERENCES

- [1] J. Frank, G. Gottwald, and S. Reich, *The Hamiltonian particle-mesh method*, In M. Griebel and M.A. Schweitzer, editors, Meshfree Methods for Partial Differential Equations, volume **26** of Lect. Notes Comput. Sci. Eng., pages 131–142, Berlin Heidelberg, 2002. Springer-Verlag.
- [2] J. Frank and S. Reich, *The Hamiltonian particle-mesh method for the spherical shallow water equations*, *Atmos. Sci. Let.*, **5**, 89–95, 2004.
- [3] J. Frank, S. Reich, A. Staniforth, A. White, and N. Wood, *Analysis of a regularized, time-staggered discretization method and its link to the semi-implicit method*, *Atmos. Sci. Let.*, **6**, 97–104, 2005.
- [4] N. Wood, A. Staniforth and S. Reich, *Improved regularization for the time-staggered discretization and its link to the semi-implicit method*, *Atmos. Sci. Let.*, **7**, 21–25, 2006.

- [5] S. Reich. *Linearly implicit time stepping methods for numerical weather prediction*, BIT, in press.
- [6] A. Staniforth, N. Wood, and S. Reich. *A time-staggered semi-Lagrangian discretization of the rotating shallow-water equations*, Q.J.R. Meteorol. Soc., in press.
- [7] M. Dubal, A. Staniforth, N. Wood, and S. Reich, *Analysis of a regularized, time-staggered discretization applied to a vertical slice model*, Atmos. Sci. Let., in press.
- [8] S. Reich, N. Wood, and A. Staniforth, *Semi-implicit methods, nonlinear balance, and regularized equations*, submitted.

Data Assimilation and the 2- and 3-body Problems

IAN ROULSTONE

(joint work with L.R. Watkinson, A.S. Lawless, N.K. Nichols)

The estimation of the initial conditions for numerical weather prediction involves the assimilation of new observations into the previous forecast, over a given time window, subject to the constraint that the final state is consistent with the equations of motion and thermodynamics. Current operational numerical weather prediction methods have generally moved towards *variational* techniques (called 4DVAR, because they assimilate information distributed in space and time). Such methods involve a *cost function*, J , which is a measure of the distance between the observations, and the previous forecast, and the model state. This is then minimised in order to find a solution that lies close to both - this solution is called the *analysis*.

We are therefore concerned with the following problem: *Given a cost*

$$(1) \quad J = \int_{t_0}^{t_1} F(t, \mathbf{x}, \dot{\mathbf{x}}) dt,$$

we wish to minimise J subject to the constraint that the dependent variables, \mathbf{x} , evolve according to the equations of motion

$$(2) \quad \dot{\mathbf{x}} = f(\mathbf{x}),$$

where $\cdot \equiv \frac{d}{dt}$, and f is some (generally nonlinear) function (or functions). The value of J depends on the path between the two end points. In 4DVAR, $F(t, \mathbf{x}, \dot{\mathbf{x}})$ is a function that measures the difference between the observations, the previous forecast, and the model state.

We can rewrite this problem by defining the Lagrangian, \mathcal{L} , which takes into account the additional information provided by the constraint:

$$(3) \quad \mathcal{L} = \int_{t_0}^{t_1} (F(t, \mathbf{x}, \dot{\mathbf{x}}) + \boldsymbol{\lambda}(t)(\dot{\mathbf{x}} - f(\mathbf{x}))) dt,$$

where $\boldsymbol{\lambda}(t)$ is a vector of Lagrange multipliers. We define $G(\mathbf{x}, \boldsymbol{\lambda}, \dot{\mathbf{x}}, \dot{\boldsymbol{\lambda}}) \equiv F(t, \mathbf{x}, \dot{\mathbf{x}}) + \boldsymbol{\lambda}(t)(\dot{\mathbf{x}} - f(\mathbf{x}))$, and the following equations are necessary conditions to ensure $\delta\mathcal{L} = 0$:

$$(4) \quad G_{\mathbf{x}} - \frac{d}{dt}G_{\dot{\mathbf{x}}} = 0, \quad G_{\boldsymbol{\lambda}} - \frac{d}{dt}G_{\dot{\boldsymbol{\lambda}}} = 0.$$

These are the Euler-Lagrange equations: the first set are the *adjoint* equations and the second set are the equations of motion. Satisfying (4) is, in general, highly non-trivial: the problem is nonlinear and the coupling between (moist) thermodynamics and dynamics can also be non-smooth. Most 4DVAR algorithms are based on the assumption that the assimilation can be linearised, so that *increments* are added to the previous forecast to arrive at a new analysis.

Operational data assimilation systems should also minimise the amount of information projected onto the fast inertia-gravity waves and optimise the amount of data projected onto the slow Rossby waves. In 4DVAR, this can be achieved by adding additional constraints to the cost function to impose *balance*. Coping with strongly nonlinear processes, with multiple timescales, will be a big challenge for the development of data assimilation systems for convective-scale forecasting. Sparsity of data also presents major challenges. Typically there are far fewer observations than degrees of freedom in the model, and it is necessary to use *qualitatively useful* information, such as the *background state* (the previous forecast), and balance conditions (such as geostrophy), applied via additional quadratic penalty terms in the cost function, to help fill the ‘data gaps’. These are known as *weak* constraints and are so-called due to the fact that they do not have to be *exactly* satisfied by the solution.

With these issues in mind, in [1] and [2] we have applied 4DVAR to the 2- and 3-body problems of celestial mechanics. The 2-body problem satisfies Kepler’s laws, and these laws provide *qualitatively useful* information that can be used in the data assimilation. The 3-body problem is a system that can exhibit instability and chaos, and can be set up so that it possesses two distinct timescales.

In the Kepler problem we have two bodies in orbit around each other, obeying Newton’s law of gravitation. We choose the origin to lie at the centre of mass, so that we have one body with *reduced mass*, $\mu \equiv (m_1 m_2)/(m_1 + m_2)$, orbiting the other body of mass $M = m_1 + m_2$. Motion is restricted to a plane. In terms of positions, \mathbf{q} , and momenta, \mathbf{p} , the equations of motion can be written (in Hamiltonian form):

$$\frac{d\mathbf{q}}{dt} = \mathbf{p}, \quad \frac{d\mathbf{p}}{dt} = -\frac{\mathbf{q}}{(q_1^2 + q_2^2)^{\frac{3}{2}}}.$$

This system conserves energy, E , and angular momentum, L :

$$E = \frac{1}{2}(p_1^2 + p_2^2) - \frac{1}{(q_1^2 + q_2^2)^{\frac{1}{2}}}, \quad L = q_1 p_2 - q_2 p_1.$$

A Störmer-Verlet scheme is used to integrate these equations:

$$(5) \quad \mathbf{P}^{n+\frac{1}{2}} = \mathbf{P}^n - \frac{h}{2} \frac{\mathbf{Q}^n}{(Q_1^{n^2} + Q_2^{n^2})^{\frac{3}{2}}}$$

$$(6) \quad \mathbf{Q}^{n+1} = \mathbf{Q}^n + h\mathbf{P}^{n+\frac{1}{2}}$$

$$(7) \quad \mathbf{P}^{n+1} = \mathbf{P}^{n+\frac{1}{2}} - \frac{h}{2} \frac{\mathbf{Q}^{n+1}}{(Q_1^{n+1^2} + Q_2^{n+1^2})^{\frac{3}{2}}},$$

where h is the timestep. A linear model is then constructed by linearizing the discrete equations (which results in the so-called *tangent linear equations*).

Define $\mathbf{x} \equiv (q_1, q_2, p_1, p_2)$ and $\boldsymbol{\lambda} \equiv (\lambda_1, \lambda_2, \lambda_3, \lambda_4)$, then the Euler-Lagrange equations (4) can be written in the Hamiltonian form

$$(8) \quad \dot{\boldsymbol{\lambda}} = \frac{\partial H}{\partial \mathbf{x}}; \quad \dot{\mathbf{x}} = -\frac{\partial H}{\partial \boldsymbol{\lambda}}$$

where

$$H(\boldsymbol{\lambda}, \mathbf{x}) = F(\mathbf{x}) - p_1\lambda_1 - p_2\lambda_2 + \frac{(\lambda_3 q_1 + \lambda_4 q_2)}{(q_1^2 + q_2^2)^{\frac{3}{2}}}$$

Among our results, we show that imposing weak penalties that constrain the energy and angular momenta of the analysis to be close to that of the previous forecast improves the subsequent forecast considerably. We introduce a background penalty: this constraint measures the distance between the model state at the initial time and the background field (previous forecast) at the same time. The constraint has the form $J_B = \alpha_1(\mathbf{x}_b(t_0) - \mathbf{x}(t_0))^T(\mathbf{x}_b(t_0) - \mathbf{x}(t_0))$, where $\mathbf{x}_b = (\mathbf{q}_b, \mathbf{p}_b)^T$ is the background state, with $\mathbf{q}_b \equiv \mathbf{q}(t_0)$ etc. The second constraint makes use of the energy conservation property of the system. Here we measure the distance between the energy of the model state at the initial time and the energy of the background at the same time. It has the form $J_E = \alpha_2(E(\mathbf{x}_b(t_0)) - E(\mathbf{x}(t_0)))^2$. We also investigate imposing a weak constraint such that the angular momentum of the analysis is close to the angular momentum of the background. This reflects the angular momentum conservation property of the two body problem. This has the form $J_L = \alpha_3(L(\mathbf{x}_b(t_0)) - L(\mathbf{x}(t_0)))^2$. In all three cases the α s are the weights.

We show that in all cases the weak constraints improve the forecast. However the behaviour of the solutions is different. If only the background penalty is imposed, we see that the error in the forecast is reduced but it is still increasing with time. When we include the energy constraint as well, there is a further reduction in the error in the forecast; however, in this case, for large values of α_2 , the error actually stops increasing. This behaviour is repeated when we impose the angular momentum constraint.

We can explain the difference in the effectiveness of the constraints by considering the inherent characteristics of the 2-body problem. We observe that the error of the unconstrained case is increasing. This behaviour can be caused by comparing two solutions that are out of phase with each other, implying that the orbital periods of the two solutions are different. From Kepler's third law we know that a change in the orbital period means a change in the semi-major axis of the

orbit. Thus we are comparing two solutions, the analysis and the truth, with different semi-major axes. However, the energy of a given orbit is dependent on the semi-major axis. Thus two solutions with different semi-major axes will have different orbital energies. Consequently, using the energy constraint helps to keep one of the qualitative features of the problem consistent from one forecast to the next. Similar results are obtained for the more complicated scenarios explored in the 3-body problem.

REFERENCES

- [1] L.R. Watkinson, *Four-Dimensional Variational Data Assimilation for Hamiltonian Problems*, PhD Thesis, University of Reading, September 2006.
- [2] L.R. Watkinson, A.S. Lawless, N.K. Nichols & I. Roulstone *Variational data assimilation for Hamiltonian problems*, Int. J. Num. Meth. Fluids, **47** (2005), 1361–1367.

Unstructured adaptive grid refinement in atmospheric and ocean modeling

LARS MENTRUP

(joint work with Jörn Behrens)

Resolving large as well as small scales and studying their interaction is one key challenge of atmospheric and oceanic simulation. Adaptivity of meshes is a fundamental means to find a deeper insight into these multiscales phenomena. At the same time computer resources are efficiently used at regions of interest, preventing the computational overkill of uniform refinement.

We first introduced amatos [1], which is a software package for adaptive grid generation. It supports planar and spherical geometries based on triangular elements. amatos relieves the researcher of the task of grid management. By using the grid generator, one basically decouples the numerical computation from grid generating and adaptation processes. Many features as FEM/SEM-support, interpolation at given points and support for semi-Lagrangian time-stepping are included in amatos. One of the latest developments is the implementation of space-filling curve ordering of indices offering advantages in a) parallelization through ease of domain decomposition, b) cache access optimization and c) very good preconditioning properties when it comes to iterative matrix solvers. More information on amatos and space-filling curves ordering can be found in [1, 3]. amatos is open source and can be downloaded on www.amatos.info.

Secondly, we presented the classic semi-Lagrangian approach for advection simulation. We showed that the discretization of the divergence-free formulation in differential form

$$\frac{d\rho}{dt} = \frac{\partial \rho}{\partial t} + a(x, t) \frac{\partial \rho}{\partial x} = 0$$

where ρ is a scalar representing density and $a(x, t) \in \mathbb{R}^d, d = 2, 3$ is a given windfield, is not mass conservative by construction. The challenge to develop

mass conservative semi-Lagrangian schemes motivated our new approach. The starting point for this task is the discretization of the integral form

$$\int_{V(x,t)} \rho(x,t) dx = \int_{V(x-\alpha(x),t-\Delta t)} \rho(x,t-\Delta t) dx$$

where $\alpha(x)$ is the upstream trajectory prescribed by the windfield $a(x,t)$. Note that for divergence-free $a(x,t)$ differential and integral form are equivalent. Defining the control volumes $V(x,t)$ can be done in different ways. We presented two different schemes implementing this new approach, namely the mass packet semi-Lagrangian method (MPSLM) [5, 8] and the cell-integrated semi-Lagrangian method (CISLM) [4]. While the MPSLM is discretizing the control volumes by sub-grid cells, so-called mass packets, the CISLM is using dual cells. Both schemes compute the upstream control volume $V(x - \alpha(x), t - \Delta t)$ and either collect the mass packets having a non-zero cut set with the control volume (MPSLM) or computing the exact intersection of $V(x - \alpha(x), t - \Delta t)$ and cells of the previous time-step grid (CISLM). Results showing mass conservation of both methods were presented.

The third part of our talk addressed an important task in grid refinement: Controlling the grid refining and coarsening process. Most grid refinement strategies at present use heuristic, physically motivated methods as refinement criterion, e.g. the gradient of a quantity of interest. In contrast, the a posteriori error estimation is a mathematically more rigorous approach based on the computed solution. A posteriori error estimation gains increasing popularity, guaranteeing reliability and efficiency of the computed error estimate. We introduced the basics of the Zienkiewicz-Zhu a posteriori error estimator. This averaging technique was proven to be reliable and efficient [6]. First tests showed encouraging results.

Finally, we presented applications based on amatos. First, results of the adaptive shallow water model on the sphere (including the poles) by Heinze, called PLASMA-FEMmE [7] were shown. For test case 5 of the Williamson test suite, the resolution at regions of interest is doubled while the computational time does not increase. PLASMA-FEMmE demonstrates very good conservation properties for the quantities of total mass (0.998), total energy (0.997) and potential enstrophy (0.994) after 15 days (1440 time-steps) of simulation time. Secondly, results of an adaptive tsunami model in development by Behrens using amatos were presented. Preliminary results modeling a tsunami event in a channel with decreasing water height over ground were shown. Both applications emphasized the mature status of the grid generator amatos.

A synopsis of techniques for adaptive atmospheric modeling can be found in [2].

REFERENCES

- [1] J. Behrens, *Adaptive mesh generator for atmospheric and oceanic simulations – amatos*, Technische Universität München, 2004.
- [2] J. Behrens, *Adaptive atmospheric modeling*, Lecture Notes in Computational Science and Engineering, **54**, Springer, 2006.

- [3] J. Behrens, *amatos: Parallel adaptive mesh generator for atmospheric and oceanic simulation*, Ocean Modelling, **10** (2005), no. 1–2, 171–183.
- [4] J. Behrens, L. Mentrup, *A Cell-Integrated Semi-Lagrangian advection scheme on adaptive unstructured triangular meshes*, submitted.
- [5] J. Behrens, L. Mentrup, *A conservative scheme for 2D and 3D adaptive semi-Lagrangian advection*, in: Recent Advances in Adaptive Computation, Contemporary Mathematics, **383** (2005), 175–189.
- [6] C. Carstensen, *All first-order averaging techniques for a posteriori finite element error control on unstructured grids are efficient and reliable*, Math. Comp., **73** (2004), 1153–1165.
- [7] T. Heinze, *An Adaptive Shallow Water Model on the Sphere*, personal communication, 2006.
- [8] L. Mentrup, *Entwicklung einer massenerhaltenden Semi-Lagrange-Methode (SLM) zur Simulation von Spurenstofftransport in der Atmosphäre auf einem adaptiven dreidimensionalen Gitter*, Diploma thesis, Technische Universität München, 2003.

The Emergence of Large Scale Coherent Structure under Small Scale Random Bombardments

ANDREW MAJDA AND XIAOMING WANG

We provide mathematical justification of the emergence of large scale coherent structure in a two dimensional fluid system under small scale random bombardments with small data assumptions. The analysis shows that the large scale structure emerging out of the small scale random forcing is not the one predicted by equilibrium statistical mechanics. But the error is very small which explains earlier successful prediction of the large scale structure based on equilibrium statistical mechanics.

REFERENCES

- [1] Majda, A.J.; Abramov, R.V.; Grote, M.J.; *Information Theory and Stochastics for Multiscale Nonlinear Systems*. AMS, Providence, RI. 2005.
- [2] Majda, A.J.; Wang, X., 2006, *The emergence of large-scale coherent structure under small-scale random bombardments*, (p 467-500) Communications on Pure and Applied Mathematics, Volume 59, Issue 4 (2006), pp.467-500.
- [3] Majda, A.J.; Wang, X., *Nonlinear Dynamics and Statistical Theories for Basic Geophysical Flows*. Cambridge University Press, 2006.

Inertia-gravity waves emitted spontaneously from quasi-balanced flow: properties and consequences

PAUL DAVID WILLIAMS

(joint work with Thomas W. N. Haine, Peter L. Read [1])

Inertia-gravity waves are observed ubiquitously throughout the stratified parts of the atmosphere and ocean. Orthodox mechanisms for inertia-gravity wave generation include dynamical instability, such as Kelvin-Helmholtz shear instability. Another possible mechanism is the interaction between the flow and a physical obstruction, which is the mechanism by which mountains generate atmospheric gravity waves. Direct forcing of the ocean by the atmosphere is an important source of oceanic gravity waves.

Despite the above insights, our understanding of the sources of inertia-gravity waves remains rudimentary. For instance, a further potential source is spontaneous emission from quasi-balanced flow [2]. This is a generalization of the classical geostrophic adjustment process [3], in which an unbalanced flow tends to establish geostrophic balance by shedding excess energy as transient inertia-gravity waves. It has been shown that even first-order balanced flows undergo a generalized adjustment process that is accompanied by the spontaneous emission of inertia-gravity waves [4]. It is proving extraordinarily difficult to determine whether or not this mechanism is a significant source of inertia-gravity waves in real geophysical flows, however [5]. This hinders the development of parameterisations of the waves in general circulation models.

The spontaneous emission of inertia-gravity waves is intimately related to the concept of the slow manifold [6, 7]. The slow manifold is a putative, invariant sub-manifold of phase space, upon which the fluid remains completely devoid of inertia-gravity waves. The strict existence of the slow manifold, and hence the possibility of a flow evolving without ever spontaneously emitting inertia-gravity waves, has long been debated. The formal non-existence of the slow manifold is now generally accepted, however.

Even accepting the inevitability of spontaneous inertia-gravity wave emission, the possibility remains that the emitted waves will be sufficiently weak that they merely perturb the slow manifold into a quasi-stochastic fuzzy manifold [8] that retains many of its useful properties. The amplitude of spontaneously-emitted inertia-gravity waves, and its dependence on the bulk flow properties (especially the Rossby number), is therefore of great interest.

In this report, I summarize the properties of observed inertia-gravity waves emitted spontaneously from quasi-balanced flow, and the consequences for loss of balance from the atmospheric and oceanic mesoscale. In a laboratory study using a rotating two-layer annulus [9], it is found that all evolving quasi-balanced flows emit inertia-gravity waves spontaneously. It has been shown [10] that the appearance of the waves is well-predicted by the radiation term derived by [4], following [11].

Two important issues arise from this study. First, the quasi-balanced flow leaks roughly 1% of its energy each rotation period into inertia-gravity waves at the peak of their generation. Extrapolation of this result suggests that the spontaneous emission mechanism might make a significant contribution to the energy budgets of the ocean and atmosphere. For example, it is crudely estimated that $O(1\text{TW})$ is being lost from balanced mesoscale ocean eddies into the internal wave field, suggesting that this mechanism might be a significant player in maintaining the deep ocean stratification.

Second, the inertia-gravity wave amplitude shows a broadly linear variation with Rossby number in the range 0.05–0.14, at constant Froude number. This is in disagreement with asymptotic and non-asymptotic theories, which predict algebraic and exponential variation, respectively [12, 13]. This suggests that the fuzzy manifold is not exponentially thin in Rossby number, as previously thought. This has potentially important implications for the fundamental dynamical concepts of balance and potential vorticity inversion.

An asymptotic renormalization theory appears to yield the observed linear Rossby number scaling. The theory is based on that of [14] in the small Rossby number (Ro) limit. The first-order renormalized equation contains only resonant triplet interactions and thus cannot generate inertia-gravity waves from quasi-balanced potential vorticity modes. In fact, if the initial inertia-gravity wave energy is zero, the equation reduces to quasi-geostrophic dynamics. The renormalized solution also contains a first-order slaved term consisting only of inertia-gravity waves, however. This term is zero initially, but increases in a few fast wave periods to be $O(\text{Ro})$. The inertia-gravity waves are slaved to the quasi-balanced flow and are not freely propagating. In this sense a slow manifold still exists because the entire flow can still be deduced from potential vorticity inversion.

REFERENCES

- [1] P. D. Williams, T. W. N. Haine, D. Ring, P. L. Read & G. L. Eyink, *Inertia-gravity waves emitted spontaneously from quasi-balanced flow: properties and consequences* submitted to J. Atmos. Sci. (2007).
- [2] R. Ford, M. E. McIntyre & W. A. Norton, *Balance and the slow quasimaniold: some explicit results*, J. Atmos. Sci. **57** (2000), 1236-1254.
- [3] C. G. Rossby, *On the mutual adjustment of pressure and velocity distributions in certain simple current systems. II* J. Mar. Res. **2** (1938), 239-263.
- [4] R. Ford, *Gravity wave radiation from vortex trains in rotating shallow water*, J. Fluid Mech. **281** (1994), 81-118.
- [5] M. E. McIntyre, *Global effects of gravity waves in the middle atmosphere: a theoretical perspective* Advances in Space Research **27** (2001), 1723-1736.
- [6] C. E. Leith, *Nonlinear normal mode initialization and quasi-geostrophic theory* J. Atmos. Sci. **37** (1980), 958-968.
- [7] E. N. Lorenz, *Attractor sets and quasi-geostrophic equilibrium* J. Atmos. Sci. **37** (1980), 1685-1699.

- [8] T. Warn & R. Menard, *Nonlinear balance and gravity-inertial wave saturation in a simple atmospheric model* Tellus **38A** (1986), 285-294.
- [9] P. D. Williams, P. L. Read, & T. W. N. Haine, *Spontaneous generation and impact of inertia-gravity waves in a stratified, two-layer shear flow* Geophys. Res. Lett. **30**(24) (2003), 2255.
- [10] P. D. Williams, T. W. N. Haine & P. L. Read, *On the generation mechanisms of short-scale unbalanced modes in rotating two-layer flows with vertical shear* J. Fluid Mech. **528** (2005), 1-22.
- [11] M. J. Lighthill, *On sound generated aerodynamically. I: General theory* Proc. R. Soc. Lond. **211** (1952), 564-587.
- [12] J. Vanneste & I. Yavneh, *Exponentially small inertia-gravity waves and the breakdown of quasigeostrophic balance* J. Atmos. Sci. **61** (2004), 211-223.
- [13] R. Plougonven, D. J. Muraki & C. Snyder, *A baroclinic instability that couples balanced motions and gravity waves* J. Atmos. Sci. **62** (2005), 1545-1559.
- [14] D. Wirossetisno, T. G. Shepherd & R. M. Temam, *Free gravity waves and balanced dynamics* J. Atmos. Sci. **59** (2002), 3382-3398.

The primary nonlinear dynamics of modal and nonmodal perturbations of monochromatic inertia-gravity waves

ULRICH ACHATZ

The importance of gravity waves for the dynamics of the middle atmosphere via their momentum and energy deposition has been known for a long time. Since the major part of the corresponding wave spectrum is at scales which cannot be resolved within state-of-the-art general circulation models these can only incorporate gravity-wave effects via parameterizations. With this regard there are still considerable uncertainties since many details of (mostly tropospheric and stratospheric) gravity-wave radiation, propagation through the middle atmosphere, and breaking, predominantly in the mesosphere-lower-thermosphere (MLT), are not sufficiently understood yet [6]. With regard to the breaking process itself, a systematic approach, starting with a linear analysis, and using the thereby identified instability patterns for distinctly perturbing a wave, had not been done yet. This might, however, be useful for the derivation of paradigms of wave breaking which could be used in improved parameterization schemes. As a first step in such a procedure, the linear stability of monochromatic gravity waves has been reinvestigated by [1] and [4, 5]. A fundamental result is that even in the absence of classic normal-mode (NM) instabilities vigorous transient growth of singular vectors (SV) is still possible. Especially for inertia-gravity waves (IGWs) this puts traditionally used instability thresholds, such as those of static instability (negative vertical buoyancy gradient) or dynamic instability (sufficiently strong vertical shear), at question.

Based on these results the breaking of an inertia-gravity wave, initiated by its leading NMs or SVs, and the resulting small-scale eddies have been investigated by means of direct numerical simulations of a Boussinesq fluid characterizing the

upper mesosphere. The focus was on the primary nonlinear dynamics, neglecting the effect of secondary instabilities. It was found that the structures with the strongest impact on the IGW and also the largest turbulence amplitudes are the NM (for a statically unstable IGW) or short-term SV (statically and dynamically stable IGW) propagating horizontally transversely with respect to the IGW, possibly in agreement with observations of airglow ripples in conjunction with statically unstable IGWs. In both cases these leading structures reduce the IGW amplitude well below the static and dynamic instability thresholds (Fig. 1). The resulting turbulent dissipation rates are within the range of available estimates from rocket soundings, even for IGWs at amplitudes low enough precluding NM instabilities. SVs thus can help explaining turbulence occurring under conditions not amenable for the classic interpretation via static and dynamic instability. Due to an important role of the statically enhanced roll mechanism in the energy exchange between IGW and eddies the turbulent velocity fields are often conspicuously anisotropic. The spatial turbulence distribution is determined to a large degree by the elliptically polarized horizontal velocity field of the IGW. Further details can be found in [2]. This work illustrates the necessity to reconsider the parameterization of IGW breaking in a broader context which also takes nonmodal instabilities into account. Moreover, a complementary paper [3] shows, in agreement with [7, 8], that the neglect of the horizontal gradients in high-frequency gravity waves causes serious errors in the estimate of the instability thresholds for these waves. Thus, present parameterization schemes cannot be seen as much more than a very coarse tool helping us to get some momentum deposition in the mesosphere, without much quantitative realism.

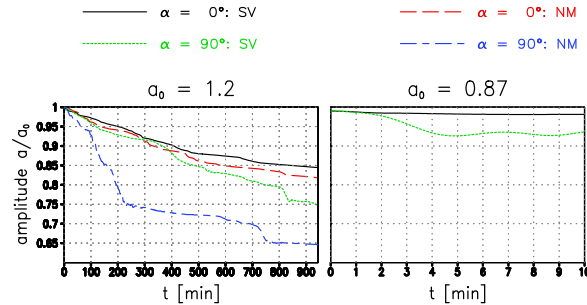


FIGURE 1. For a (right) statically and dynamically stable IGW (initial amplitude with respect to the overturning threshold $a_0 = 0.87$, no unstable NM) or a statically unstable IGW (left, $a_0 = 1.2$), the time dependence of the IGW amplitude a , normalized by a_0 , from integrations after a perturbation by the leading SVs or NMs at azimuth angles $\alpha = 0, 90^\circ$.

REFERENCES

- [1] U. Achatz, *On the role of optimal perturbations in the instability of monochromatic gravity waves*, Phys. Fluids, **17**, (2005), 094107 1–27.
- [2] U. Achatz, *The primary nonlinear dynamics of modal and nonmodal perturbations of monochromatic inertia-gravity waves*, J. Atmos. Sci., (2006) in press.
- [3] U. Achatz, *Modal and nonmodal perturbations of monochromatic high-frequency gravity waves: Primary nonlinear dynamics*, J. Atmos. Sci., (2006), in press.
- [4] U. Achatz and G. Schmitz, *Shear and static instability of inertia-gravity wave packets: Short-term modal and nonmodal growth*, J. Atmos. Sci., **63**, (2006), 397–413.
- [5] U. Achatz and G. Schmitz, *Optimal growth in inertia-gravity wave packets: Energetics, long-term development, and three-dimensional structure*, J. Atmos. Sci., **63**, (2006), 414–434.
- [6] D. C. Fritts, and M. J. Alexander, *Gravity wave dynamics and effects in the middle atmosphere*. Rev. Geophys., **41**, (2003), 1003, doi:10.1029/2001RG000106.
- [7] D. C. Fritts, C. Bizon, J. A. Werne, and C. K. Meyer, *Layering accompanying turbulence generation due to shear instability and gravity-wave breaking*. J. Geophys. Res., **108**, (2003), 8452, doi:10.1029/2002JD002406.
- [8] D. C. Fritts, S. L. Vadas, K. Wan, and J. A. Werne, *Mean and variable forcing of the middle atmosphere by gravity waves*. J. Atmos. Sol.-Terr. Phys., (2006), **68**, 247–265.

A Resonant Instability of Finite-Amplitude Mountain Waves

DAVID J MURAKI

(joint work with Youngsuk Lee, David Alexander & Craig Epifanio)

When density-stratified air is forced by winds over elevated terrain, the vertical displacement of the flow results in a downstream pattern of dispersing waves. The effects of these gravity waves can often be visualized through clouds which do not drift with the winds, but remain stationary with respect to the topography. Such vertical disturbances to the flow are important in the understanding of the microscale variations in cloud and precipitation patterns for alpine communities (and ski resorts). Intense wave activity is also an aviation hazard when encountered as in-flight turbulence.

Linear theories for stratified flow over topography were first established during the 1940's with the pioneering works of Lyra [1], Queney [2] and Scorer [3]. The first significant theory to address nonlinearity occurred soon thereafter, when

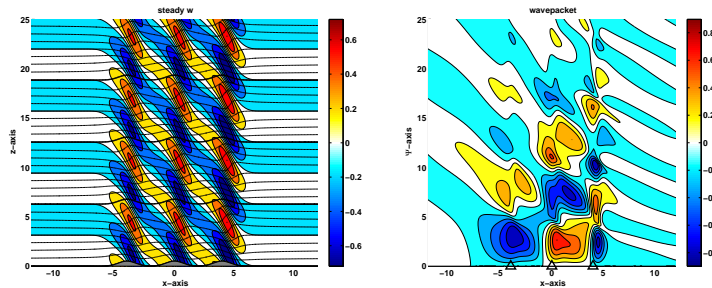


FIGURE 1. The left panel shows the vertical motion field (shading) for steady, hydrostatic flow over three mountains, along with the corresponding streamlines (solid). The right panel shows the disturbance streamfunction for the most unstable mode (growth rate ≈ 0.08 & frequency ≈ 0.32).

Long [4] noted that the steady theory for stratified flow over two-dimensional topography could be exactly expressed as a single equation for the streamfunction.¹ Furthermore, conditions of uniform upstream wind and constant density stratification (under a Boussinesq assumption) represent a remarkable special case where the theory reduces to the linear Helmholtz equation.

A counterpoint to this theory of stable, steady waves over topography is the well-established fact that periodic plane gravity waves are subject to a nonlinear instability. Floquet theory [7, 8, 9] has shown that a sinusoidal gravity wave, even of infinitesimal amplitude, is parametrically unstable through resonant wave interactions (see also the review by Staquet & Sommeria [10])). The possibility that this resonance mechanism has implications for topographic flow was noted in the original hydrostatic simulations of Klemp & Lilly [11], where the theoretical steady solutions were not achieved for flow past periodic topography.

The steady mountain waves are known to be unstable for topographic heights for which there are overturning streamlines/isentropes [12]. However, recent two-dimensional simulations for non-periodic topography clearly show that an oscillatory instability of steady flow over two (or more) isolated peaks can occur well-below the overturning threshold (Epifanio & Muraki, in preparation). For hydrostatic steady mountain waves, a linear stability analysis produces unstable modes that well-reproduce the simulations, and identifies the instability mechanism as a triad resonance.

REFERENCES

- [1] G. Lyra, *Über den Einfluß von Bodenerhebungen auf die Strömung einer stabil geschichteten Atmosphäre*, Beitr. Phys. Freien Atmos., **26** (1940), 197–206.

¹Very early appearances of the non-Boussinesq version of the streamfunction theory are found in Dubreil-Jacotin [5, 6]. The context for her studies addressed surface water waves, rather than the topographic flow problem.

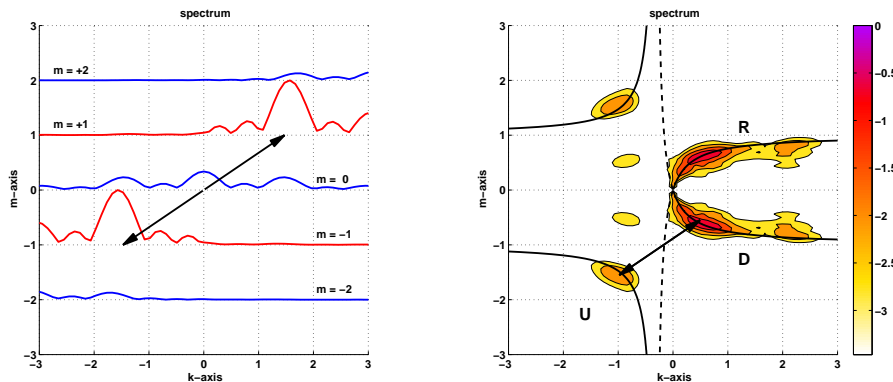


FIGURE 2. The left panel shows the spectral amplitudes of the steady waves (as obtained from an isentropic coordinate geometry). Because of 2π -periodicity in the vertical, the spectrum is discrete in the vertical wavenumber m . The right panel shows the log spectral amplitudes of the disturbance streamfunction. The triad resonance is identified by the observation that the wavevector of the maximum spectral peak of the steady solution connects two of the spectral wavepackets (U,D) of the unstable mode.

- [2] P. Queney, *The problem of air flow over mountains: A summary of theoretical results*, Bull. Amer. Meteor. Soc., **29** (1948), 16–26.
- [3] R.S. Scorer, *Theory of waves in the lee of mountains*, Quart. J. Roy. Met. Soc., **75** (1949), 41–56.
- [4] R.R. Long, *Some Aspects of the Flow of Stratified Fluids. I. A Theoretical Investigation*, Tellus, **5** (1953), 42–58.
- [5] M.L. Dubreil-Jacotin, *Complément à une note antérieure sur les ondes de type permanent dans les liquides hétérogènes*, Atti della R. Acc. Naz. dei Lincei, **21** (1935), 344–346.
- [6] M.L. Dubreil-Jacotin, *Sur les théorèmes d'existence relatifs aux ondes permanentes périodiques à deux dimensions dans les liquides hétérogènes*, J. Math. Pures Appl., **16** (1937), 43–67.
- [7] R. Mied, *The occurrence of parametric instabilities in finite-amplitude internal gravity waves*, J. Fluid Mech., **78** (1976), 763–784.
- [8] P. Drazin, *On the instability of an internal gravity wave*, Proc. R. Soc. Lond. A, **356** (1977), 411–432.
- [9] J. Klostermeyer, *On parametric instabilities of finite-amplitude internal gravity waves*, J. Fluid Mech., **119** (1982), 367–377.
- [10] C. Staquet & J. Sommeria, *Internal gravity waves: From instabilities to turbulence*, Ann. Rev. Fluid Mech., **34** (2002), 559–593.
- [11] J. Klemp & D. Lilly, *Numerical simulation of hydrostatic mountain waves*, J. Atmos. Sci., **35** (1979), 78–107.

- [12] J. Scinocca & W. Peltier, *The instability of Long's stationary solution and the evolution toward severe downslope windstorm flow. part i: Nested grid numerical simulations*, J. Atmos. Sci., **50** (1993), 2245–2263.

Spherical Hamiltonian Isentropic 2-Layer Model for Atmospheric Dynamics

ONNO BOKHOVE

(joint work with Marcel Oliver)

Introduction Recently, it has been shown that the numerical Hamiltonian particle mesh method of Frank, Gottwald and Reich [4] arises from a parcel Eulerian-Lagrangian (EL) formulation [2,3]. A parcel Eulerian-Lagrangian Hamiltonian formulation consists of a non-autonomous Hamiltonian description of a particular fluid parcel with as single parcel Hamiltonian function the sum of its kinetic energy (the velocity magnitude squared) and an Eulerian potential evaluated at the parcel's position. However, the fluid is a continuum collection of such particular fluid parcels. The Eulerian potential depends on an Eulerian (pseudo)density and, furthermore, this (pseudo)density is related to all fluid parcel by an integral relation which thus establishes the continuum nature of the fluid. Bokhove and Oliver [2,3] show that several geophysical fluid systems have a parcel EL Hamiltonian formulations, which are readily related to corresponding Eulerian Hamiltonian formulations. The advantages of the new parcel formulation are that it provides new insights into Hamiltonian systems and sometimes simplifies the use of mathematical techniques. Bokhove [1] first used these EL formulations to study balanced models with asymptotic theory and to revisit classic parcel instabilities. As an example, a two-layer model with an isentropic tropospheric and an isentropic stratospheric layer will be derived here on the sphere within the parcel EL framework. Subsequently, it can be shown that the Eulerian Hamiltonian formulation of the two-layer equations readily follows from the parcel EL formulation. Further questions under investigation are whether numerical Hamiltonian particle mesh methods remain worthwhile in the presence of weak forcing and dissipation.

Parcel Eulerian-Lagrangian Hamiltonian formulation Consider an isentropic two-layer atmosphere on the sphere. In the troposphere the potential temperature (or entropy) is taken constant, $\theta = \theta_2$, and, similarly, in the stratosphere the potential temperature is constant $\theta = \theta_1$ with $\theta_1 > \theta_2$. The variables in these layers and at their interfaces are sketched in Fig. 1. The pressure at the bottom topography at $r = r_2(\lambda, \phi)$ is $p_2(\lambda, \phi, t)$ with r the radial coordinate, λ and ϕ the latitude-longitude coordinates, and t the time. The pressure at the tropopause, the interface between troposphere and stratosphere at $r = r_1(\lambda, \phi)$, is $p_1(\lambda, \phi, t)$. The pressure at the top $r = r_0(\lambda, \phi, t)$ of the stratosphere is $p_0 \approx 0$. In these layers the horizontal velocity depends on the latitude-longitude coordinates and time. When the horizontal length and velocity scales along the sphere are much

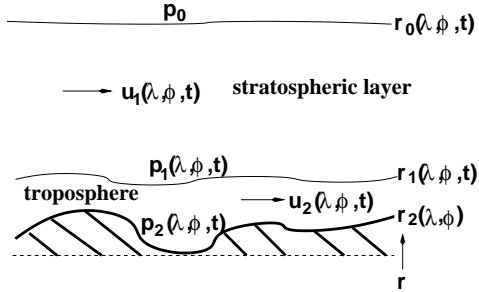


FIGURE 1. Sketch of an atmosphere consisting of an isentropic tropospheric and isentropic stratospheric layer.

larger than the vertical ones this is a leading order approximation. Furthermore, hydrostatic balance holds to leading order in the radial or vertical direction.

We use subscripts $\alpha = 1, 2$ for the variables in and associated with the tropospheric and stratospheric layers. These are dropped when no confusion arises. Consider a fluid parcel in one of the layers, on a rotating Earth. It has coordinates $X^1 = \lambda$ and $X^2 = \phi$. The corresponding velocities follow from the spherical geometry as $U = R \cos \phi \dot{\lambda}$ and $V = R \dot{\phi}$ with $\dot{\lambda} = d\lambda/dt$ and $\dot{\phi} = d\phi/dt$, using $r \approx R$. Related to these velocities are the following covariant (bold lower indices) and contravariant (bold upper indices) vectors

$$(1) \quad U_1 = U^1 R^2 \cos^2 \phi = U R \cos \phi \quad \text{and} \quad U_2 = U^2 R^2 = V R.$$

The kinetic energy on a sphere rotating with a speed Ω is

$$(2) \quad E_{\text{kin}} = \frac{1}{2} \left(R^2 \cos^2 \phi (\dot{\lambda} + \Omega)^2 + (R \dot{\phi})^2 \right) = \frac{1}{2} (\tilde{U}^2 + \tilde{V}^2)$$

for each layer. The effective potential for each layer α is

$$(3) \quad V = M(\lambda, \phi) + \frac{1}{2} \Omega^2 R^2 \cos^2 \phi$$

with Eulerian Montgomery potential $M = M(X^1, X^2)$ and a centrifugal force contribution. The Euler-Lagrange equations for one fluid parcel then follow from the variational principle $0 = \delta \int_{t_0}^{t_1} E_{\text{kin}} - V dt$. The associated canonical Hamilton's equations subsequently emerge via a Legendre transformation. Instead, we prefer the following non-canonical formulation. The non-canonical Hamiltonian equations for each layer parcel in this spherical shell geometry then become

$$(4) \quad \frac{dX^1}{dt} = \frac{U_1}{R^2 \cos^2 X^2} = \frac{\partial H}{\partial U_1} \quad \text{and} \quad \frac{dX^2}{dt} = \frac{U_2}{R^2} = \frac{\partial H}{\partial U_2}$$

$$(5) \quad \frac{dU_1}{dt} = 2 \Omega R^2 \cos X^2 \sin X^2 \frac{\partial H}{\partial U_1} - \frac{\partial H}{\partial X^1}$$

$$(6) \quad \frac{dU_2}{dt} = -2 \Omega R^2 \cos X^2 \sin X^2 \frac{\partial H}{\partial U_2} - \frac{\partial H}{\partial X^2}$$

with in each layer the Hamiltonian

$$(7) \quad H = \frac{1}{2} (U_1 U^1 + U_2 U^2) + M(X^1, X^2, t) = \frac{1}{2} (U^2 + V^2) + M(\lambda, \phi, t).$$

Montgomery potentials The next step is to derive the Montgomery potentials M_α for $\alpha = 1, 2$. In the troposphere the potential temperature is constant $\theta = \theta_2$ and the ideal gas law $p = \rho R T$ is used with temperature $T = \theta \eta^\kappa$, density ρ and gas constant R . We can therefore rewrite the following expression

$$(8) \quad (\nabla p)/\rho + \nabla(g r) = \nabla(\theta \Pi + g r) = \nabla M,$$

where $\Pi = c_p \theta \eta^\kappa$ is the Exner function, $\eta = p/p_r$ with reference pressure p_r , and $\kappa = R/c_p$ the ratio of R over the specific heat c_p at constant pressure. We have assumed that hydrostatic balance holds in the radial direction, which thus obtains the form $\partial M/\partial r = 0$ after using (8) in the respective layers. After integration of this hydrostatic balance relation from the Earth's surface at $r = r_2$ to $r < r_1$ one obtains

$$(9) \quad M = c_p \theta_2 \eta^\kappa + g r = M_2 = c_p \theta \eta_2^\kappa + g r_2.$$

Integration of hydrostatic balance from $r > r_1$ to $r = r_0$ in the stratosphere gives likewise

$$(10) \quad M = c_p \theta_1 \eta^\kappa + g(r - R_0) = g(r_0 - R_0)$$

with $p_0 \approx 0$ and a constant reference height R_0 . Using continuity of pressure $p_1 = p_2$ at interface r_1 , one finds

$$(11) \quad M_1 = c_p \theta_1 \eta_1^\kappa + c_p \theta_2 (\eta_2^\kappa - \eta_1^\kappa) + g(r_2 - R_0).$$

In addition, pseudo-densities $\sigma_1 = p_1/g$ and $\sigma_2 = (p_2 - p_1)/g$ are defined such that $M_\alpha = M_\alpha(\sigma_1, \sigma_2, z_2)$.

To derive the Eulerian Hamiltonian formulation on the sphere from the parcel Hamiltonian formulation (4)–(7), relations between functional and function variational and time derivatives are required as in [2,3]. The mass of a layer column is $dM = da db = \sigma R^2 \cos x^2 dx^1 dx^2$. By definition

$$(12) \quad \sigma_\alpha(x^1, x^2, t) = \iint \sigma_\alpha(\tilde{x}^1, \tilde{x}^2, t) \delta(x^1 - \tilde{x}^1) \delta(x^2 - \tilde{x}^2) d\tilde{x}^1 d\tilde{x}^2$$

$$(13) \quad = \iint \frac{\delta(x^1 - \chi_\alpha^1) \delta(x^2 - \chi_\alpha^2)}{\sqrt{\mu}} da db$$

with parcel coordinates $\tilde{x}^1 = \chi_\alpha^1(a, b, t)$, $\tilde{x}^2 = \chi_\alpha^2(a, b, t)$ and parcel labels $(a, b)^T$, and $\sqrt{\mu} = R^2 \cos \phi_\alpha$. For a particular label $(A, B)^T$: $(X^1(t), X^2(t))^T = \chi(A, B, t)$. These integral relations reveal the continuum nature of the parcel EL Hamiltonian formulation, (4)–(7) and (12), since the M_α 's depend on these pseudo-densities.

Conclusion The parcel EL Hamiltonian formulation has been constructed for an isentropic two-layer model of atmospheric dynamics on a sphere. From this EL formulation one can derive the corresponding Eulerian Hamiltonian formulation in a relatively easy way. Details of similar derivations can be found in Bokhove and Oliver [2,3].

REFERENCES

- [1] O. Bokhove, *Wave-vortex interactions in the atmosphere, and climate prediction*, Proceedings of the ICTAM04 Conference in Warsaw, Poland, Eds. Witold Gutkowski and Tomasz Kowalewski (2005) 103–116.
- [2] O. Bokhove and M. Oliver, *Parcel Eulerian-Lagrangian fluid dynamics for rotating geophysical flows*, Proc. Roy. Soc. A. **462** (2006a), 2563–2573.
- [3] O. Bokhove and M. Oliver, *Isentropic-Isothermal Two-Layer Model for Atmospheric Dynamics*, In preparation for Q.J. Roy. Met. Soc. (2006b) 13 pp.
- [4] J. Frank, G. Gottwald, and S. Reich, *A Hamiltonian Particle-Mesh Method for the Rotating Shallow Water Equations*, In M. Griebel and M.A. Schweitzer, Eds., Meshfree Methods for Partial Differential Equations, Vol. 26, pp. 131–142, Springer.

On the motion and structure of 3D - mesoscale vortices

EILEEN MIKUSKY

(joint work with Antony Owinoh, Rupert Klein)

The purpose of the talk is to illustrate how perturbation methods can be employed to derive a system of reduced model equations describing the motion and structure of mature hurricane-like vortices with typical wind speeds of $\sim 30 \text{ m s}^{-1}$ and radial scales of $\sim 300 \text{ km}$. Regarding the mechanisms controlling the motion and structure of hurricane-like vortices, the role of scale interactions associated with diabatic processes on vortex-scales and a vertically sheared background flow on synoptic scales ($\sim 1000 \text{ km}$) is of particular interest. The two major questions the authors try to answer are 1.) Are there mesoscale processes that may help a vortex to sustain its coherence in the presence of a vertically sheared background flow? 2.) Are hurricane-like vortices primarily steered by its environmental flow or are there additional effects related to diabatic effects that cause a deflection of the synoptic-scale vortex motion from its environmental steering flow?

Our interest on these issues is motivated by recent studies that identify mesoscale processes to play a key role in determining the hurricane-like vortex structure by creating asymmetries in the near core region. For instance, numerical simulations for mature tropical cyclones carried out by [1] have shown that after 48 h and in the presence of a 5 m/s environmental shear throughout the troposphere, the vortex remained in its vertically upright position while a strongly asymmetric, quasi-steady vertical motion pattern was observed with maximum upward motion downshear left of the center. In this relatively strong environmental shear this is a somewhat surprising result, since one would expect that the vortex becomes tilted once a vertical background shear has been imposed and eventually shears away due to the differential advection. Thus, the question is raised what mechanisms cause such asymmetries and in which manner are they responsible for maintaining the vortex coherence in vertical shear flows.

The derivation of reduced model equations is carried out using an unified approach to meteorological modelling based on multiple-scale asymptotic methods [2], [3]. To this class of asymptotic methods belong both multiple-scale expansions and matched asymptotics which are useful mathematical tools to study the interactions of processes acting on different length and time scales. In analogy to the work of [4] who studied the motion and core structure of geostrophic vortices in the framework of a shallow water model, we employ the method of matched asymptotics for our studies. In a first step single scale inner and outer expansions have been used to construct reduced model equations in leading orders describing the vortex structure on mesoscales and synoptic scales, respectively. Then, based on these equations analytical solutions for the velocity fields have been derived. Eventually, a matching of these velocity fields made it possible to derive equations for the synoptic scale vortex motion that account for net-effects of mesoscale processes in the vortex-scale region.

Considering adiabatic vortices (diabatic effects are excluded) embedded in a background flow with weak vertical shear, leading order solutions for the vortex motion have been derived that describe how the vortex is steered by its vertically constant background flow in leading order. From next higher order equations, corrections for the vortex motion have been obtained that describe how the differential advection induces a vortex tilt. Interestingly, the direction of the vortex tilt is fixed as long as the background flow is strong. For weak background flows, however, the vortex tilt makes a precession motion. The latter vortex behaviour is in agreement with observations made by [5]. Studying the impact of the background flow induced vortex tilt on the mesoscale vortex structure, a relation between the vortex tilt and wavenumber-one asymmetries in the vertical velocity and potential temperature patterns has been found. This is also known as the adiabatic lifting mechanism which has been first observed by [6].

Considering diabatic vortices (diabatic effects are included) things change dramatically. It turns out that in leading order the vortex is not only steered by its background flow, but a modification is caused by the net effect of mesoscale processes on vortex-scales which are strongly related to diabatic effects. Regarding the vortex tilt two different observations can be made. In the absence of net-heating effects due to small-scale convection, the vortex tilt is reduced at least by one order. However, if a net-heating due to small-scale convection is turned on we get a nonzero tilt in leading order. Although no detailed studies on that issue have been done so far it is believed, however, that the tilt of diabatic vortices must not be seen as a result of small-scale convective processes. From the experience of the behaviour of dry adiabatic vortices it is rather expected that small-scale convective heating can be seen as a result of a vortex tilt induced by the vertical shear of an environmental flow. This argumentation is motivated by observations of lightnings in hurricane-like vortices. In particular, a statistical analysis made by [7] has shown that there are prefered regions of lightnings depending on the direction in which the vertical shear vector points.

Finally, it is worth to point out that regarding the axisymmetric vortex structure, the asymptotic analysis of the governing equations of diabatic vortices yields a system of equations that can be seen as an extended version of Eliassen's balanced vortex model [8] which in terms of the vortex tilt also accounts for the influence of an environmental flow on the secondary circulation.

REFERENCES

- [1] Frank W.M., Ritchie E.A., *Effects of vertical wind shear on hurricane intensity and structure*, Mon. Wea. Rev. **129** (2001), 2249-2269.
- [2] Klein R., *An Applied Mathematical View of Theoretical Meteorology* invited presentation at ICIAM 2003, Sydney, Australia , SIAM Proceedings in Applied Mathematics **116** (2004).
- [3] Klein R., Majda A.J., *Systematic Multiscale Models for Deep Convection on Mesoscales*, Theoretical and Computational Fluid Dynamics, submitted, Aug. (2005)
- [4] Ting L., Ling G. *Studies on the motion and core structure of a geostrophic vortex*, Scientia Sinica **31** (1988), 694-705
- [5] Reasor P.D., Montgomery M.T. , *Three-dimensional alignment and corotation of weak, TC-like vortices via linear vortex Rossby waves* J. Atmos. Sci. **58** (2001), 2306-2330.
- [6] Frank W.M., Ritchie E.A., *Effects of environmental flow upon tropical cyclone structure*, Mon. Wea. Rev. **127** (1999), 2044-2060.
- [7] Kirsten L. Corbosiero, *The Effects of Vertical Wind Shear on the Distribution of Convection in Tropical Cyclones* Mon. Wea. Rev. **130** (2003) 2110-2123
- [8] Arnt Eliassen, *Slow Thermally of Frictionally Controlled Meridional Circulation in a Circular Vortex* Astrophysica Norvegica **V** (1950) 19-60

Compressible atmospheric modeling at all scales

OSWALD KNOTH

A time discretization method for the dry compressible atmospheric equations in conservation form is introduced and the solution of the linear equations involved is outlined. To formulate the prognostic equations in variables that have conservation properties, we define flux quantities

$$(1) \quad \mathbf{V} = \rho \mathbf{v} = (\mathbf{U}, \mathbf{V}, \mathbf{W}), \quad \Theta = \rho \theta$$

and we write the prognostic compressible equations in the form:

$$\begin{aligned} \frac{\partial \rho}{\partial t} + \nabla(\rho \mathbf{v}) &= 0 \\ \frac{\partial \rho \mathbf{v}}{\partial t} + \nabla(\rho \mathbf{v} \circ \mathbf{v}) &= \nabla \tau - \nabla p - \rho \mathbf{g} - 2\Omega \times (\rho \mathbf{v}) \\ \frac{\partial \rho \theta}{\partial t} + \nabla(\rho \mathbf{v} \theta) &= \nabla(\rho \nu_\theta \nabla \theta) + Q_\theta. \end{aligned}$$

Pressure is obtained from the diagnostic equation of state

$$(2) \quad p = \rho R \theta (p/p_0)^\kappa.$$

After spatial discretization an ordinary differential equation

$$y' = F(y)$$

is obtained which we integrate in time by a special Rosenbrock-method, Lanser et al. [1].

$$\begin{aligned} w^{n+1} &= w^n + \frac{5}{4}k_1 + \frac{3}{4}k_2 \\ Sk_1 &= \tau F(w^n) \\ Sk_2 &= \tau F(w^n + \frac{2}{3}k_1) - \frac{4}{3}k_1 \\ S &= I - \gamma\tau J, \quad J = F'(w^n) \end{aligned}$$

with $\gamma = \frac{1}{2} + \frac{1}{6}\sqrt{3}$.

The above described Rosenbrock method allows a simplified solution of the linear systems without loosing the order. When $J = J_A + J_B$ the matrix S can be replaced by $S = (I - \gamma\tau J_A)(I - \gamma\tau J_B)$. A further simplification can be reached by omitting some parts of the Jacobian or replacement of the derivatives by the same derivatives of a simplified operator $\tilde{F}(w^n)$. For instance higher order interpolation formulae are replaced by the first order upwind method. This further simplification of the matrix however reduces the method to second order. The structure of the Jacobian

$$J = \begin{pmatrix} \frac{\partial F_\rho}{\partial \rho} & \frac{\partial F_\rho}{\partial \mathbf{V}} & 0 \\ \frac{\partial F_V}{\partial \rho} & \frac{\partial F_V}{\partial \mathbf{V}} & \frac{\partial F_V}{\partial \Theta} \\ 0 & \frac{\partial F_\Theta}{\partial \mathbf{V}} & \frac{\partial F_\Theta}{\partial \Theta} \end{pmatrix}.$$

A zero block 0 indicates that this block is not included in the Jacobian or is absent. The derivative with respect to ρ is only taken for the Buoyancy term in the vertical momentum equation. Note that this type of approximation is the standard approach in the derivation of the Boussinesq approximation starting from the compressible Euler equations. The matrix J can decomposed as

$$J = J_T + J_P = \begin{pmatrix} \frac{\partial F_\rho}{\partial \rho} & 0 & 0 \\ \frac{\partial F_V}{\partial \rho} & \frac{\partial F_V}{\partial \mathbf{V}} & 0 \\ 0 & 0 & \frac{\partial F_\Theta}{\partial \Theta} \end{pmatrix} + \begin{pmatrix} 0 & \frac{\partial F_\rho}{\partial \mathbf{V}} & 0 \\ 0 & 0 & \frac{\partial F_V}{\partial \Theta} \\ 0 & \frac{\partial F_\Theta}{\partial \mathbf{V}} & 0 \end{pmatrix}$$

or

$$J = J_T + J_P = \begin{pmatrix} \frac{\partial F_\rho}{\partial \rho} & 0 & 0 \\ 0 & \frac{\partial F_V}{\partial \mathbf{V}} & 0 \\ 0 & 0 & \frac{\partial F_\Theta}{\partial \Theta} \end{pmatrix} + \begin{pmatrix} 0 & \frac{\partial F_\rho}{\partial \mathbf{V}} & 0 \\ \frac{\partial F_V}{\partial \rho} & 0 & \frac{\partial F_V}{\partial \Theta} \\ 0 & \frac{\partial F_\Theta}{\partial \mathbf{V}} & 0 \end{pmatrix}.$$

The first part of the splitting J_T is called the transport/source part and contains the advection, diffusion and source terms like Coriolis, curvature, Buoyancy, latent heat, and so on. The second matrix is called the pressure part and involves the pressure gradient and the derivative of the divergence with respect to momentum

of the density and potential temperature equation. The difference between the two splitting approaches is the insertion of the derivative of the gravity term in the transport or pressure matrix. The first splitting damps sound waves and can be reduced to a Poisson-like equation, whereas the second splitting damps sound and gravity waves but the dimension of the system is doubled. Both systems are solved by preconditioned CG-like methods. The transport/source system

$$(I - \gamma\tau J_{AD} - \gamma\tau J_S)\Delta w = R$$

is preconditioned from the right with the matrix

$$P_r = (I - \gamma\tau J_{AD})^{-1}$$

and from the left with the matrix

$$P_l = (I - \gamma\tau J_S)^{-1}.$$

where the matrix J_{AD} is the derivative of the advection and diffusion operator where the unknowns are coupled between grid cells. The matrix J_S assembles the source terms. Here the coupling is between the unknowns of different components in each grid cell. The matrix

$$P_l(I - \gamma\tau J_{AD} - \gamma\tau J_S)P_r$$

can be written using the Eisenstat trick in the form

$$(I - \gamma\tau P_l J_{AD})P_r = (I + P_l((I - \gamma\tau J_{AD}) + I))P_r.$$

Therefore we have to store only the LU-decomposition of the matrix $(I - \gamma\tau J_S)$. The matrix $(I - \gamma\tau J_{AD})$ is inverted by a fixed number of Gauss-Seidel iterations. In the parallel case we use one cell overlap.

The second matrix of the splitting approach looks in case of the first splitting

$$(I - \gamma\tau J_P) = \begin{pmatrix} V_F & \gamma\tau \text{GRADD}_\Theta \\ \gamma\tau \text{DIV} D_\mathbf{V} & V_C \end{pmatrix}$$

where V_F , V_C , $D_\mathbf{V}$, and D_Θ are diagonal matrices. The matrices GRAD and DIV are related by the requirement

$$\text{GRAD} = -\text{DIV}^T$$

Elimination of the momentum part gives a Helmholtz equation for the increment of the potential temperature. This equation is solved by a CG-method with multigrid as a preconditioner. For the second splitting the resulting matrix is twice in dimension and no more symmetric.

To illustrate the integration method a simulation for the 2-D density current is presented. This simulation follows the benchmark case analyzed by Straka et al. [2]. A density current is generated within a neutrally stable atmosphere by cold bubble that descends to the surface and spreads out laterally due to the negative buoyancy of the cold air. The parameters are taken from Straka et al.. The resolution is $\Delta x = \Delta z = 100$ m and the time step is chosen automatically and varies between 4 and 10 seconds. The evolving density current is displayed in Fig. 1 and agree well with the reference results by Straka et al.

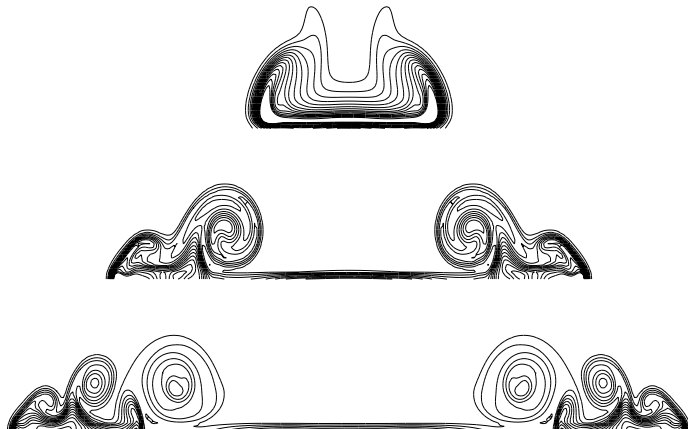


FIGURE 1. Potential temperature field for Straka et al. [2] 2-D density current benchmark case for 300 s, 600 s, and 900s.

REFERENCES

- [1] D. Lanser, J.G. Blom and J.G. Verwer *Time integration of the shallow water equations in spherical geometry*, J. Comp. Phys. **171** (2001), 373–393.
- [2] J.M. Straka, R.B. Wilhelmson, L.J. Wicker, J.R. Anderson and K.K. Droege-meier *Numerical Solutions of a Nonlinear Density-Current - A Benchmark Solution and Comparisons*, Int. J. Num. Meth. in Fluids, **17** (1993), 1–22.

Time-splitting techniques in nonhydrostatic compressible modeling

ALMUT GASSMANN

Numerical weather forecasting models on high resolutions demand for very efficient time integration methods for the full compressible nonhydrostatic equations. One possibility is the split-explicit time integration method, in which processes of different time scales are integrated each with appropriate time steps. In the field of weather prediction models the method of Klemp and Wilhelmson (1978) is most widespread to be found. In this approach, slow advective processes are separated from fast ones connected with the propagation of sound waves and gravity waves. Advective tendencies are computed once in a large time step and hold constant during the short time step integration. An essential issue in research (e. g. Skamarock and Klemp, 1992) was the question of numerical stability of such schemes. With our recent work (Gassmann, 2005; Gassmann and Herzog, 2006) we could give a guideline for delegating the particular terms in the equations to either the slow or the fast processes and show the linear numerical stability of such a split-explicit two-time-level scheme. The method was then implemented into the LM (Lokal-Modell: Doms and Schättler, 1999) of DWD (German Weather Service),

and currently it is in a test phase for operational use at MeteoSwiss. One great practical advantage of the new scheme over the older ones is that a radiative upper boundary condition for gravity waves (Klemp and Durran, 1983; Bougeault, 1983; Herzog, 1995) could be implemented directly without difficulties.

The first part of the talk was devoted to the investigation of the sound-advection system and its split-explicit numerical treatment with three different two-time-level schemes: first, the Euler scheme in which the slow advective tendencies appear as a function of the current large time step, second, the method proposed by Wicker and Skamarock (1998) in which a Runge-Kutta advection method is merged with the split-explicit technique, and thirdly, a newly proposed method that computes fast steps until the midpoint of the large time step in order to provide those values for the computation of slow advective tendencies. The actual advection scheme can be chosen more freely, the only constraint is that the advective tendency is a function of this midpoint estimate. In case of the Euler scheme it could be shown that the numerical splitting error term leads to instability. This error term is present also in case of the other two variants, but it does not lead to significant instabilities. The newly proposed scheme has the smallest error. This scheme also treats waves propagating in opposite directions very similar, which is not observed with the other schemes.

The second part of the talk addressed the problem of splitting the nonhydrostatic equations into a slow and a fast equation part. We have to pick the terms responsible for the propagation of sound and gravity waves for the fast equation part. The remaining terms contributing to the slow part are then the momentum advection terms and the horizontal advection terms for the thermodynamic variables (temperature and pressure). The vertical advection terms for these variables constitute the Brunt-Väisälä-frequency and thus belong to the gravity wave part. Once the mode separation is done, stable numerical schemes are needed for each, the slow and the fast model parts alone. In a NWP-model (Numerical Weather Prediction model) implicit methods are needed at least in the vertical. In the horizontal direction, a forward-backward method (Mesinger, 1977) is applied for the fast part.

For stabilizing split-explicit schemes, divergence damping is usually applied (e. g. Skamarock and Klemp, 1992). But the actual model implementations often only add this damping term to the horizontal momentum equation, but not – as required – to the vertical momentum equation, too. It is now shown, how this shortcut deteriorates the phase properties of the gravity modes severely. Consequently, one should use complete divergence damping or the off-centering of the implicit weights. This last option reveals the best results when performing a stability analysis of the complete splitting scheme.

The last part of the talk gave some examples of the presented new splitting method in the LM. It could be demonstrated how a false splitting into slow and fast terms destroys the forecast in comparison to a well performed splitting. One great advantage of the new splitting technique is the applicability of the radiative

upper boundary condition for gravity waves (Klemp and Durran, 1983; Bougeault, 1983).

With all these investigations the splitting approach for nonhydrostatic modeling is now based on a thorough linear analysis, which was not the case before.

REFERENCES

- [1] Ph. Bougeault, *A non-reflective upper boundary condition for limited-height hydrostatic models*, Monthly Weather Review **111** (1983), 420–429.
- [2] G. Doms and U. Schättler, *The nonhydrostatic limited-area-model LM (Lokal-Modell) of DWD, part I: Scientific documentation*, Deutscher Wetterdienst, Geschäftsbereich Forschung und Entwicklung, (1999).
- [3] A. Gassmann, *An improved two-time-level split-explicit integration scheme for non-hydrostatic compressible models*, Meteorology and Atmospheric Physics **88**, (2005), 23–38.
- [4] A. Gassmann and H.-J. Herzog, *A consistent time-split numerical scheme applied to the nonhydrostatic compressible equations*, Monthly Weather Review, (2006), accepted to be published.
- [5] H.-J. Herzog, *Testing a radiative upper boundary condition in a nonlinear model with hybrid vertical coordinate*, Meteorology and Atmospheric Physics **55** (1995), 185–204.
- [6] J. B. Klemp and D. R. Durran, *An upper boundary condition permitting internal gravity wave radiation in numerical mesoscale models*, Monthly Weather Review **111** (1983), 430–444.
- [7] J. B. Klemp and R. B. Wilhelmson, *The simulation of three-dimensional convective storm dynamics*, Journal of the Atmospheric Sciences **35** (1978), 1070–1096.
- [8] F. M. Mesinger, *Forward-backward scheme and its use in a limited area model*, Contributions to Atmospheric Physics **50** (1977), 200–210.
- [9] W. C. Skamarock and J. B. Klemp, *The stability of time-split numerical methods for the hydrostatic and the nonhydrostatic elastic equations*, Monthly Weather Review **120** (1992), 2109–2127.
- [10] J. L. Wicker and W. C. Skamarock, *A time-splitting scheme for the elastic equations incorporating second-order Runge-Kutta time differencing*, Monthly Weather Review **126** (1998), 1992–1999.

Waves in rotating fluids: geometric effects

LEO R.M. MAAS

Geophysical fluid dynamics is characterized by the importance of earth rotation (interpreted as a stratification in angular momentum), density stratification and irregularity of the fluid's domain. It is interesting to observe that both types of stratification give rise to wave phenomena in the interior of the ocean or atmosphere that are quite different from those encountered strictly at the surface (see

[7]). In particular, these waves are prone to a strong focusing principle. Irrespective of forcing location, the location of so-called *wave attractors* is determined by forcing frequency, stratification rate, rotation rate and geometry. These attractors are the locations where inviscid theory predicts the waves being focused to and occur “almost always”. The result of focusing of wave energy is that the waves mix fluid around these attractors (particularly at the boundary reflections where the focusing takes place). Interestingly, the attractors themselves have a strong, fractal dependence on the lumped parameter containing the previously mentioned information on the wave and the environment. Thus, while the waves are described in a strictly linear manner, their structure exhibits many features from nonlinear dynamics, owing to the fact that the geometry of the underlying characteristics (that form the backbone of the analytical solutions) is strongly influenced by the nonlinear shape of the boundary.

Previous theoretical work has focused on elucidating the nature of these waves and the attractors that are formed. This has first been performed separately for stratified, non-rotating fluids – well described as a 2D problem ([8]) – and later for homogeneous, rotating fluids. The former give rise to internal gravity waves, the latter to inertial waves. In nature, the two restoring mechanisms come, admittedly, in a combined form, but it is worthwhile to address them separately too. Here attention is given to inertial waves in a rotating, homogeneous, rigid-lid fluid. Very few container shapes are known for which stationary, regular, inviscid, linearized inertial wave patterns can be computed, notably the axial, finite-sized annulus and the axial ellipsoidal spheroid. Recently, this was extended to the rotating, rectangular box, provided the box is positioned horizontally, i.e. has its sides either parallel or perpendicular to the rotation axis ([6]). In this case vertical standing modes separate from the horizontal (generalized eigenvalue) problem. The horizontal problem is similar to the classical [9]) problem, concerned with rotationally modified gravity waves, described in the shallow water approximation in a rectangular fluid domain. Once this geometric symmetry is broken, by taking a sloping side wall, inertial wave attractors are produced and, following the mixing of angular momentum, a cyclonic mean flow is generated ([5]). Inertial wave attractors are observed in the laboratory for five frequency regimes (and one exceptional frequency for which a regular wave is predicted). The observations suggest the existence of an ‘inertial wave manifold’ and the waves approaching the attractor suggest there to be propagation along the manifold. But, while their horizontal structure can to some extent be unravelled experimentally ([3, 4]), the exact shape of this manifold and the dynamics on it still need to be elucidated.

By taking a rigid, flat surface and a finite-amplitude, exponential bottom the homogeneous fluid case is studied more carefully, as it gives rise to a paradox. On the one hand the appearance of an inertial wave attractor in the cross-channel direction is predicted. On the other hand, assuming a small aspect-ratio of maximum depth over channel width, as a zeroth order expansion in this small parameter, a standard expression for a topographic Rossby waves can be derived. These waves are derived from the same set of linear, inviscid rotating Euler equations, and yet

have disparate properties: Rossby waves are regular, vertically uniform and have anisotropic, westward phase propagation, while in this geometry inertial waves are singular, vertically nonuniform, and apparently horizontally isotropic. The inertial waves seem to be the more fundamental of the two: no approximation is needed to describe them. How is the paradox resolved? Does the infinite series (of which the topographic Rossby wave is just the zeroth order term) diverge locally? Or, does it co-exist with the inertial wave, as two different type of waves. More work is needed to come to a conclusion.

REFERENCES

- [1] M. Muster, *Computing certain invariants of topological spaces of dimension three*, Topology **32** (1990), 100–120.
- [2] M. Muster, *Computing other invariants of topological spaces of dimension three*, Topology **32** (1990), 120–140.
- [3] A.M.M. Manders & L.R.M. Maas, *Observations of inertial waves in a rectangular basin with one sloping boundary*, Journal of Fluid Mechanics **493** (2003), 59–88.
- [4] A.M.M. Manders & L.R.M. Maas, *On the three-dimensional structure of the inertial wave field in a rectangular basin with one sloping boundary*, Fluid Dynamics Res. **35** (2004), 1–21.
- [5] L.R.M. Maas, *Wave focusing and ensuing mean flow due to symmetry breaking in rotating fluids*, Journal of Fluid Mechanics **437** (2001), 13–28.
- [6] L.R.M. Maas, *On the amphidromic structure of inertial waves in a rectangular parallelepiped*, Fluid Dynamics Research **33** (2003), 373–401.
- [7] L.R.M. Maas, *Wave attractors: linear yet nonlinear*, International Journal of Bifurcation & Chaos **15** (2003), 2757–2782.
- [8] L.R.M. Maas & F.P.A. Lam *Geometric focusing of internal waves*, Journal of Fluid Mechanics **300** (1995), 1–31.
- [9] G.I. Taylor, *Tidal oscillations in gulfs and basins*, Proceedings of the London Mathematical Society Series 2 **3** (1921), XX, 148–181.

The spontaneous generation of inertia-gravity waves in idealized baroclinic life cycles

RIWAL PLOUGONVEN AND CHRIS SNYDER

Plougonven, Chris Snyder

Flows on the synoptic scale in the oceans and atmosphere are predominantly 'balanced' (verifying balance relations such as geostrophy and hydrostatic). This has allowed the development of '*balanced models*' which simplify the dynamics by filtering out the gravity waves. Understanding the spontaneous generation of gravity waves from balanced motions is a necessary step to better understand the limitations of these models ([2]). A second motivation is that, although it is known from observations that jets and fronts (predominantly balanced features of the flow) are

important sources of gravity waves ([6] and refs therein), they remain too poorly understood as such to be properly parameterized in Global Circulation Models.

Now, both observation ([3] and refs. therein) and numerical studies ([4, 10]) of spontaneous generation in atmospheric mid-latitude flows have emphasized upper-level jet exit regions as a key region of the flow where large amplitude inertia-gravity waves are found. Although it has often been assumed that this was due to generation of the waves there, the role of propagation has not properly been investigated. Another puzzling fact is that, although gravity waves are known from two-dimensional studies of frontogenesis [9] to be generated from surface fronts, such generation has not been found in three-dimensional simulations of baroclinic instability which do display frontogenesis.

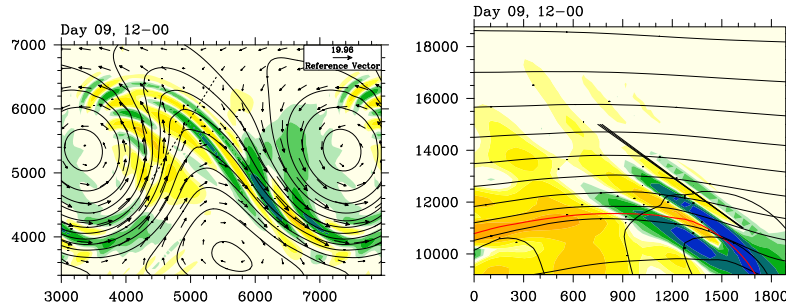


FIGURE 1. Gravity waves generated in an idealized baroclinic life-cycle. The left-panel shows a horizontal cross-section ($z = 13\text{ km}$) of divergence (colors) and horizontal wind in the reference frame of the baroclinic wave; x and y indicated in km. The right panel shows a vertical cross-section through the dashed line indicated in the left panel; horizontal coordinate in km, z in m. The red line indicates the tropopause. The black segments are the prediction of the slope of the phase lines, obtained from a coarse-grained knowledge of the background flow.

In order to understand and quantify the generation of gravity waves from jets and fronts, we have carried out numerical simulations of baroclinic life cycles in a periodic channel on the f -plane, using the Weather and Research Forecast Model. Such idealized simulations have been widely used in dynamic meteorology as representative of mid-latitude synoptic systems. Ongoing work on these simulations has already shown that:

- the emission of gravity waves occurs in specific regions of the flow, where temperature gradients collapse (surface and upper-level fronts). The simulations have shown a richer array of regions generating gravity waves than were previously described [8].
- consideration of propagation effects (wave-capture, [1]) provides valuable information regarding the localization, orientation and intrinsic frequency

of some of the excited gravity waves [7]. Knowledge of the large-scale flow is sufficient to predict the angle of the phase lines to the horizontal (cf. Fig. 1). Hence, jet exit regions play a key role for reasons related to the propagation of the gravity waves. This does not rule out that they may also be key regions for generation; it rather shows that generation and propagation cannot be thought of separately.

REFERENCES

- [1] O. Bühler and M.E. McIntyre. *Wave capture and wave-vortex duality*. J. Fluid Mech., 534:67–95, 2005.
- [2] R. Ford, M. E. McIntyre, and W. A. Norton. *Balance and the slow quasi-manifold: some explicit results*. J. Atmos. Sci., 57:1236–1254, 2000.
- [3] F. Guest, M. Reeder, C. Marks, and D. Karoly. *Inertia-gravity waves observed in the lower stratosphere over Macquarie Island*. J. Atmos. Sci., 57:737–752, 2000.
- [4] D. O’Sullivan and T.J. Dunkerton. *Generation of inertia-gravity waves in a simulated life cycle of baroclinic instability*. J. Atmos. Sci., 52(21):3695–3716, 1995.
- [5] R. Plougonven and H. Teitelbaum. *Comparison of a large-scale inertia-gravity wave as seen in the ecmwf and from radiosondes*. Geophys. Res. Lett., 30(18):1954, 2003.
- [6] R. Plougonven, H. Teitelbaum, and V. Zeitlin. *Inertia-gravity wave generation by the tropospheric mid-latitude jet as given by the fastex radiosoundings*. J. Geophys. Res., 108(D21):4686, 2003.
- [7] R. Plougonven and C. Snyder. *Gravity waves excited by jets: propagation versus generation*. Geoph. Res. Lett., 32(L18892):doi:10.1029/2005GL023730, 2005.
- [8] R. Plougonven and C. Snyder. *Inertia-gravity waves spontaneously generated in idealized baroclinic life cycles*. in revision for J. Atm. Sci., 2006.
- [9] C. Snyder, W.C. Skamarock, and R. Rotunno. *Frontal dynamics near and following frontal collapse*. J. Atmos. Sci., 50(18):3194–3211, 1993.
- [10] F. Zhang. *Generation of mesoscale gravity waves in upper-tropospheric jet-front systems*. J. Atmos. Sci., 61(4):440–457, 2004.

Exponential smallness of inertia-gravity-wave generation

JACQUES VANNESTE

(joint work with I. Yavneh, E. I. Ólafsdóttir and A. B. Olde Daalhuis)

The mid-latitude dynamics of the atmosphere and oceans is characterised by a large time-scale separation between the slow large-scale motion (termed balanced motion), and the fast inertia-gravity waves (IGWs). The corresponding frequency ratio ϵ is small for IGWs of all scales in the quasi-geostrophic regime, with small Rossby and Burger numbers, thought to be the most relevant at mid-latitudes.

Together with the slowness of the external forcing, this explains why the levels of IGW activity typically encountered are very low.

The explanation can be formalised by writing the equations of motion in the form

$$\frac{\partial s}{\partial t} = N_s(s, f; \epsilon), \quad \frac{\partial f}{\partial t} + \mathcal{L}f = N_f(s, f; \epsilon),$$

separating the slow variables s from the fast variables f . Here, N_s and N_f group the nonlinear terms, and \mathcal{L} is a linear operator, with spectrum $\text{spec } \mathcal{L} \subset \{i\omega : \omega \in \mathbf{R}, |\omega| > \epsilon^{-1}\}$ [1]. For $\epsilon = 0$, there is an invariant slow manifold $f = 0$, corresponding physically to geostrophic balance. For $\epsilon \neq 0$, slow manifolds can also be constructed using iterations or expansions in powers of ϵ : these are not invariant but, formally, can have an arbitrary accuracy ϵ^N (in the sense that the vector field $(\partial_t s, \partial_t f)$ makes an $O(\epsilon^N)$ angle with the manifold). Optimal-truncation arguments then suggest (and in some cases prove) that an exponential accuracy can be achieved [2]. Since motion transverse to a slow manifold is interpreted as IGWs, this indicates that in suitably initialised balanced flows, IGW-phenomena can at most be exponentially weak in ϵ .

We demonstrate that exponentially weak IGW phenomena do occur by analysing two models of IGW generation in a simple horizontal Couette flow in a Boussinesq (and for simplicity hydrostatic) rotating stratified fluid. The first is a form of spontaneous generation that arises when a vortex, taken with Gaussian potential-vorticity distribution, is placed in the Couette flow. In the linear approximation which we employ, the potential vorticity evolves slowly through simple advection. Other fields, such as the vertical component of the vorticity ζ , exhibit the generation and subsequent propagation of IGW-packets. This can be estimated asymptotically by expansion of the linearised equations of motion in terms of sheared modes of the form

$$(1) \quad \zeta(x, y, z, t) = \int \hat{\zeta}(k, l, m, t) \exp[i(kx + (l - \Sigma kt)y + mz)] dx dy dz,$$

where Σ is the shear and (k, l, m) can be interpreted as components of a wavevector. This reduces the problem to the study of (uncoupled) ordinary differential equations for the amplitudes $\hat{\zeta}(k, l, m, t)$. These equations have been studied in [3] and [4], where it is shown that IGW oscillations appear through a Stokes phenomenon. The amplitude of the oscillations, which is exponential small in the Rossby number $\epsilon = |\Sigma|/f_C \ll 1$, where f_C is the Coriolis frequency, and their form can be estimated explicitly using exponential asymptotics. Carrying out the triple integration in (1) using asymptotic and numerical methods provides a detailed description of the wavepacket emitted [5]. Compared with entirely numerical approaches, our asymptotic treatment has the advantage of removing ambiguities in the initialisation procedure (the initial state can be chosen entirely free of IGWs), and in the diagnostic of IGWs (which are completely separated from the balanced motion).

Our second model reassesses the instabilities of a horizontal Couette flow in a channel [6, 7]. Because the velocity profile has no inflection point, this flow is

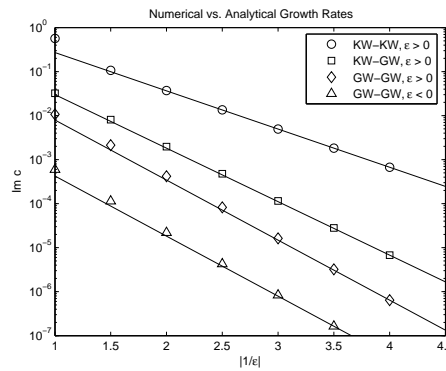


FIGURE 1. Growth rates of the unbalanced instabilities of a horizontal Couette flow in a channel as a function of the Rossby number ϵ . Asymptotic (curves) and numerical (symbols) results are compared for different modes instabilities associated with the interactions between pairs of Kelvin and/or inertia-gravity waves.

stable in any balanced approximation, however accurate. Studying the Boussinesq equations reveals that the flow is nonetheless unstable, through unbalanced instabilities which involve the linear interaction of pairs of waves, either IGWs or Kelvin waves (KWs). Because the two waves involved in instabilities are exponentially localised in different parts of the channel, their interaction is exponentially weak, and the growth rates are exponentially small, with rough asymptotics $\sigma \asymp \exp(-\Psi/\epsilon)$, where $\Psi = 2, 2.8$ and π , for the fastest-growing instability associated with KW-KW, KW-IGW and IGW-IGW interactions, respectively [8] (see Figure 1). Only the latter type of instabilities is possible when the shear is cyclonic, i.e. $\Sigma f_C < 0$.

The two models studied illustrate distinct mechanisms of wave generation by balanced motion. In the first model, it is the spontaneous evolution of an initially perfectly balanced state that leads to IGW emission through what might term a conversion mechanism, corresponding mathematically to a Stokes phenomenon; in the second model, an instability of a (steady) balanced flow leads to the amplification of a small unbalanced perturbation. What is exponentially small differs between the two models — wave amplitude vs. growth rate — but in both case a significant level of unbalance can only be achieved if the Rossby number ceases to be small.

REFERENCES

- [1] T. Warn, O. Bokhove, T. G. Shepherd and G. K. Vallis, *Rossby number expansions, slaving principles, and balance dynamics*, Quart. J. R. Met. Soc. **121** (1995), 723–739.
- [2] R. S. MacKay, *Slow manifolds*, in *Energy Localisation and Transfer*, World Scientific (2004), 149–192.

- [3] J. Vanneste and I. Yavneh, *Exponentially small inertia-gravity waves and the breakdown of quasi-geostrophic balance*, J. Atmos. Sci. **61** (2004), 211–223.
- [4] E. I. Ólafsdóttir, A. B. Olde Daalhuis and J. Vanneste, *Multiple Stokes multipliers in a inhomogeneous differential equation with a small parameter*, Proc. R. Soc. London A**461** (2005), 2243–2256.
- [5] E. I. Ólafsdóttir, A. B. Olde Daalhuis and J. Vanneste, *Inertia-gravity-wave generation by a sheared three-dimensional vortex*, in preparation (2006).
- [6] P. J. Kushner, M. E. McIntyre and T. G. Shepherd, *Coupled Kelvin wave and mirage-wave instabilities in semi-geostrophic dynamics*, J. Phys. Ocean. **28** (1998), 513–518.
- [7] I. Yavneh, J. C. McWilliams and J. Molemaker, *Non-axisymmetric instability of centrifugally-stable Stratified Taylor-Couette flow*, J. Fluid Mech. **448** (2001), 1–21.
- [8] J. Vanneste and I. Yavneh, *Unbalanced instabilities of rotating stratified shear flows*, in preparation (2006).

Macroturbulence and Hadley Circulation Dynamics

TAPIO SCHNEIDER

(joint work with Simona Bordoni and Christopher C. Walker)

In Earth's atmosphere, large-scale eddy momentum fluxes strongly influence the strength of the summer Hadley cells but less strongly influence the strength of the cross-equatorial winter Hadley cells. Where frictional processes and the vertical advection of momentum by the mean meridional circulation can be neglected—in the upper branches of the circulation where streamlines are horizontal—the mean zonal momentum balance in a statistically steady state is approximately

$$(1) \quad (f + \bar{\zeta})\bar{v} = f(1 - \text{Ro})\bar{v} \approx \mathcal{S},$$

with local Rossby number $\text{Ro} = -\bar{\zeta}/f$, eddy momentum flux divergence \mathcal{S} , and with the bar denoting a zonal and temporal mean along isobaric surfaces (other symbols have their usual meaning). The local Rossby number in the upper branches of the Hadley circulation, where streamlines are horizontal, is a nondimensional measure of the influence of eddy momentum fluxes on the strength of the circulation, or, because the absolute vorticity $f + \bar{\zeta} = f(1 - \text{Ro}) = -(a^2 \cos \phi)^{-1} \partial_\phi \bar{m}$ is proportional to the meridional gradient of absolute angular momentum per unit mass $\bar{m} = (\Omega a \cos \phi + \bar{u})a \cos \phi$, it is a nondimensional measure of the flatness of angular momentum contours in the meridional plane [e.g., 4]. If $\text{Ro} \rightarrow 0$, angular momentum contours are vertical; the mean meridional circulation is tied to the eddy momentum flux divergence. If $\text{Ro} \rightarrow 1$, angular momentum contours are horizontal; the eddy momentum flux divergence approaches zero, and the mean meridional circulation decouples from the eddy momentum flux divergence. In Earth's atmosphere, the local Rossby number in the upper branches of the Hadley circulation, where streamlines are horizontal, varies from $\text{Ro} \lesssim 0.2$ in the summer

cells to $\text{Ro} \gtrsim 0.5$ in the cross-equatorial winter cells, with intermediate values in the equinox cells [8]. Regionally, in the Asian monsoon anticyclone, the local Rossby number can reach about 0.7 according to monthly-mean reanalysis data [7].

Depending on whether eddy momentum fluxes strongly or weakly influence their strength, Hadley cells respond differently to variations in thermal driving. The strength of a Hadley cell with $\text{Ro} \rightarrow 0$ in the upper branch does not respond directly to variations in thermal driving. It only responds indirectly through changes in eddy momentum flux divergence and, possibly, through changes in the Hadley cell extent, which affects the relevant value of the Coriolis parameter in the zonal momentum balance (1) [8]. The strength of a Hadley cell with $\text{Ro} \rightarrow 1$ in the upper branch—a Hadley cell in the angular momentum-conserving limit in which streamlines and angular momentum contours coincide—responds directly to variations in thermal driving [3, 1, 2]. The seasonal variations of the local Rossby number in the upper branches of Earth's Hadley circulation lie between these extremes and suggest that the character of a Hadley cell's response to variations in thermal driving may change in the course of the seasonal cycle.

I presented simulations with an idealized general circulation model (GCM) with zonally symmetric boundary conditions that showed that, over wide parameter ranges, the strength of the Hadley circulation displays clear scaling relations with regime transitions. For circulations with hemispherically symmetric thermal driving, the strength of the Hadley circulation typically, albeit not always, scales with the strength of the eddy momentum flux divergence near the latitude of its streamfunction extremum [8]. The regime transitions in the scaling behavior of the Hadley circulation are regime transitions in the scaling behavior of large-scale eddy fluxes, which can be understood by considering the interaction of eddies with the mean flow and particularly with the mean thermal stratification [8, 6]. For circulations with hemispherically asymmetric thermal driving, the cross-equatorial Hadley cell is in one of two regimes distinguishable according to whether eddy momentum fluxes strongly or weakly influence the strength of the cell. In the course of a simulated seasonal cycle, the cross-equatorial Hadley cell undergoes transitions between the two regimes, which resemble the transitions in Earth's tropical circulation associated with the onset and end of monsoons [5].

REFERENCES

- [1] Held, I. M., and A. Y. Hou, 1980: Nonlinear axially symmetric circulations in a nearly inviscid atmosphere. *J. Atmos. Sci.*, **37**, 515–533.
- [2] Lindzen, R. S., and A. Y. Hou, 1988: Hadley circulations for zonally averaged heating centered off the equator. *J. Atmos. Sci.*, **45**, 2416–2427.
- [3] Schneider, E. K., 1977: Axially symmetric steady-state models of the basic state for instability and climate studies. Part II. Nonlinear calculations. *J. Atmos. Sci.*, **34**, 280–296.
- [4] Schneider, T., 2006: The general circulation of the atmosphere. *Ann. Rev. Earth Planet. Sci.*, **34**, 655–688.

- [5] Schneider, T., and S. Bordoni, 2007: Regime transitions in the seasonal cycle of the Hadley circulation and possible implications for monsoon dynamics. *J. Atmos. Sci.*. To be submitted.
- [6] Schneider, T., and C. C. Walker, 2006: Self-organization of atmospheric macro-turbulence into critical states of weak nonlinear eddy–eddy interactions. *J. Atmos. Sci.*, **63**, 1569–1586.
- [7] Uppala, S. M., and Coauthors, 2005: The ERA-40 reanalysis. *Quart. J. Roy. Meteor. Soc.*, **131**, 2961–3012.
- [8] Walker, C. C., and T. Schneider, 2006: Eddy influences on Hadley circulations: Simulations with an idealized GCM. *J. Atmos. Sci.*, **63**. In press. Preprint available at www.gps.caltech.edu/~tapiro.

Linear baroclinic instability in the world's oceans

K. SHAFER SMITH

Satellite altimetric observations of the ocean surface reveal a circulation dominated by turbulent flow on scales of 50 to 250 km, the oceanic mesoscale. The apparent eddy dominance at the oceanic mesoscale was first noted, however, from ship-going observations in the early 1970s. Using available data, Gill, Green, and Simmons [1] noted the concurrence of eddy activity with steep isopycnal gradients, and pointed out that the oceanic mean available potential energy resulting from these isopycnal gradients is about 1000 times larger than the kinetic energy of the gyre-scale circulation. These two facts, they argued, are consistent with the hypothesis that eddies are generated by baroclinic instability. Baroclinic instability develops in flow where both rotation and stratification are important, as they are at the oceanic mesoscale, and acts to convert mean available potential energy to eddy kinetic energy. Gill et al. also perform some simple linear instability calculations and show that the resulting growth rates are roughly consistent with observed eddy timescales.

Recent analyses of the global statistics of eddies using satellite altimetry [2] are consistent with most aspects of this picture, demonstrating that eddy activity, for example, is well correlated with estimates of the Eady growth rate $f/Ri^{1/2}$ from hydrographic data. Stammer [2] also analyzes the horizontal *scale* of the observed eddies, and argues that it is linearly correlated with the local first deformation scale. In the simplest examples of linear baroclinic instability, such as the Eady and Phillips models [see, e.g., 3], the scale of fastest linear growth is also near the deformation scale, and so this apparent correlation seems to be reasonable. Therefore, one might argue that the observed eddy structure can be largely predicted and understood through linear theory. Is this a reasonable conclusion?

While the fundamentals of baroclinic instability theory have been understood for half a century, and great progress has been made in understanding its relation to the mean *atmospheric* circulation, no systematic investigation of even the linear instability of the mean ocean state has been presented in the literature. This state of affairs is due to the fact that, earlier than the past decade, data for the

ocean has been very sparse. It is only recently that global hydrographic atlases have approached completeness, and so a program of systematic investigation of the ocean's linear instability characteristics has not been feasible until now. The present report discusses the methods and results of such a program, with the explicit goal of comparing observed eddy statistics to those predicted by linear theory. The null hypothesis is that the entire field is described by the local linear instability of the slowly-varying mean state.

The dataset of Gouretski and Koltermann [4, denoted GK04 hereafter] provides monthly, seasonal and annual averages of temperature and salinity gridded at 1/2 degree in the horizontal, on 45 fixed depth levels, from 72S to 90N at all longitudes. In the present study we use annually averaged data, though comparisons were made to seasonally averaged results, showing negligible differences. Where data is not available from observations, an objective analysis (or Gauss-Markov) method is used to interpolate existing data. Notably, the GK04 dataset interpolation is performed in such a way that neutral stability is ensured (this is not the case for the World Ocean Atlas 2001 dataset). See GK04 for details and an explicit comparison to the World Ocean Atlas 2001 dataset.

The intrinsic buoyant stability of the dataset allows for the straightforward computation of “neutral” density [5] for the entire world ocean. Neutral density is a locally referenced density and so represents the dynamically active component of the buoyancy field.

Before proceeding to the velocity and instability calculations, we compute the vertical modes of the density field, or in other words the vertical structure of resting solutions to the quasigeostrophic equations [see, e.g., ref. 3]. Specifically, we seek solutions $\phi_m = \phi_m(z)$ with eigenvalues λ_m to the Sturm-Liouville eigenvalue equation

$$(1) \quad -\frac{f^2 \rho_0}{g} \frac{d}{dz} \left(\frac{\phi_m}{d\rho/dz} \right) = -\lambda_m^2 \phi_m, \text{ with } \left. \frac{d\phi}{dz} \right|_0 = \left. \frac{d\phi}{dz} \right|_{-H} = 0,$$

for each vertical profile of neutral density $\rho = \rho(z)$. In the above, $f = 2\Omega \sin(\theta)$ is the Coriolis parameter at latitude θ , with rotation rate Ω , g is the gravitational acceleration and ρ_0 is the mean density for that vertical profile, and we have assumed a flat bottom and rigid lid. The resulting eigenvalues λ_m are the local internal deformation wavenumbers, or the reciprocals of the Rossby deformation radii, and the eigenfunctions ϕ_m form a complete set onto which other continuous functions of z satisfying the same boundary conditions as ϕ_m can be projected.

We follow Chelton et al. [6] and compute solutions to (1) numerically, using centered differences. Note as a technical point that there are a number of GK04 profiles with levels at which the centered estimate of the vertical derivative of the density between two prescribed depth levels is zero. At these points we simply skip down to the next level at which there is an increase in density, and so always retrieve a non-zero vertical profile of the density derivative. The resulting contours of the first deformation radii are plotted in figure 1.

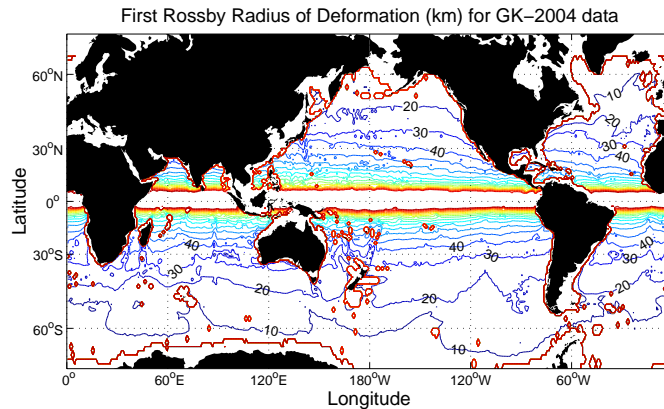


FIGURE 1. The first internal deformation radii, plotted in 10 Km intervals from 10 Km to 200 Km, as calculated from the GK04 dataset.

Next we compute the thermal wind velocity field for the entire dataset as follows. The hydrostatic pressure field is calculated from the density field, and horizontal centered differences are then used to estimate the horizontal isopycnal gradients. The horizontal gradients are then used to compute the velocity field through geostrophic balance. The arbitrary offset is fixed by removing the barotropic component of the flow.

Given the density structure and vertical profiles of the vertical shear of the mean horizontal velocity field, one can calculate the linear baroclinic instability for each profile, assuming a doubly-periodic domain (reasonable if one assumes that local vertical, as opposed to horizontal or boundary-induced inhomogeneities produce the instability connected to the eddies). However, rather than proceed with a vertical differencing of the local quasigeostrophic linearized about the mean, we first project the equations onto a truncated set of the local vertical modes.

This latter step is taken for the following reasons. Sharp vertical gradients, prevalent particularly near the surface, result generically in baroclinic instabilities at very small horizontal scales (less than 1 Km) and with fast growth rates (less than 1 day) [7]. It seems unreasonable to expect that, if such instabilities are truly present, the annually averaged mean state could possibly represent the shorter timescale mean that actually leads to such instabilities. In other words, such small and fast instabilities will surely alter the local mean on short timescales. Rather we seek to quantify the instability of the slowly varying mean state, and so avoid the fast-small modes by considering only the instability of the first N baroclinic modes. *A posteriori*, it will be apparent that this neglect of sharp gradients is not significant to the story. Even with the filtered data, the resulting horizontal scales of maximum growth will turn out to be uniformly smaller than the observed eddy scales.

Projection of the mean velocities onto the neutral vertical modes has a second, related effect. Geostrophically balanced horizontal gradients of buoyancy at the top surface yield vertical shears at the upper surface. Thus when such gradients are present, the mean velocity does not satisfy the same boundary condition at $z = 0$ as the vertical modes ϕ_m calculated in (1). Therefore the surface component of the mean shear (or equivalently the horizontal buoyancy gradient itself) will be effectively removed from the calculation by projection onto the vertical modes. This removes instabilities of the Charney and Eady type, leaving only instabilities due to sign changes of the interior mean potential vorticity gradient via the Charney-Stern-Pedlosky criterion [see, again, ref. 3]. Eady instabilities, caused by interactions of edge waves at the upper and lower surfaces, are not expected since there are negligible gradients of buoyancy in the oceanic abyss. Charney-type instabilities, however, resulting from the interaction of the upper surface and interior flow, are likely to exist in many places in the ocean. However, like the sharp vertical gradients in the interior, with oceanic parameters these instabilities are also uniformly small and fast, and so we neglect them with the same rationale.

Given the mean zonal and meridional velocities, $\bar{u}(z) = (\bar{u}(z), \bar{v}(z))$, at a given horizontal location, we compute the projections

$$\vec{U}_m = \int_{-H}^0 \bar{u}(z) \phi_m(z) dz \longrightarrow \sum_n \bar{u}_n \phi_{mn} \Delta_n$$

where Δ_n is the discretized vertical spacing, ϕ_{mn} is the m -th vertical mode, discretized with index n replacing the coordinate z , and \bar{u}_n is the discretized velocity profile. For a given profile, up to 45 depth levels may be present, yielding a total of 44 baroclinic vertical modes. We project the velocity onto only the first 15 modes.

The complete linear instability problem projected onto vertical modes is then

$$(2) \quad A_{ij} \psi_j = -\omega \psi_i,$$

where ω is the frequency and

$$A_{ij} = \frac{1}{K^2 + \lambda_i^2} \left[k\beta \delta_{ij} + \sum_m \vec{K} \cdot \vec{U}_m \varepsilon_{ijm} (\lambda_m^2 - \lambda_j^2 - K^2) \right]$$

with β the northward gradient of the Coriolis parameter, and $\vec{K} = (k, \ell)$ the horizontal wavevector with modulus K . The triple interaction coefficient ε_{ijm} is calculated by the integral of the product of vertical modes i , j and m , over the full depth of the domain, and δ_{ij} is the Kronecker delta. At each gridpoint, we solve (2) for each wavenumber on a 100×100 grid with moduli ranging from $\lambda_1/5$ to $20\lambda_1$. This is sufficient to capture all the growth for all profiles checked.

The maximum growth rates at each horizontal location yield values ranging from about $1/30$ to $1/2$ days $^{-1}$, as expected (not shown). More interestingly and to the point, figure 2 plots the ratio of the scale of maximum growth L_{\max} to the local deformation scale (shown in figure 1). The resulting scales of maximum growth, even after filtering small scale growth via the projection onto a truncated set of vertical modes, is everywhere smaller than the local first deformation radius.

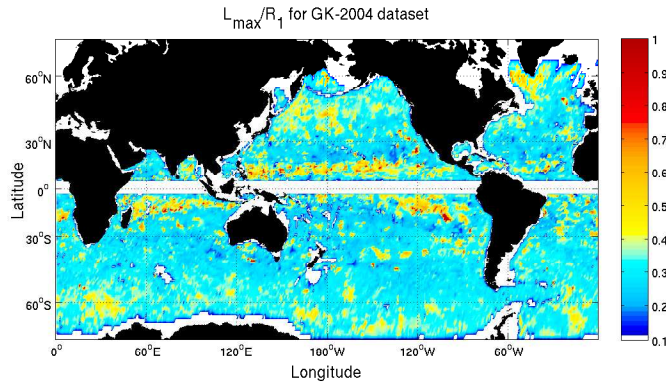


FIGURE 2. The scale of maximum baroclinic growth for the GK04 dataset, nondimensionalized by the local radius of deformation.

Stammer [2] demonstrates that the observed eddy scales, by contrast, are everywhere *larger* than the local deformation scale. Stammer proposes a linear correlation with the deformation scale $R_1 = \lambda_1^{-1}$, given by $L_{\max} = 0.8R_1 + 88$. Moreover, the raw data, seen in figures 21a and 24 of Stammer's paper, indicate that a linear fit is only marginally justified. To make the matter stark, in the Antarctic Circumpolar Current (ACC), where deformation scales are of order 10 Km (see figure 1), the observed eddy scale is nearly 100 Km. Given that the scale of maximum linear baroclinic growth is another 1/3 smaller than the deformation scale, one can safely conclude that linear theory, while fairly accurate in predicting timescales and locations of eddy activity, completely fails to predict the spatial scale of the eddies. Nonlinear studies of baroclinic growth in the presence of vertical shears and density structures similar to those found in the ACC [8] indicate that a strong inverse cascade should ensue, resulting in an eddy scale much larger than the scale of maximum linear growth. One can thus further conclude that a strong nonlinear cascade of energy is necessary to explain the observed eddy statistics.

REFERENCES

- [1] A. E. Gill, J. S. A. Green, and A. J. Simmons, *Energy partition in the large-scale ocean circulation and the production of mid-ocean eddies*, Deep-Sea Research **21** (1974), 499–528.
- [2] D. Stammer, *Global characteristics of ocean variability estimated from regional TOPEX/Poseidon altimeter measurements*, Journal of Physical Oceanography **27** (1997), 1743–1769.
- [3] J. Pedlosky, *Geophysical Fluid Dynamics*. Springer, New York, 2nd edition, 1987.

- [4] V. V. Gouretski and K. P. Koltermann, *WOCE global hydrographic climatology, a technical report*, Berichte des BSH **35** (2004), 1–52.
- [5] D. R. Jackett and T. J. McDougall, *A neutral density variable for the world's oceans*, Journal of Physical Oceanography **27** (1997), 237–263.
- [6] D. B. Chelton, R. A. deSzoeke, M. G. Schlax, K. E. Naggar, and N. Siwertz, *Geographical variability of the first baroclinic Rossby radius of deformation*, Journal of Physical Oceanography **28** (1998), 433–460.
- [7] R. M. Samelson, *Note on a baroclinic analog of vorticity defects in shear*, Journal of Fluid Mechanics **382** (1999), 367–373.
- [8] K. S. Smith and G. K. Vallis, *The scales and equilibration of mid-ocean eddies: Forced-dissipative flow*, Journal of Physical Oceanography **32** (2002), 1699–1721.

Participants

Dr. Ulrich Achatz

Leibniz-Institut für
Atmosphärenphysik an d. Universität
Rostock e.V.
Schloßstraße 6
18225 Kühlungsborn

Prof. Dr. Oliver Bühler

Center for Atmosphere Ocean Science
Courant Institute of Math. Sc.
New York University
251 Mercer Street
New York, NY 10012-1110
USA

Prof. Dr. Joseph Biello

Department of Mathematics
University of California
1, Shields Avenue
Davis, CA 95616-8633
USA

Prof. Dr. Paola Cessi

Scripps Institution for
Oceanography, Physical Oceanography
University of California San Diego
8602 La Jolla Shore Drive
La Jolla CA 92037
USA

Dr. Onno Bokhove

Department of Applied Mathematics
Twente University
P.O.Box 217
NL-7500 AE Enschede

Daan T. Crommelin

New York University
Courant Institute of Mathematical
Sciences
251 Mercer Street
New York, NY 10012
USA

Prof. Dr. Elie Bou-Zeid

Departement de Mathematiques
Ecole Polytechnique Federale
de Lausanne
CH-1015 Lausanne

Prof. Dr. Stamen Dolaptchiev

Potsdam-Institut für Klimafolgen-
forschung (PIK)e.V.
Telegrafenberg A31
14412 Potsdam

Prof. Dr. Grant Branstator

National Center for Atmospheric
Research
Climate & Global Dynamics Division
Boulder, CO 80307
USA

Prof. Dr. Joseph Egger

Institut für Theoretische
Meteorologie
Universität München
Theresienstraße 37
80333 München

Prof. Dr. Yann Brenier

Laboratoire J.-A. Dieudonne
Universite de Nice
Sophia Antipolis
Parc Valrose
F-06108 Nice Cedex 2

Prof. Dr. Gavin Esler

Department of Mathematics
University College London
Gower Street
GB-London, WC1E 6BT

Dr. Almut Gassmann

Meteorologisches Institut Bonn
Universität Bonn
Auf dem Hügel 20
53121 Bonn

Prof. Dr. Marcus Grote

Mathematisches Institut
Universität Basel
Rheinsprung 21
CH-4051 Basel

Prof. Dr. David Michael Holland

New York University
Courant Institute of Mathematical
Sciences
251 Mercer Street
New York, NY 10012
USA

Prof. Dr. Boualem Khouider

Dept. of Mathematics and Statistics
University of Victoria
P.O.Box 3045
Victoria, BC V8W 3P4
CANADA

Prof. Dr. Rupert Klein

FB Mathematik und Informatik
Freie Universität Berlin
Takustr. 7
14195 Berlin

Dr. Oswald Knoth

Institut für
Troposphärenforschung e.V.
Permoserstr. 15
04318 Leipzig

Dr. Leo Maas

Netherlands Institute for Sea
Research
P.O.Box 59
NL-1790 AB den Burg Texel

Prof. Dr. Andrew J. Majda

Courant Institute of
Mathematical Sciences
New York University
251, Mercer Street
New York, NY 10012-1110
USA

Lars Mentrup

Zentrum Mathematik
Technische Universität München
Boltzmannstr. 3
85747 Garching bei München

Dipl.Met. Eileen Mikusky

Potsdam-Institut für Klimafolgen-
forschung (PIK)e.V.
Telegrafenberg A31
14412 Potsdam

Prof. Dr. Paul A. Milewski

Department of Mathematics
University of Wisconsin-Madison
480 Lincoln Drive
Madison, WI 53706-1388
USA

Prof. Dr. Adam Hugh Monahan

School of Earth and Ocean Sciences
University of Victoria
PO Box 3055 STN CSC
Victoria, BC V8W 3P6
CANADA

Prof. Dr. Mitchell Moncrieff

NCAR-National Center for
Atmospheric Research
Foothill Lab
1850 Table Mesa Drive
Boulder Co 80305-3000
USA

Prof. Dr. David James Muraki

Dept. of Mathematics
 Simon Fraser University
 8888 University Dr.
 Burnaby, B.C. V5A 1S6
 CANADA

Dr. Christian Schoof

Dept. of Earth and Ocean Sciences
 The University of British Columbia
 6339 Stores Road
 Vancouver, BC V6T 1Z4
 CANADA

Dr. Antony Z. Owino

Fachbereich Mathematik
 und Informatik
 Freie Universität Berlin
 Arnimallee 2-6
 14195 Berlin

Prof. Dr. Shafer Smith

New York University
 Courant Institute of Mathematical
 Sciences
 251 Mercer Street
 New York, NY 10012
 USA

Prof. Dr. Vladimir Petoukhov

Potsdam-Institut für Klimafolgen-
 forschung (PIK)e.V.
 Telegrafenberg A31
 14412 Potsdam

Prof. Dr. Bjorn Stevens

Department of Atmospheric and
 Oceanic Sciences
 University of California
 Box 951565
 Los Angeles, CA 90095-1565
 USA

Dr. Riwal Plougonven

Lab. de Meteorologie Dynamique
 Ecole Normale Supérieure
 24, rue Lhomond
 F-75231 Paris Cedex 05

Prof. Dr. Esteban G. Tabak

Courant Institute of
 Mathematical Sciences
 New York University
 251, Mercer Street
 New York, NY 10012-1110
 USA

Prof. Dr. Sebastian Reich

Institut für Mathematik
 Universität Potsdam
 Postfach 601553
 14415 Potsdam

Prof. Dr. Edriss S. Titi

Department of Computer Science
 and Applied Mathematics
 The Weizmann Institute of Science
 P.O.Box 26
 Rehovot 76100
 ISRAEL

Dr. Ian Roulstone

Department of Mathematics and
 Statistics
 University of Surrey
 Guildford
 GB-Surrey GU2 7XH

Dr. Jacques Vanneste

School of Mathematics
 University of Edinburgh
 James Clerk Maxwell Bldg.
 King's Buildings, Mayfield Road
 GB-Edinburgh, EH9 3JZ

Prof. Dr. Tapio Schneider

California Institute of Technology
 Mail Code 100-23
 1200 E. California Blvd.
 Pasadena CA 91125
 USA

Dr. Xiaoming Wang
Department of Mathematics
Florida State University
Tallahassee, FL 32306-4510
USA

Prof. Dr. Vladimir Zeitlin
Lab. de Meteorologie Dynamique
Ecole Normale Supérieure
24, rue Lhomond
F-75231 Paris Cedex 05

Dr. Paul Williams
Department of Meteorology
University of Reading
Earley Gate
PO Box 243
GB-Reading RG6 6BB

